

Electrochemical Studies of Actinides using bis(trifluoromethylsulphonyl)imide [NTf₂] based Room temperature Ionic Liquids

By

Kavitha Jayachandran

CHEM01201404004

Bhabha Atomic Research Centre, Mumbai

A thesis submitted to the

Board of Studies in Chemical Sciences

In partial fulfillment of requirements

for the Degree of

DOCTOR OF PHILOSOPHY

of

HOMI BHABHA NATIONAL INSTITUTE



October, 2019

Homi Bhabha National Institute

Recommendations of the Viva Voce Committee

As members of the Viva Voce Committee, we certify that we have read the dissertation prepared by **Kavitha Jayachandran** entitled “**Electrochemical Studies of Actinides using bis(trifluoromethylsulphonyl)imide [NTf₂] based Room temperature Ionic Liquids**” and recommend that it may be accepted as fulfilling the thesis requirement for the award of Degree of Doctor of Philosophy.

Chairman: Dr. (Smt.) Smruti Dash		Date: 18-10-2019
Guide/ Convener: Dr. S. Kannan		Date: 18-10-19
Examiner: Dr. A. K. Srivastava		Date: 18/10/2019
Member 1: Dr. P.K. Mohapatra		Date: 18.10.2019
Member 2: Dr. (Smt.) Sangita D. Kumar		Date: 18.10.2019
Member 3: Dr. A.K. Pandey		Date: 18.10.2019
Technology Advisor: Dr. (Smt.) Ruma Gupta		Date: 18.10.2019.

Final approval and acceptance of this thesis is contingent upon the candidate's submission of the final copies of the thesis to HBNI.

I/We hereby certify that I/we have read this thesis prepared under my/our direction and recommend that it may be accepted as fulfilling the thesis requirement.

Date: 18-10-19

Place: Mumbai

Guide


(S. Kannan) 18-10-19

STATEMENT BY AUTHOR

This dissertation has been submitted in partial fulfillment of requirements for an advanced degree at Homi Bhabha National Institute (HBNI) and is deposited in the Library to be made available to borrowers under rules of the HBNI.

Brief quotations from this dissertation are allowable without special permission, provided that accurate acknowledgement of source is made. Requests for permission for extended quotation from or reproduction of this manuscript in whole or in part may be granted by the Competent Authority of HBNI when in his or her judgment the proposed use of the material is in the interests of scholarship. In all other instances, however, permission must be obtained from the author.



Kavitha Jayachandran

DECLARATION

I, hereby declare that the investigations presented in the thesis have been carried out by me. The work is original and has not been submitted earlier as a whole or in part for a degree /diploma at this or any other Institution / University.



Kavitha Jayachandran

List of Publications

REFFEREED JOURNALS

1. “Redox and Photophysical Behaviour of Complexes of NpO_2^+ Ions with Carbomyl methyl phosphine oxide in 1-Hexyl-3-methylimidazolium bis (trifluoromethyl sulfonyl)imide Ionic Liquid”
Kavitha Jayachandran, Ruma Gupta, Mahesh Sundararajan, Santosh K. Gupta, Manoj Mohapatra, S.K.Mukerjee, *Electrochimica Acta* 224(2017)269–277.
2. “Extraction and Electrochemical investigations of Pu(IV) employing green solvent system containing new bifunctional ligand and Bmim[NTf₂] ionic liquid”
Kavitha Jayachandran, Ruma Gupta, Bal Govind Vats and S. Kannan,
Journal of Radioanalytical and Nuclear Chemistry 318 (2018) 1009–1014.
3. “Remarkably Enhanced Direct Dissolution of Plutonium Oxide in Task Specific Ionic Liquid: Insights from Electrochemical and Theoretical Investigations”
Kavitha Jayachandran, Ruma Gupta, K.R.S. Chandrakumar, Dibakar Goswami, D.M Noronha, Sumana Paul and S. Kannan, *Chemical Communications*, 55 (2019) 1474-1477.
4. “Electrochemical investigations of U, Pu and Np employing N, N-dioctyl, α -hydroxy acetamide in (Omim[NTf₂])”
Kavitha Jayachandran, Jayashree S Gamare, Ruma Gupta, Bal Govind Vats and S. Kannan (to be communicated.)

Other Publications:

Symposium:

1. Thermodynamic and Electrochemical investigations of NpO_2^+ in 1-Butyl -3-methylimidazolium bis (trifluoro methyl sulfonyl) imide (Bmim[NTf₂]) ionic liquid”, **Kavitha Jayachandran** and Ruma Gupta, 21st Symposium on Thermal Analysis, (THERMANS-2018) at Goa University, India.
2. “Direct Dissolution of Plutonium Oxide in Task Specific Ionic Liquid”, Ruma Gupta, **Kavitha Jayachandran**, D.M Noronha and S. Kannan, 14th Biennial DAE-BRNS Symposium on Nuclear and Radiochemistry NUCAR-2019, held at DCC Anushaktinagar -Mumbai.

Dedicated to

My Family

ACKNOWLEDGEMENTS

I wish to express my deepest and sincere gratitude to my guide, Prof. S. Kannan, Head, Fuel chemistry Division, B.A.R.C. for his valuable guidance, constant encouragement and persistent motivation. His advice and comments have been priceless and played a significant role in documenting my work.

I convey my heartfelt gratitude to Dr. S. K. Mukherjee, former guide & Head, Process Development Division for his tremendous support and encouragement.

I take this opportunity to express my sincere regards and deepest appreciation to my technical advisor Dr. (Smt) Ruma Gupta, for sharing her experimental expertise and scientific knowledge with me. Without her help it would not have been possible to carry out the electrochemical studies of actinides and completing my Ph.D.

It gives me a great pleasure to acknowledge my senior colleague Dr. I.C.Pius with whom I started my first scientific endeavour after joining FCD, BARC, for sharing his work experience and scientific knowledge with me and for providing me the training necessary for handling radioactive materials .

I would also like to thank my senior colleagues Dr. P.R.Nair, Smt. Mary Xavier, Dr.(Smt) J.V. Kamat, for sharing their experimental expertise and scientific knowledge with me.

I would take this opportunity to thank the respected members of my doctoral committee Prof. Smruti Dash (Chairman), Prof. P.K.Mohapatra (member) and Prof. (Smt.) Sangita D Kumar(member), Prof. Ashok K Pandey (member), Prof. S.K.Aggarwal (ex-Chairman and Former Head FCD) and Dr. P.S. Dhami (ex-member) for their critical reviews and valuable suggestions during the annual progress reviews and presynopsis presentation.

I am thankful to all my collaborators especially Dr. K. R.S. ChandraKumar and Dr. Mahesh Sundararajan of Theoretical Chemistry Section, Chemistry Group, BARC for theoretical studies, Dr. Dibakar Ghosh of Bio Organic Division for Synthesis of ionic liquid, Dr. S.K. Gupta and Dr.M. Mohapatra for luminescence studies, Dr.(Smt.) Sumana Paul, Fuel Chemistry Division for providing alpha spectrometry experiments. I am also thankful to Dr. (Smt) Manjulata Sahu, Radioanalytical Chemistry Division for providing DSC data and Shri Karthik Dutta of Bio organic Division, BARC for NMR analysis.

My sincere thanks to Dr. S. Chaudhury, Head Actinides Processing Section and all of my colleagues from Actinides Processing Section, FCD for their help, suggestion and encouragement. I would like to express my sincere gratitude to Dr. P.K Pujari Associate Director, Radiochemistry and Isotope Group (RC&IG) for his constant support and encouragement throughout the work.

I am thankful to my colleagues Shri Rahul Agarwal and Dr. Balgovind Vats, Smt Jayashree Gamare for sharing their knowledge and scientific understanding during the fruitful discussions with me throughout the work.

This thesis would not have been accomplished without the support and encouragement of numerous people including my well wishers, my friends and colleagues who contributed in many ways to the successful completion of this thesis. I cannot imagine my current position without the blessings of my teachers and will always be indebted to them.

Most importantly, I owe my heartfelt gratitude to my parents, parent-in-laws and family for their constant encouragement, care and never fading love. Their blessings and good wishes have helped me to achieve what I am today.

Finally, I would like to express my endless thanks and appreciations to my husband, Jayachandran for his support and care and also to my children Abhinav and Jahnavi for their encouragement and support.

October, 2019

Kavitha Jayachandran
FCD, BARC

CONTENTS

	Page No.
<i>Synopsis</i>	<i>i-ix</i>
<i>List of figures</i>	<i>x-xii</i>
<i>List of tables</i>	<i>xiii</i>
<i>List of abbreviations</i>	<i>xiv</i>
<i>List of symbols</i>	<i>xv</i>
I. Introduction	1-31
1.1 General Actinide Chemistry	2
1.1.1 Electronic Configuration	2
1.1.2 Solution Chemistry	3
1.1.3 Oxidation States	4
1.1.4 Redox Reactions	5
1.1.5 Disproportionation	7
1.1.6 Complex Formation	8
1.1.7 Hydrolysis and Polymerisation	8
1.1.8 Electronic Spectroscopy of Actinides ions	9
1.1.9 Coordination chemistry of the Actinide Elements	10
<i>i) Neutral mono-functional extractants</i>	11
<i>ii) Neutral bi and tri- functional extractants</i>	11
1.2 Spent Nuclear Fuel Reprocessing	13
1.2.1 Purex Process	14
1.2.2 Pyrochemical Process	14
1.2.3 Need for alternative solvent	15
1.3 Room Temperature Ionic liquids	17
1.3.1 History of room temperature ionic liquids – in brief	17
<i>i) First generation RTILs</i>	18
<i>ii) Second generation RTILs</i>	18
<i>iii) Third generation RTILs</i>	18
1.3.2 Cations and Anions	19

1.3.3	Attraction of ILs	19
1.3.4	Properties of Ionic Liquids	20
	<i>i) Melting Point</i>	20
	<i>ii) Viscosity</i>	21
	<i>iii) Density</i>	22
	<i>iv) Vapour pressure</i>	22
	<i>v) Radiation and thermal stability</i>	23
	<i>vi) Polarity</i>	24
	<i>vii) Coordinating ability</i>	24
	<i>viii) Environmentally benign (Green Solvent)</i>	25
1.3.5	Task-specific Ionic Liquids	25
1.3.6	Applications of ionic liquids	26
	1.3.6.1 Application of ionic liquids in nuclear fuel cycle	27
	i) As diluents	28
	ii) As extractant	29
	1.4 Scope of the work	30
II.	Electrochemical methods and characterization techniques	32-60
	2.1. Electrochemical Methods	33
	2.1.1 Faradaic and Non-Faradaic processes	33
	2.1.2 Overview of electrode processes	34
	2.1.2.1 Interfacial Region	34
	2.1.2.2 Electrical Double Layer	35
	2.1.2.3 Charging Currents	37
	2.1.3 Electrode Kinetics	38
	2.1.4 Mass Transport	39
	<i>i) Diffusion</i>	39
	<i>ii) Convection</i>	40
	<i>iii) Migration</i>	41
	2.1.5 Practical Electrochemistry	42
	2.1.6 Voltammetric Techniques	44
	2.1.6.1 Cyclic Voltammetry (CV)	46
	2.1.6.2 Chronoamperometry (CA)	54

2.2. Materials & Chemicals	55
2.2.1 Radiotracers	55
2.2.2 Ionic liquids	55
2.2.3 Solvents and materials	55
2.2.4 Extractants	55
2.3 Characterization techniques	56
2.3.1 Radiation Detectors	56
2.3.2 Alpha Liquid Scintillation Counter	56
2.3.3 Gamma Counting	57
2.3.4 Alpha Spectrometry	57
2.3.5 Ultraviolet and Visible (UV-VIS) Spectroscopy	57
2.3.6 Fourier Transfer Infra-red Spectrometer	58
2.3.7 NMR spectrometer	58
2.3.8 Thermal studies	58
2.3.9 Luminescence studies	59
2.3.10 Computational Details	59
III. Electrochemical investigations of Np using RTIL employing CMPO as extractant	61-81
3.1. Introduction	62
3.2. Experimental	64
3.3. Results and Discussions	66
3.3.1. <i>Extraction of Np by CMPO</i>	66
3.3.2. <i>Electrochemical Investigations</i>	67
3.3.2.1 <i>Cyclic Voltammetry</i>	67
3.3.2.2 <i>Chronoamperometry</i>	71
3.3.3. <i>UV-Vis Spectroscopy</i>	72
3.3.4. <i>Time resolved fluorescence spectroscopy</i>	73
3.3.5. <i>Computational Results</i>	77
3. 4. Conclusions	80
IV. Electrochemical studies of actinides using New Bifunctional ligands as extractant	82-104
4.1. Introduction	83
4.2. Experimental	85

4.2.1	Synthesis and Characterization of Ligands	86
4.3.	Results and discussions	87
4.3.1	<i>Electrochemical investigations of Pu employing N, N-dioctyl carbamoyl methyl) (2- pyridyl-N-Oxide) sulfide (NOSCO) in (C₄mim[NTf₂])</i>	
4.3.1.1	Extraction Studies	87
4.3.1.2	Effect of Ligand concentration	87
4.3.1.3	Electrochemical Studies	89
4.3.2	<i>Electrochemical investigations of U, Pu and Np employing N, N-dioctyl, α-hydroxy acetamide in (C₈mim[NTf₂])</i>	
4.3.2.1	Electrochemical Studies of Uranium	97
4.3.2.2	Electrochemical Studies of Plutonium	99
4.3.2.3	Electrochemical Studies of Neptunium	101
4.4	Conclusions	103
V.	Direct Dissolution of PuO₂ powder in Task specific ionic liquid and its electrochemical studies	105-123
5.1	Introduction	106
5.2	Experimental Section	107
5.3	Results and Discussion	110
5.3.1	<i>DSC and TG Studies</i>	110
5.3.2	<i>UV-VIS spectroscopy</i>	111
5.3.3	<i>Electrochemical Studies</i>	112
5.3.4	<i>Computational Details</i>	119
5.3.5	<i>Alpha Spectrometry</i>	121
5.4	Conclusions	122
VI.	Conclusions & perspectives	124-128
6.1	Electrochemical studies of Np(V) in RTIL diluents with conventional extractant	125
6.2	Electrochemical studies of actinides in RTIL diluents with newly synthesized extractants such as : NOSCO and DoHyA	126
6.3	Direct dissolution of plutonium oxide and its electrochemical studies in TSIL	127
6.4	Future perspectives	128
	REFERENCES	129-150

SYNOPSIS

Chemistry of actinide elements is an essential part of the development of nuclear technology that began at the end of the 19th century. Nuclear technology has vital uses in research, medicine and general industries, but the most prominent use is in the generation of nuclear energy from the fission of heavier actinides. As India is following closed fuel cycle, it is important to recycle the spent nuclear fuel (SNF), a complex mixture of chemical elements, consisting of various radioactive isotopes. Currently, approximately 10,000 metric tons of SNF is generated per year [1]. At present, PUREX process is employed for reprocessing of SNF [2-4]. This method is based on the selective liquid-liquid extraction of uranium and plutonium from other elements in the nitric acid solution of dissolved SNF using 30% tri-n-butyl phosphate in kerosene. The process starts with the dissolution of spent fuel rods in hot concentrated (8 M) nitric acid.

The alternative method is non aqueous pyrochemical method for reprocessing of SNF. It has several advantages, such as minimum waste generation, low criticality concern and feasibility or reprocesses the high burn-up, and short cooled fuels. This method exploits the differences in the thermodynamic stabilities of various actinides and fission products for the dissolution of used nuclear fuel in the inorganic molten salt media followed by the electrochemical recovery of actinides [5]. Usually, the inorganic molten salt is composed of a eutectic of alkali or alkaline earth chloride. Therefore, the processing temperature in this method is invariably above 800K depending upon the composition of chosen eutectic. Hence, there is an urge for an alternative medium to reprocess the SNF in ambient temperature.

Room temperature ionic liquids (RTIL) have attracted considerable attention as possible replacements for conventional molecular organic solvents in biphasic liquid-liquid extraction systems for the separation of metal ions. The potential advantages of using a water-immiscible ionic liquid (IL) in such separations include exceedingly low volatilities and low

flammabilities, the efficient extraction of metal ions that are difficult to extract with molecular organic solvents [6-8], and the possibility of easily coupling liquid-liquid extraction and electrorefining [9]. RTILs offer large electrochemical window and superior conductivity for their potent use in electrochemical investigations over conventional solvents. Dialkyl substituted imidazolium cation based ionic liquids are usually air and moisture stable and have been used extensively in the electrochemical studies [10]. For application in nuclear fuel cycle, the radiolytic stability is a very crucial factor. RTILs, containing imidazolium and pyridinium cation, are fairly stable to radiolytic degradation due to the presence of aromatic rings. For imidazolium cation based ionic liquids, physical properties such as density, surface tension, refractive index, etc. are not considerably affected upon irradiation, but the viscosity is reported to be slightly higher due to the polymerization of the imidazolium cation [11]. Till now there is still inadequate data for the basic understanding of the electrochemical behaviour of actinides in ILs.

CMPO is considered as an efficient extractant for actinides extraction from SNF and have been extensively studied [12, 13]. Although there have been numerous experimental studies on extractabilities of actinides by CMPO, many unclear scientific issues still remain for example the behaviour of the extracted species in ionic liquids, its transport properties in ILs, structures of the extracted complexes, photophysical characteristics and the corresponding kinetic properties. Despite of the differences in oxidation and reduction chemistry of the actinides, electrochemical techniques have poorly been applied for nuclear fuel reprocessing. There is a need to develop selective extractants for safe recovery and recycling of actinides from the SNF. Researchers have proposed many ligands with different functional groups for the extraction of actinides from spent fuel [14–17].

The present thesis deals with the extraction and electrochemical behaviors of actinide ions with two new bifunctional ligands namely: (N, N-dialkyl carbamoyl methyl) (2-pyridyl-

xide) sulfide (NOSCO type) [11] and N, N-dioctyl- α -hydroxy acetamide (DoHyA) in ionic liquids 1-butyl-3-methylimidazolium bis (trifluoromethanesulphonyl) imide ($[C_4mim][NTf_2]$) and 1-octyl-3-methylimidazolium bis (trifluoromethanesulphonyl) imide $[C_8mim][NTf_2]$ respectively.

Furthermore, task specific ionic liquids (TSILs) can also be employed for extensive studies of lanthanides and actinides. Herein, functional groups are covalently, attached to either the cationic or anionic part of the ionic liquid so as to enhance the extractability of lanthanide and actinide complexes. In spite of the usage of ionic liquids for the separation of f-block elements, the primary issue of poor solubility of lanthanides and actinides in ILs is still unsolved. Hence, there is a need for extensive research to understand the behaviour of the complexes involving the f-block elements in TSILs and their electrochemical behaviour so as to find the simplest approach of recovering actinide species without generating waste. The most important actinide oxides in the nuclear industry are UO_2 and PuO_2 [18]. The present thesis envisages an approach for direct dissolution of PuO_2 in protonated betaine bis (trifluoromethylsulfonyl) imide) $[Hbet][NTf_2]$ and electrodeposit plutonium from the solution of TSIL and PuO_2 .

The thesis is divided into five chapters. The brief description of the each chapter is given below:

Chapter 1: Introduction

This introductory chapter gives an overview of the nuclear fuel cycle. The solution chemistry of actinide ions is important for their separation and, therefore, is briefly mentioned. A brief introduction to reprocessing of the spent nuclear fuel and different types of new bifunctional ligands relevant to the extraction of actinide ions from the spent fuel are also discussed. A brief introduction of RTILs including its properties, application in nuclear fuel cycle and the task specific ionic liquids are presented. Finally, the scope for the present study that deals

with the importance of introducing electrochemical methods for the separation and recovery of actinides from the nitric acid medium is also explained.

Chapter 2: Electrochemical methods and characterization techniques

This chapter gives mainly emphasis on electrochemical methods, instrumentation and the basic fundamental aspects of voltammetric and characterization techniques. Electrochemistry is the study of electron transfer reactions between electrodes and reactant molecules, therefore the overview of electrode processes are also explained. The electrochemical experiments are performed by the use of three electrodes system which offers a great degree of control and repeatability as compared to two electrodes system. Various other characterization techniques such as: radiometric, spectrophotometry, NMR, TG/DTA, density functional theory etc. employed during the present studies is explained.

Chapter 3: Electrochemical and spectroscopic studies of neptunium in [C_nmim] [NTf₂] based ionic liquids using CMPO as an extractant

This chapter deals with the electrochemical, theoretical and luminescence studies of $\text{NpO}_2^+/\text{NpO}_2^{2+}$ with carbamoyl methyl phosphine oxide (CMPO) ligand in ionic liquid [C_nmim] [NTf₂] (Figure 1).

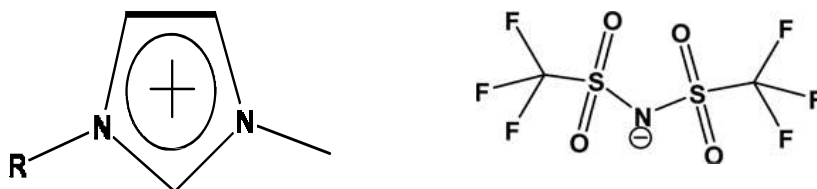


Figure 1: Structural formula of Alkyl methyl imidazolium bis(trifluoromethylsulfonyl) imide

To understand the role of ionic liquid in these studies, the redox behavior, complexation, and photophysical characteristics NpO_2^+ complexes are carried out. The electrochemical behavior of NpO_2^+ extracted by CMPO in 1-Hexyl-3-methylimidazolium bis(trifluoromethylsulfonyl)

imide [C₆mim] [NTf₂] (IL) was studied at glassy carbon (GC) electrode. The redox reaction of NpO₂⁺ to NpO₂²⁺ and vice versa in [C₆mim] [NTf₂] is quasi-reversible (Figures 2 and 3) and controlled by diffusion as well as charge transfer kinetics. The transport properties and kinetics of NpO₂⁺ are deduced from electrochemical calculations.

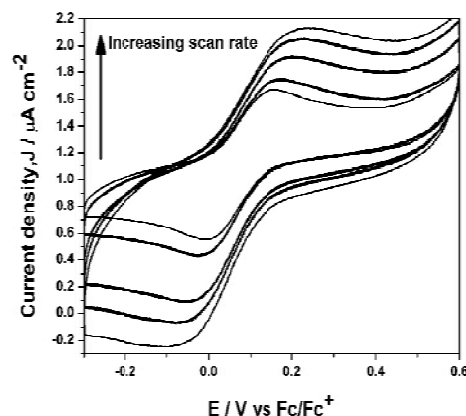
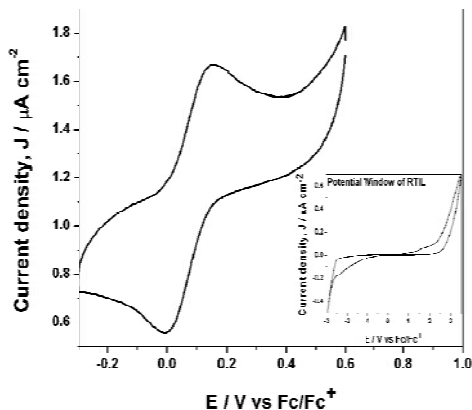


Figure 2: Cyclic voltammogram of NpO₂⁺ in C₆mimNTf₂ ILs. Inset shows the potential window of C₆mimNTf₂.

Figure 3: Cyclic voltammograms of NpO₂⁺ in C₆mimNTf₂ ILs recorded at different scan rates.

Chapter 4: Electrochemical studies of actinides in [C_nmim][NTf₂] ionic liquid employing New Bifunctional Ligands

This chapter comprises the electrochemical studies and extraction of Pu, U and Np employing two new bifunctional ligand system (N, N-dialkyl carbamoyl methyl) (2-pyridyl-N-Oxide) sulfide C₅H₄NOSCH₂CONR₂, (where R = octyl) (NOSCO) and N, N-dioctyl - α -hydroxy acetamide (DoHyA). Cyclic voltammetry (CV) studies of these actinide ions in aqueous as well as in ([C₄mim] [NTf₂] + NOSCO) and ([C₈mim] [NTf₂] + DoHyA) media respectively have been carried out. Shifts of cathodic and anodic peak potentials of Pu(IV) in cyclic voltammograms were observed towards negative potentials in the extended electrochemical window for ionic liquid medium compared to aqueous medium (Figure 4). The diffusion

coefficient and heterogeneous charge transfer coefficient are calculated for both aqueous and ionic liquid media.

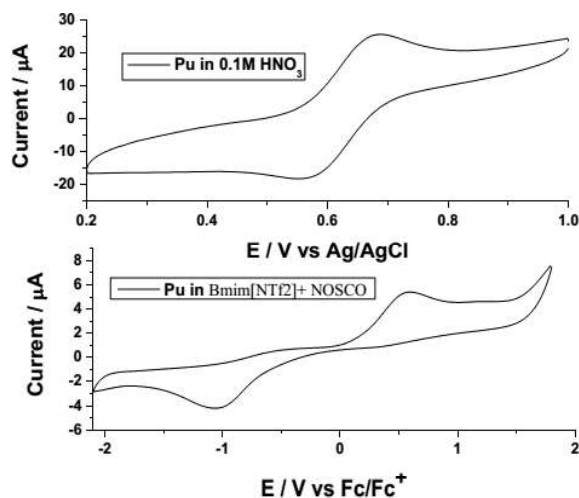


Figure 4: Comparison of cyclic voltammograms of Pu(IV) obtained in ionic liquid and aqueous solution

Chapter 5 - Task Specific Ionic Liquid for Direct Dissolution of Plutonium Oxide

This chapter explains the direct dissolution of plutonium oxide (PuO₂) in Protonated 1-carboxy-N, N, N-trimethylmethanaminium bis (trifluoromethylsulfonyl) imide [Hbet][NTf₂] task specific ionic liquid (TSIL). This chapter also explains an attractive possibility to electrodeposit plutonium from the solution of TSIL and PuO₂ (Figure 5). The carboxyl functional group attached to the TSIL plays a key role in facilitating the dissolution of plutonium ions (Figure 6) by making strong bonding. In addition, the electrochemical and thermodynamic properties of plutonium in [Hbet][NTf₂] at glassy carbon electrode are also investigated. The diffusion coefficient and heterogeneous charge transfer coefficient of plutonium at the electrode – electrolyte inter phase are determined at various temperatures. Furthermore, the fundamental nature of the interaction between the betaine based TSIL and plutonium ions was theoretically studied.

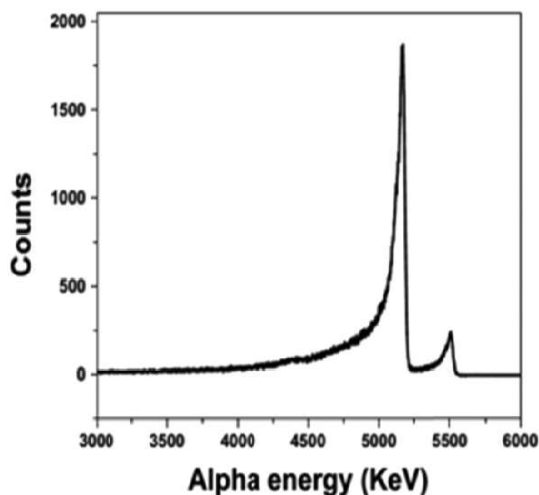


Figure 5: Alpha spectra of the stainless steel planchette after the electrochemical deposition of plutonium.

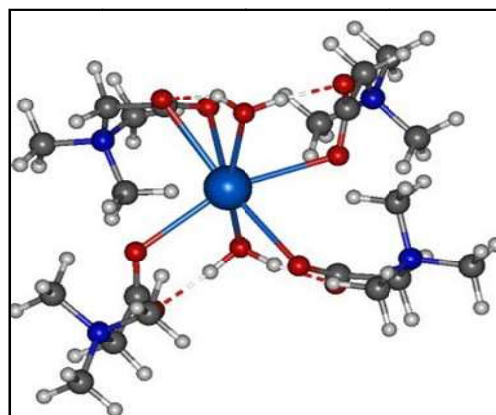


Figure 6: Optimized Structure of $[Hbet][NTf_2]$ recorded at various scan rates

Chapter 6 – Conclusions & perspectives

This chapter deals with the electrochemical studies of actinide ions separated from aqueous acidic solutions using conventional ligand and new bifunctional ligands in room temperature ionic liquids as diluents. The results revealed that the extraction of metal ion was remarkable when ionic liquids are used as diluents. The major findings of the work included in this thesis are summarized in this Chapter along with the future perspectives.

REFERENCES

1. E. Amaral, K. Brockman, H.G. Forsström, International perspectives on spent fuel management, IAEA, management of spent fuel from nuclear power reactors, 18, IAEA doc. STI/PUB/1295 (2007).
2. D.D. Sood, S.K. Patil, J. Radioanal. Nucl. Chem. 203 (1996) 547–573.
3. C. Musikas, W. Schultz, J.-O. Liljenzin, in: J. Rydberg, M. Cox, C. Musikas, G. Choppin (Eds.), Solvent Extraction Principles and Practice, 2nd ed., Marcel Dekker, Inc., New York, 2004, pp. 507–557.

4. K.L. Nash, C. Madic, J. Mathur, J. Lacquement, in: J.J. Katz, L.R. Morss, N.M. Edelstein, J. Fuger (Eds.), *The Chemistry of the Actinide and Transactinide Elements*, Vol. 1, Springer, Dordrecht, The Netherlands, 2006, pp. 2622– 2798.
5. T. Koyama, Y. Sakamura and M. Iizuka, *ECS Trans.*, 2010, 33(7), 339–349.
6. J.P. Hallett, T. Welton, *Chem. Rev.* 111 (2011) 3508–3576.
7. T. Welton, *Chem. Rev.* 99 (1999) 2071–2083.
8. Z. Kolarik, *Solvent Extr. Ion Exch.* 31 (2013) 24–60.
9. A.P. Abbott, G. Frisch, J. Hartley, K.S. Ryder, *Green Chem.* 13 (2011) 471–481.
10. J. Dupont, P.A.Z .Suarez (2006) Physico-chemical processes in imidazolium ionic liquids. *Phys Chem Chem Phys* 8:2441–2452.
11. P. K. Mohapatra (2017) Actinide ion extraction using room temperature ionic liquids: opportunities and challenges for nuclear fuel cycle application. *Dalton Trans* 6:1730–1747.
12. G.F. Vandegrift, R.A. Leonard, M.J. Steindler, E.P. Horwitz, L.J. Basile, H. Diamond, D.G. Kaline, L. Kaplan, Report ANL-84-45, Argonne National Laboratory, Argonne, IL, 1984.
13. E.P. Horwitz, D.G. Kalina, H. Diamond, G.F. Vandegrift, W.W. Schulz, *Solvent Extr. Ion Exch.* 3 (1985) 75–109.
14. C. Cuillerdier, C. Musikas, P.L. Hoel, X. Nigond Vitart (1991) Malonamides as new extractants for nuclear waste solutions. *Sep Sci Technol* 26(9):1229– 1244.
15. S. A. Ansari, P.N. Pathak, P.K. Mohapatra, V. K. Manchanda (2012) Chemistry of diglycolamides: promising extractants for actinide partitioning. *Chem Rev* 112(3):1751–1772.
16. J.H. Matonic, M. P. Neu, A. E. Enriquez, R.T. Paine, B. L. Scott (2002) Synthesis and crystal structure of a ten-coordinate plutonium(iv)ion complexed by 2-

[(diphenylphosphino) methyl] pyridine N, P-dioxide: $[\text{Pu}(\text{NO}_3)_3\{2\text{-}[(\text{C}_6\text{H}_5)_2\text{P}(\text{O})\text{CH}_2]\text{C}_5\text{H}_4\text{NO}\}_2] [\text{Pu}(\text{NO}_3)_6]_{0.5}$. J. Chem Soc. Dalton Trans 11:2328–2332.

17. B. G. Vats, J. S. Gamare, S. Kannan, I. C. Pius, D. M. Noronha, M. Kumar (2017) Synthesis, structural and extraction studies of new bifunctional ligand with uranium. Inorg Chim Acta 467:1–6.
18. I. Billard, A. Ouadi and C. Gaillard, Anal. Bioanal. Chem., 2011, 400, 1555–1566.

Chapter 1

Introduction

1.1.General Actinide Chemistry

To understand the extraction and complexation behaviour of actinides, a brief survey of general actinide chemistry is necessary. The actinides are fourteen elements having 5f electrons, which follows actinium in the periodic table of elements. Although all known isotopes of actinides are radioactive, the half lives of Thorium-232 and Uranium –235 & 238 are sufficiently long for them to be present in appreciable concentrations in nature. Therefore much of the earlier work on actinides has been devoted to thorium and uranium. Plutonium, the most important element in the actinide series, occurs in nature only in trace quantities [1]. It is the most studied element in the actinide series and these studies were conducted using synthetically prepared plutonium. Neptunium (Np) is one of the actinides produced in nuclear reactors and is located between U and Pu in the Periodic Table, suggesting that its chemical properties are qualitatively similar to those of U and Pu.

1.1.1. Electronic Configuration

In actinides, electrons are filled successively in the 5f orbital analogous to the lanthanides, where 4f orbital are filled successively [2]. In the beginning of the series up to Am, the energy of the 6d shell is lower and this shell preferred over 5f shell and thereafter the 5f shell is lower in energy compared to 6d. . The ground state electronic configurations of actinides are given in the Table 1.1[3].

Table 1.1. Electronic Configuration of Actinide Elements

Atomic No.	Element	Electronic Configuration
89	Ac	(Rn Core) $6d^1 7s^2$
90	Th	“ $6d^2 7s^2$
91	Pa	“ $5f^2 6d^1 7s^2$
92	U	“ $5f^3 6d^1 7s^2$
93	Np	“ $5f^4 6d^1 7s^2$
94	Pu	“ $5f^6 7s^2$
95	Am	“ $5f^7 7s^2$
96	Cm	“ $5f^7 6d^1 7s^2$
97	Bk	“ $5f^9 7s^2$
98	Cf	“ $5f^{10} 7s^2$
99	Es	“ $5f^{11} 7s^2$
100	Fm	“ $5f^{12} 7s^2$
101	Md	“ $(5f^{13} 7s^2)$
102	No	“ $(5f^{14} 7s^2)$
103	Lr	“ $(5f^{14} 6d^1 7s^2)$

Predicted configuration in parenthesis

1.1.2 Solution Chemistry of Actinides

The chemical behaviour of early members of actinides, as manifested by multiplicity of oxidation states, has proved extremely useful in their laboratory or industrial separations, which essentially exploit their redox reactions and their chemical behaviour in different oxidation states. Whereas the possibility of coexistence of various oxidation states, in the

same solution, for some of their members, their susceptibility to undergo changes in oxidation states under experimental conditions, due to preferential complexing of some oxidation state or due to the tendency to undergo disproportion reaction, the hydrolysis usually accompanying polymer formation and the influence of their nuclear properties on their chemistry, make their chemical studies on one hand very complex while on the other hand challenging as well as rewarding [4].

1.1.3 Oxidation States

Unlike in lanthanides, in actinides, first few electrons entering the 5f orbital are not effectively shielded and therefore they are easily ionizable [5]. Actinides from protactinium to plutonium are therefore able to exhibit higher oxidation states. As 5f shell is successively filled, the increased nuclear charge causes contraction of the 5f shell, with consequent better shielding of 5f shell from neighbouring atoms [5] and therefore higher oxidation states become more difficult to achieve and thus post americium actinides predominantly exhibit only 3+ oxidation state in aqueous solutions. Different oxidation states exhibited by the actinide ions in solution are given in Table 1.2. The ionic species formed by the actinides in aqueous solutions are M^{3+} , M^{4+} , MO_2^+ , and MO_2^{2+} . The higher charge of pentavalent and hexavalent ions are responsible for hydrolysis and subsequent formation of oxygenated species even in highly acidic solutions [5-7]. The heptavalent state, the highest oxidation state shown by neptunium, plutonium and americium is stable only in concentrated alkaline medium, the actinide species being present as MO_5^{3-} [9,10] ion. However, species $[MO_2(OH)]^{3-}$ for heptavalent state is inferred from spectral studies [11].

Table 1.2. Oxidation State of Actinide elements

Atomic No:	Actinide element	Oxidation State
89	Ac	<u>3</u>
90	Th	(2), (3), <u>4</u>
91	Pa	(3), 4, <u>5</u>
92	U	3, 4, 5, <u>6</u>
93	Np	3, 4, <u>5</u> , 6, 7
94	Pu	3, <u>4</u> , 5, 6, 7
95	Am	(2), <u>3</u> , 4, 5, 6, 7
96	Cm	<u>3</u> , 4
97	Bk	(2), <u>3</u> , 4
98	Cf	(2), <u>3</u> , (4)
99	Es	(2), <u>3</u>
100	Fm	2, <u>3</u>
101	Md	2, <u>3</u>
102	No	<u>2</u> , 3
103	Lr	<u>3</u>

The most stable oxidation states in aqueous solutions are underlined; those not known in aqueous solutions are within parenthesis.

1.1.4 Redox Reactions

The existence of multiple oxidation states of actinides make their chemistry complicated, but this is conveniently utilized for devising methods for their mutual

separations as well as separations from other elements. The values of formal potentials of uranium and plutonium couples are given in Figure 1.1 [12, 13].

Actinide ions show a widely varying degree of complexation with a particular ligand and this result in considerable changes in formal potentials from one medium to other. Although knowledge of formal potentials [14-16] helps in choosing reagents to obtain required oxidation states of actinide, it fails to give any information about the time required for completion of the reaction. The M^{4+}/M^{3+} and MO_2^{2+}/MO^{2+} couples are reversible, whereas M^{4+}/MO_2^{2+} couples is not reversible because of the slowness introduced in making and breaking of metal oxygen bond. The data on the kinetics of redox reactions of actinides have been reviewed by Newton [17, 18] and more data on the redox reactions have been reviewed by Nash and Sullivan[19].

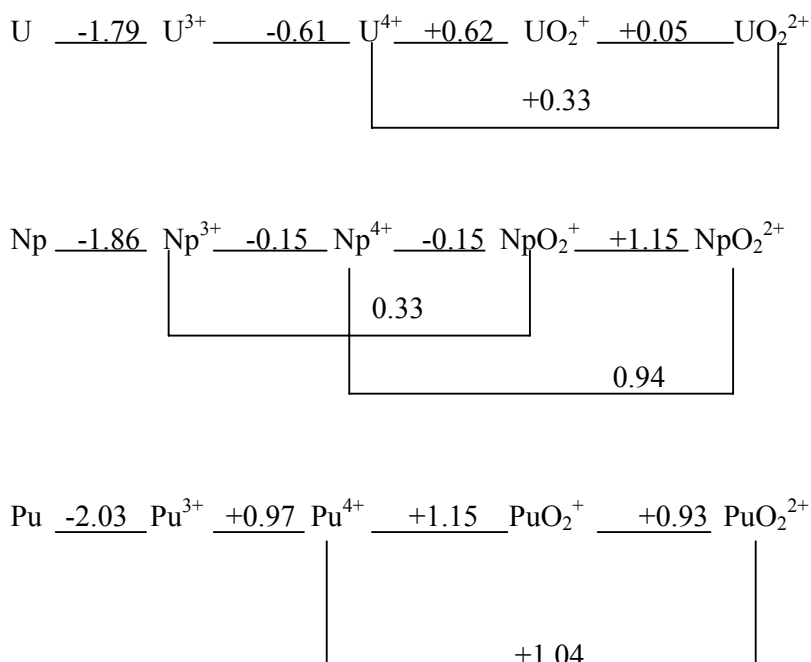


Figure 1.1 Reduction Potential of U, Np and Pu ions in 1M HClO₄ medium

1.1.5 Disproportionation

Disproportionation is a self oxidation-reduction reaction. One of the prerequisites for disproportionation to occur is that the element should exist in solution at least in three oxidation states. The disproportionation reactions of MO_2^+ and M^{4+} ions are given below: -



It can be inferred from the above reactions that, the presence of high H^+ ion concentration and the presence of complexing agents like oxalate, sulphate, phosphate, which form stronger complexes with M^{4+} ion as compared with MO_2^+ ion, favour the disproportionation reaction of MO_2^+ ion and the reverse is true in the case of disproportionation of M^{4+} ion.

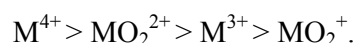
Although many transition metals exhibit multiple oxidation states, only few instances are known where different oxidation states co-exist simultaneously in appreciable concentrations. This is mainly governed by the potentials of the redox couples involved. Plutonium, having redox potentials of different couples very close to each other, exhibits the unique property of co-existence of four oxidation states, ranging from +3 to +6 in equilibrium in appreciable concentrations.



The equilibrium constants for the above reaction have been reported as 8.2 in 1M HCl and 3.2 in 0.1M HNO_3 [20,21]. Because of the above mentioned reaction, it becomes difficult to stabilize certain oxidation states and extreme care should be taken to avoid even partial change in the oxidation state during the course of experiments.

1.1.6 Complex Formation

The electronic configuration of anion is the most important factor determining the extend of complex formation. As actinides ions are considered as hard cations [22, 23] and their complex forming tendencies are primarily guided by electrostatic interaction. The variations shown in the complex formation by the actinides, can be explained to a considerable extend, based on their ionic potential, which is defined as the ratio of charge to radius. The general trend of formation of complexes with a given ligand is [24, 26]

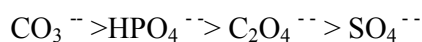


In few cases, however, the reversal in the order of MO_2^{2+} and M^{3+} is observed.

Among anions, the relative ability to form complexes with actinide ions varies relative to their tendency to bind with hydrogen ion. That is, the weaker the acid formed by the anion (except F^-), the stronger the complex it forms with the actinide ion. The over-all complexing sequence for singly charged ligands is [25]



and for doubly charged anions the sequence is



1.1.7 Hydrolysis and Polymerisation

All metal ions in aqueous solutions interact extensively with water molecules and exist as aquo cation [26, 27]. The hydrated cations act as Bronsted acids and the tendency to release hydrogen ion depends on the charge and size of the ion [28].



In actinides the trend of hydrolysis is similar to that of its complex formation. Hydrolysis, in fact is one form of complex formation, where the ligand is OH^- ion, but it is treated separately, as it could lead to polymerization and precipitation. The degree of

hydrolysis is in the order of: $M^{4+} > MO_2^{2+} > M^{3+} > MO_2^+$ for a particular actinide element [29]. The degree of hydrolysis increases with increase in atomic number in the case of M^{4+} and M^{3+} ions and the reverse is the order in the case of MO_2^{2+} and MO_2^+ ions.

In general, the hydrolysis of tetravalent actinides leads to polymerization resulting in the formation of a complex mixture of hydrolytic products and polymers, so their study becomes a difficult task. In many cases, only the first hydrolysis constant of actinides has been reported. The hydrolytic behaviour of plutonium is of special interest, as after first hydrolysis, there is a slow irreversible [30] polymerization leading to species with molecular weight ranging from few thousands to as high as 10^{10} amu [31]. The presence of polymer is indicated by bright green colour and its absorption spectrum is markedly different from the monomeric Pu(IV). The polymer spectrum has a characteristic absorption peak [32] at 610 nm. The presence of polymer can pose serious problems in reprocessing. Depolymerisation can be achieved by the use of high acidity and its rate can be hastened by increasing temperature, and by adding strong complexing and oxidizing agents [33, 34].

1.1.8 Electronic Spectroscopy of Actinide ions

The absorption/ emission spectra of actinide ions arise due to the electronic transitions and absorption bands appear mainly from three types of transitions, viz. i) f-f transition, ii) f-d transition, and iii) charge transfer bands [35]. In f-f transitions, the electronic transition occur between the two 5f-5f orbital which is generally Laporte forbidden. The bands are sharp because the transitions take place in the inner shell and are, therefore, not affected much by the surrounding environment. The energy differences between the various energy levels are of such an order of magnitude that the bands due to 5f-5f transitions appear in UV, visible and near IR regions. On the other hand, in case of f-d transitions the absorption bands are broad as these transitions are influenced by the surrounding environment. As transitions

take place between the orbital of different azimuthal quantum numbers, they are Laporte allowed and, therefore, these bands are relatively more intense. In case of charge transfer transitions, the bands occur due to the transition between the 5f orbital of actinide ions and the ligand orbital or the reverse. Therefore, the nature of ligand plays an important role. These transitions are significantly affected by the surrounding environment. As a consequence, the charge transfer bands are broad.

Yang and Group [36] have studied the complexation of Np (V) with carbonate solely by using spectrophotometry, whereas Ansari *et al.* [37] have carried out complexation with Glutaramide using spectrophotometry, micro calorimetry and DFT calculations. Taylor and Hindman in their respective work [38, 39] discusses about the electronic spectroscopy of neptunyl ions. However recently some work has been initiated wherein solid and solution state luminescence spectroscopy of neptunyl (VI) has been studied [40, 41].

1.1.9 Coordination Chemistry of the Actinide ions

Coordination chemistry of the actinide ions has gained enormous interest due to its high coordination numbers encountered in the complexes than that of the other elements. The coordination number in f-block metal ions is governed by the size and charge of the metal ions; this is due to the very small crystal field effect on the f-orbitals. Actinide ions are hard Lewis acids and their interaction with ligands is almost exclusively electrostatic in nature (even though in some actinide complexes there is evidence of a small degree of covalent nature). The coordination chemistry of the actinyl ion is of utmost importance in the nuclear reprocessing industry. The actinide-ligand complex formation in organic solvents is of direct importance to understanding and developing new biphasic aqueous-organic actinides separation chemistry, which is basis of existing reprocessing schemes. All earlier actinides (Th to Pu) utilize their f electrons more readily and thus can exist in a range of oxidation

states from +3 to +7 in aqueous solutions. As actinides are hard Lewis acids, their coordination chemistry mostly deals with hard donor ligands like oxygen. Phosphine oxides and phosphonates are continuing to attract a great deal of increased attention because of their relevance in actinide separation in nuclear fuel reprocessing such as in the PUREX process (Plutonium Uranium Redox Extraction) [42].

There are various types of neutral extractants having different donor groups, they were studied and classified according to the number of donor centers present in the molecule, such as mono-functional, bi-functional, tri-functional etc. The extraction, electrochemical and theoretical properties of these extractants are completely different from each other and giving interesting geometries around the metal ions.

i) Neutral mono-functional extractants

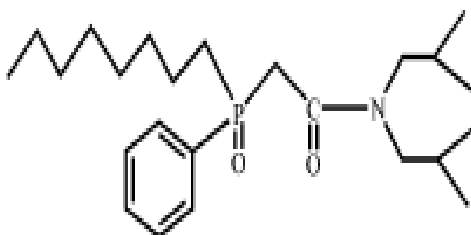
Tributyl phosphate (TBP), an alkyl phosphate based ligand is a monofunctional extractant, which is known as the workhorse for the nuclear reprocessing industry, the aqueous route reprocessing-PUREX process [43, 44]. In PUREX process, U(VI), Pu(IV) and Np(V) metal ions are extracted into organic phase by using 30% TBP in kerosene from ~ 3M HNO₃ and leaving rest of the fission products in the aqueous stream. A large number of studies have been reported using many monofunctional analogues of phosphates like: substituted amides [45-47], phosphine oxides [48], N-oxides [49] and suphoxides [50,51] for the extraction of actinides from spent nuclear fuel.

ii) Neutral bi and tri- functional extractants

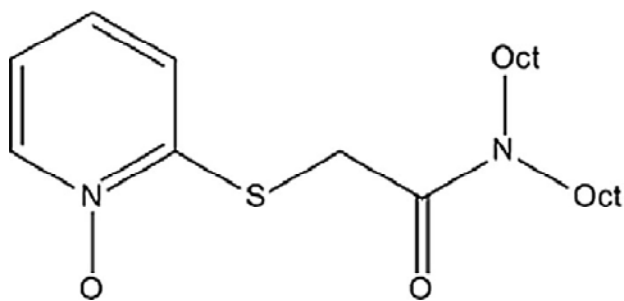
Bi-functional extractants, such as: carbamoyl methyl phosphonates (CMP), carbamoyl methyl phosphine oxides (CMPO), bis(diaklyl phosphine oxides) and malonamides and trifunctional ligands such as: tetraalkyl diglycolamides have shown excellent extraction properties for the trivalent actinides in addition to that of tetra and hexavalent actinide ions. The compounds of actinides with the neutral donor ligands such as

ketones, sulfoxides, amides, phosphates and phosphine oxides have been well characterized and thoroughly studied. The bi-functional chelating ligands such as: CMP, CMPO and malonamides are very well known for their superior extractability with respect to the extraction of actinide ions from acid media [46, 52-56].

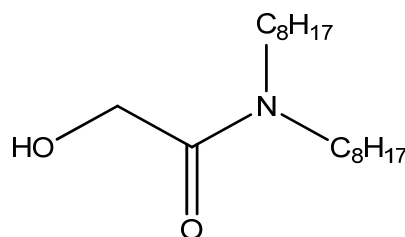
For actinide extraction from SNF, CMPO is considered as an efficient extractant and have been extensively studied [57-60]. Suzuki and co workers studied the extraction behaviour of Np (V) from nitric acid solution by CMPO in the presence and absence of TBP using n-dodecane and decalin as the diluents and predicted that Np(V) could be extracted by CMPO [61]. They also studied the extraction of Np (V) from nitric acid solutions containing U(VI) by CMPO and confirmed that the distribution ratio of Np(V) increased because of the formation of the cation–cation complex of Np(V)–U(VI) in CMPO solution [62]. Apart from this, other actinides viz. Am(III) Pu(IV), and U(VI) were also extracted successfully employing CMPO as an extractant [63-67]. The scope of actinide chemistry is very large and out of variety of extractants explored for the recovery of plutonium and uranium from the nuclear waste solutions, the following ligands have been used in present studies (Figure 1.2).



Octyl-(phenyl)-N, N-diisobutylcarbamoyl methyl phosphine oxide (CMPO)



(N, N-dialkyl carbamoyl methyl) (2-pyridyl-N-Oxide) sulfide (NOSCO)



N, N-dioctyl, α -hydroxy acetamide (DoHyA)

Figure 1.2: Structural formula of important ligands used in present study.

1.2 Spent Nuclear Fuel Reprocessing

Nuclear energy provides about 11% of the world's electricity from about 450 power reactors [68]. It is one of the world's largest sources of low-carbon power and is free from emitting greenhouse gases or other environmental contaminants and hence a solution for mitigating climate changes. Nuclear energy is trusted to be one of the most feasible options to meet the increasing worldwide demand of energy as the fossil fuel resources are limited [69]. The disposal of radioactive waste is a major drawback for the more widespread acceptance of nuclear energy.

The two different technologically feasible methods existing for reprocessing of SNF are aqueous-based conventional, PUREX (plutonium uranium recovery by extraction) process [70] and non aqueous-based pyrochemical process [71].

1.2.1 Purex Process

The Plutonium Uranium Reduction Extraction (PUREX) process is employed for the reprocessing of the spent nuclear fuel throughout the world [72]. The PUREX process involves the dissolution of used nuclear fuel in nitric acid medium followed by the selective liquid-liquid extraction of uranium and plutonium from other elements in the nitric acid solution of dissolved SNF using 30% tri-n-butyl phosphate in n-dodecane/kerosene. The process starts with the dissolution of spent fuel rods in hot concentrated (8 M) nitric acid. Pu is preferentially stripped back from loaded organic phase by conversion of Pu^{4+} to Pu^{3+} while 0.1 M HNO_3 was found to be useful for the quantitative recovery of U from the loaded TBP phase.

1.2.2 Pyrochemical Process

For reprocessing SNF using non aqueous pyrochemical method has several advantages, such as low criticality concern, minimum waste generation and feasibility or reprocesses the high burn-up, and short cooled fuels. This method exploits the difference in the thermodynamic stabilities of various actinides and fission products for the dissolution of used nuclear fuel in the inorganic molten salt media followed by the electrochemical recovery of actinides [73, 74]. Usually, the inorganic molten salt is composed of a eutectic of alkali or alkaline earth chloride. Therefore, the processing temperature in this method is invariably above 800K depending upon the composition of chosen eutectic. In view of this, the pyrochemical method also has few challenges with respect to the plant design, requirement of

inert atmosphere, high-temperature operation and corrosion problems, and so forth. The actinides being highly electropositive generally react rapidly and in some cases viciously with water to evolve hydrogen and give metal oxides. In order to obtain the pure metals, anhydrous molten salt processes have been developed. However, its practical application is limited by the high temperatures and strongly corroding properties of molten salt media [75-77].

The solubility of the charge bearing metal ions in the organic solvents are very less as they tend to remain in the aqueous phase due to ion-dipole interaction. For the extraction of metal ions in the organic phase, the charge on the metal ions must be neutralized so as to enhance the solubility in non-polar organic solvents. Therefore, a suitable extractant (ligand) molecule is generally added in the organic solvent which upon complexation with metal ions forms neutral hydrophobic species which are then extracted into the organic phase. In such cases, the extraction of metal ions may follow one of the following extraction mechanisms.

1.2.3 Need for Alternative Solvents

From environmental and economic point of view, the use of solvent is wasteful. The problem with the solvent is not much with their use but the inefficiencies in recovering them completely. In chemical reactions, solvents are used to facilitate the reaction, and after the completion of the reactions, they are removed from the products or reused for the same reaction. Removal of residual solvents from products is achieved by either evaporation or distillation. Therefore, most of the solvents used are highly volatile. This volatility has led to major public concern for atmospheric pollution which may lead to dizziness, nausea, and other long term effects including respiratory tract infection or sometimes cancer. Government and Environmentalist agencies are implementing various laws to reduce such types of pollutions.

Alternative solvents strategies should allow for the efficient reusability and recovery of the solvent after use. Compounds which used as alternative solvents are water, supercritical CO₂ [78], ionic liquids, and fluoruous compounds. Figure 1.3 shows the schematic representation of the alternative solvents used in the reaction. Water always cannot form homogenous mixture with all reagents used in reaction. Carbon dioxide is widely used as extracting solvents and fluoruous compounds forms homogenous reaction mixture with similar polarity reagents while using in chemical reaction.

Whereas ionic liquids, can be tailor made and imparts tunable properties by changing the composition of the salt used. Thus, it warrants the development of alternative approaches that could lend a hand to solve several concerns with current methodology including non proliferation issues, criticality safety, apparatus corrosion, and stiffness of the process.

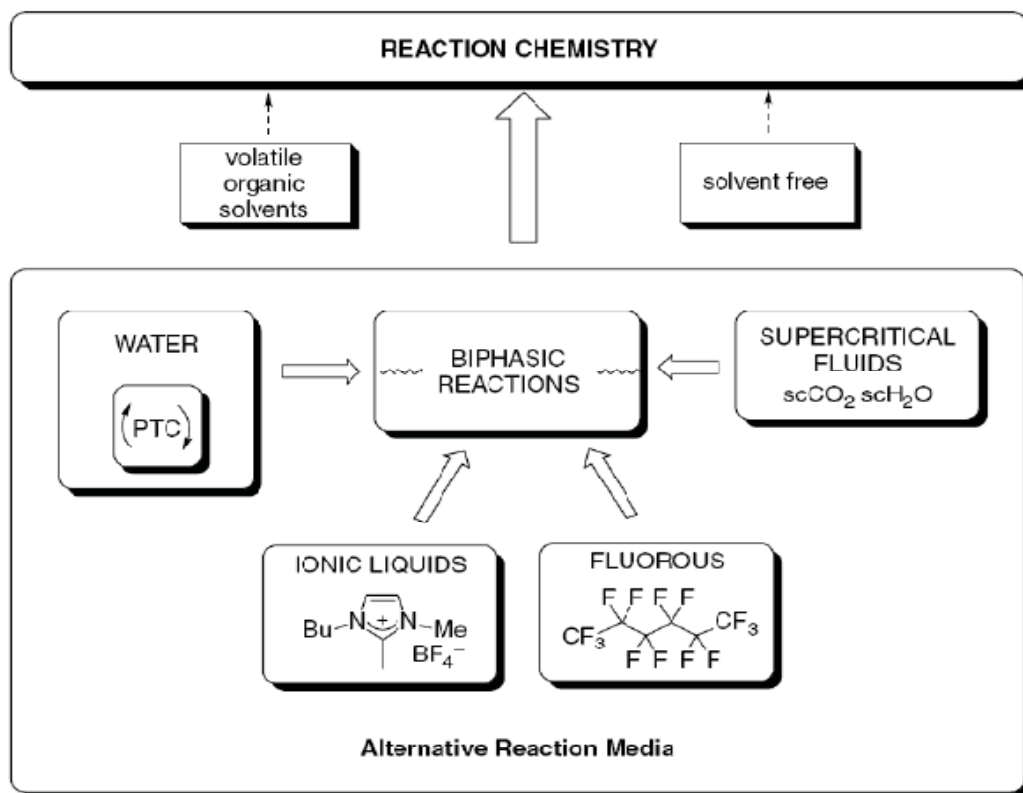


Figure 1.3: Diagrammatic Representation of Alternative reaction media (Dave et al., 2005)

1.3 Room Temperature Ionic liquids

Room temperature ionic liquids (RTIL) have attracted considerable attention as possible replacements for conventional molecular organic solvents in biphasic liquid-liquid extraction systems for the separation of metal ions. The potential advantages of using a water-immiscible ionic liquid (IL) in such separations include exceedingly low volatilities and low flammabilities, the efficient extraction of metal ions that are difficult to extract with molecular organic solvents [79-81], and the possibility of easily coupling liquid-liquid extraction and electrorefining [82]. In addition, the physico-chemical properties (in particular, polarity, polarizability, and molar volume) of individual ILs can be tuned over wide ranges by varying the constituent cations or anions. They are known to possess high electrical conductivity and good charge transport properties. Combined with their distinctive solvation ability to a wide variety of inorganic, organic, and organometallic species, ILs have inherent advantages for various electrochemical applications [83–85].

1.3.1 History of Room Temperature Ionic Liquids

Ionic liquids are not new materials – they have been known for over a century [86-89]. In 1914, Paul Walden's synthesised ethylammonium nitrate and it is published in ionic liquid research. This technology was only recently improved so that it might be performed on the industrial level [90-93]. Roughly some twenty years later, the significance of ILs for electrochemical applications such as electrodeposition of metals like aluminium was recognized [94-97]. Alas, ionic liquids first used for this kind of application were based on complex metal ions such as AlCl_4^- , which easily undergo hydrolysis and are highly corrosive. A significant step forward was the development of a set of ionic liquids that could be handled under ambient conditions [98, 99]. Soon it was realized that such ILs have unique properties as VOCs (volatile organic compounds) as solvent replacements and are materials with new

and unique combinations of physical properties. These days it is often the unique materials properties set, neither available in molecular compounds nor in typical crystalline salts, that turn out to be the true advantage of ILs [100-103]. It is estimated that more than one million simple ionic liquids can be synthesized, each with a different set of chemical and physical properties [104, 106]. The intrinsic nonvolatility, high thermal stability, large liquidus ranges and unique properties possible with many ILs have enhanced the interest in IL chemistry over the years [100-103]. Thus, ionic liquids truly offer the possibility to design a solvent for a certain application by the right choice of the cation and anion and their combination, which somehow justifies their being promoted as “designer solvents” [106]. Even more, the increasing social pressure for new green technologies has led to growing academic and industrial interest in IL technologies.

- i) First generation RTILs:** They are based on chloroaluminate (AlCl_4^- or Al_2Cl_7^-) anions. They are highly hygroscopic in nature. Due to the high reactivity of these RTILs towards water, there is limitation of their applications in practical purposes.
- ii) Second generation RTILs:** The draw backs in first generation RTILs, lead to development of “second generation RTILs”, which are mostly composed of air stable anion, such as BF_4^- , PF_6^- . However, these are highly viscous and produce detectable amount of HF acid formed by hydrolysis in the presence of trace amount of water [98].
- iii) Third generation RTILs:** They are composed of perfluorinated anion containing RTILs such as Tf_2N , fluoroalkylphosphate (FAP) and address the problem of second generation RTILs. These are mostly hydrophobic in nature and characterized with low melting points, low viscosity, and low conductivity [107]. However, RTILs composed of these anions are more expensive and show stronger binding ability towards the Lewis acid metal ions. Due to the presence of fluorine which is toxic and harmful for human beings, disposal of these RTILs become more complicated. This problem leads to the realization

of non-fluorinated orthoborate, carborane anion containing RTILs which are low coordinating and cheaper than other RTILs.

1.3.2 Cations and Anions

Room temperature Ionic liquids are typically salts with large nitrogen or phosphorus containing organic cations with linear alkyl chains (Figure 1.4). Many researchers have worked imidazolium cations.

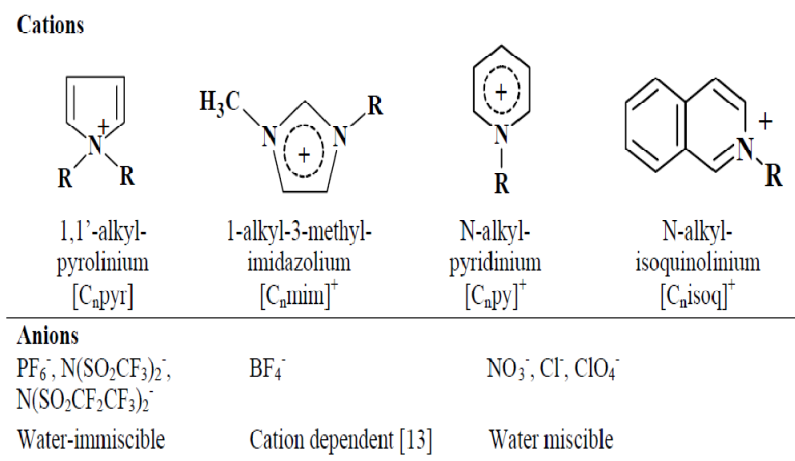


Figure 1.4: Representative cations and anions for IL composition (n indicates the no: of carbons in the alkyl chain)

1.3.3 Attraction of Ionic Liquids

Since the late 1990s, ILs has attracted the attention of chemist around the world for various reasons. ILs has opened up a new face of chemistry. Before 1998, there were relatively fewer studies of chemistry at temperature below 100°C in a liquid environment that was entirely ionic compared with the chemistry in a molecular environment. The scientific potential for research on ILs is virtually unlimited. Till date, more than 1500 IL have been reported in the literature. In theory at least, a million or so ILs are possible. An almost limitless number of IL systems are possible by mixing two or more simple ILs. Unlike

organic molecular solvents, ILs has negligible vapour pressure and therefore do not evaporate under normal conditions. They are non flammable and remains stable at temperature higher than conventional organic molecular solvents, they show wide electrochemical window. Their physical, chemical, and biological properties can be “tuned “or “tailored” by simply (a) switching anion or cation, (b) by designing specific functionalities in to the cation and/or anion, and (c) by mixing two or more simple IL, because IL consist of cation and anion, they have dual functionality. Therefore, they impart a unique architectural platform compared with molecular liquids. Consequently, ILs can potentially be exploited as solvents and new material for wide ranging applications such as, electrochemistry, organic and inorganic chemistry, biochemistry, material science and pharmaceuticals. ILs could contribute significantly to the development of green chemistry and green technology by replacing toxic, flammable volatile organic solvents, reducing or preventing chemical wastage and pollution and improving the safety of chemical process and products.

1.3.4 Properties of Ionic Liquids

Ionic Liquids have several fascinating properties out of which some of them relevant to the present thesis are i) negligible or near zero vapor pressure, ii) High radiation and thermal stability, iii) Tunable properties i.e, the properties of a particular ionic liquids can be changed by changing cation – anion combination, iv) Polar and coordinating nature, v) Enviromentally benign. Below, are the brief descriptions of some of the properties of RTILs.

i) Melting Point

The melting point of ionic liquid salts is directly proportional to the strong electrostatic interaction between the oppositely charged ions, which is related to the lattice energy of the salt as given below.

$$E = k (Q_1 Q_2) / d \quad \dots\dots\dots (1.1)$$

Where Q_1 and Q_2 are the charges on cation and anion respectively, d is the inter nuclear distance between the ions and 'k' is the Madelung constant. As the inter nuclear distance (d) increases the lattice energy (E) decreases. As a result, the melting point of the ionic salt decreases. For example, the melting point of NaCl is 803°C which is due to the strong electrostatic interaction between Na^+ and Cl^- ions. This strong interaction between two ions is due to the symmetrical nature of both ions and equal size of both the ions. If Na^+ ion is replaced by an asymmetric, bulky organic cation such as imidazolium cation, the melting point of the resulting crystal decreases drastically nearly 10 – 12 times that of NaCl, due to the increase in the interionic distance between the oppositely charged ions. In other words, these bulky and unsymmetrical ions will have low lattice energies due to the steric hindrance offered by oppositely charged ions which prevents the close approach of oppositely charged ions and hence the compound exists in liquid state at room temperature.

ii) Viscosity

The viscosities of RTILs are higher than that of conventional solvents and aqueous solvents [108]. It is obvious that the viscosity increases with increasing alkyl chain length, due to the increased possibility of Vander Waals interactions between the cations [109]. Along with the cations, RTIL anions also influence the viscosity. It depends upon the symmetry and tendency of the anion to form hydrogen bond. RTIL impurities have a significant effect on viscosity as well as other properties. Seddon et al. [110] studies show the effect of presence of water, sodium chloride, and organic solvents on the physical properties of ILs. For example, C_4mimBF_4 with 0.01M Cl^- ion has a viscosity of $154 \text{ (mPa s}^{-1}\text{)}$ and with 0.5 M Cl^- ion $201 \text{ (mPa s}^{-1}\text{)}$. However, the viscosities of ammonium based ionic liquids are much higher than that of imidazolium based ionic liquids [111].

iii) Density

In separation processes the density of the ionic liquids plays a vital role, which is one of the main applications of ionic liquid. The simple halide based ionic liquids have significantly lower densities and with increase in the hydrophobicity of the anions such as PF_6^- or NTf_2^- ion, the density increases. The density decreases with increase in the alkyl chain length of the cation moiety, since the addition of CH_2 groups affects the effective packing. Mikkola et al [111] reported that the density of quaternary ammonium based ionic liquids with long alkyl chain (e.g., Aliquat 336) is lower than that of water.

iv) Vapour pressure

Even at high temperatures due to the ionic nature, ionic liquids possess negligibly vapour pressure. Therefore the volatile products, and even products with low vapour pressures, can be isolated from ionic liquids by distillation. However, some ionic liquids can be distilled at low pressure without decomposition [112] and even can be separated thermally [113]. Seddon and co-workers have demonstrated that some ionic liquids can be distilled at 473-573 K under reduced pressure. Rebelo et al. [114] have performed distillation of 1-decyl-3-methylimidazolium and 1 dodecyl-3-methylimidazolium bis triflamide ionic liquids under reduced pressure, and predicted normal boiling points based on the data obtained from surface tension and density measurements. The predicted values of boiling temperatures were in the order of $[\text{BF}_4]^- > [\text{PF}_6]^- > [(\text{CF}_3\text{SO}_2)_2\text{N}]^-$ for a given cation (e.g. 1-alkyl-3-methylimidazolium cation). Zaitsau et al. [61] have reported the vapour pressure of a series of 1-alkyl-3-methylimidazolium triflimide based ionic liquid (alkyl = ethyl, butyl, hexyl and octyl).

v) Radiation and thermal stability

Ionic liquids generally have high radiation and thermal stability. Rouzo et.al [115] investigated the radiochemical stability of imidazolium-based ionic liquids constituted of the C_4mim^+ cation and associated with four commonly used anions (X^- : Tf_2N^- , TfO^- , PF_6^- and BF_4^-) under gamma irradiation for high irradiation doses (up to 2.0 MGy). The degradation of ionic liquid increased in the order $NTf_2^- < OTf^- < PF_6^- < BF_4^-$. Allen et al. [116] have investigated the radiation stability of 1, 3 - dialkylimidazolium nitrate and chloride ionic liquids under α^- , β^- and γ^- radiation fields. The results indicate that their stabilities were comparable with that of benzene, and more than the mixture of tributylphosphate and odourless kerosene under similar irradiation conditions. These ionic liquids were stable up to 400 kGy. The enhanced stability was attributed to the combination of properties of ionic salt and aromaticity. Berthon et al. [117] have studied the gamma radiolysis of $C_4mimNTf_2$ and C_4mimPF_6 . It was reported that the properties such as density, surface tension and refractive index were unchanged upon irradiation up to 600 kGy. The overall concentrations of radiolysis products did not exceed 1 mol% when irradiated up to 1200 kGy. Berthon et al [118] have investigated the radiolysis of ionic liquid containing quaternary ammonium cation. $MeBu_3NTf_2$ was reported to be stable at high radiation doses. The primary radiolytic products of the anion (F^\bullet and CF_3^\bullet) combine with the radiolytic products of cation (Bu^\bullet , Me^\bullet and H^\bullet) to form degradation products in small concentrations.

Most ILs has a high thermal stability because of their negligible vapour pressure. The thermal stability of different ionic liquids is nearly independent of cations but it decreases with increase in the anion hydrophilicity [119]. Bonhote et al.[120] have found that $C_2mimNTf_2$ was stable up to 400 °C and decomposed rapidly between 440°C and 480°C whereas C_2mimTA (TA = trifluoroacetate) was only stable to 150 °C and then decomposed rather slowly to 250°C.

vi) Polarity

Polarity is related to the physical properties such as melting and boiling points, solubility, and intermolecular interactions [121]. Ionic liquids have been considered as polar solvents, such as those suitable for charged compounds, possibly because of their ionic nature. The first polarity investigation of ionic liquids using the solvatochromic dye method postulated that imidazolium-based ILs possess a polarity similar to lower alcohols [122]. Various methods were subsequently developed to determine the polarity of ILs [123-128]. Bonhote et al. [120] have reported that the polarity of 1-ethyl-3-methylimidazolium bis(trifluoromethanesulphonyl) imide similar to that of ethanol, and the apparent low dielectric constant was attributed to ion-pairing in the pure state. Seddon and co-workers have reported the polarity of 1, 3- dialkylimidazolium based ionic liquids using absorption spectrum of solvatochromic dye Nile Red, and observed that the spectral features of tested ionic liquids were similar to that of short chain alcohols [128]. Dzyuba et al. [129] have studied the polarity of ionic liquids, by incorporating functional groups such as hydroxy and alkoxy groups at C1 position of 1, 3-dialkylimidazolium cation, and observed an increase in the polarity.

vii) Coordinating ability

The coordinating ability is a tendency to donate electrons to form a chemical bond [130]. A decade ago, ILs were generally perceived as non-coordinating, which implied that their anions were non coordinating as well [131-135]. However, the recent reports confirm that ionic liquids are indeed coordinating in nature [136 – 138]. In traditional imidazolium IL systems, the coordinating abilities are determined by the anionic part rather than the cations [139]. The chloride or bromide displays strong coordinating abilities, and this has been proven by several characterization techniques like crystallographic as well as NMR and IR

studies [140, 141]. The ionic liquid bearing the anions such as NTf_2^- and $[\text{SO}_3\text{CF}_3]^-$ are assumed to be non-coordinating because the negative charge is highly delocalized over electronegative fluorine atoms. However, recent studies suggest that NTf_2^- is a versatile coordinating anion that can interact with transition metals in various modes. For example, N-methyl-N-propylpyrrolidinium bis (trifluoromethanesulfonyl) imide [136] reacts with YbI_2 , forming a complex in which the NTf_2^- anions coordinate with the Yb center in a chelating mode using the two oxygen atoms as donors. Ionic liquids can be designed to coordinate deliberately by incorporating coordination groups (task specific ionic liquids).

viii) Environmentally benign

Ionic liquids are the potential solvents for clean and green approach to solve the problems encountered due to the green house effect and global warming issues. Ionic liquids are the most viable candidates for a new, clean and green technology; where waste streams are minimal and atom-efficiency is increased and as a result, environmental and cost benefits could be achieved. This is possible because of ionic liquids' "immeasurably" low vapor pressure under normal conditions. Some issues have recently been raised against the greenness of the ionic liquids [142, 143]. However, due to infinite designing possibilities, ILs can be made non-toxic, readily degradable, and even edible by a proper cation-anion combination [144, 145]. Recently, an article on greenness of ionic liquids is reported by Welton [146].

1.3.5 Task-specific Ionic Liquids

Davis et al. (2004) have introduced task specific ILs. These are ILs designed with functionalised cations and or anions that imparts specific properties or reactivity to the ILs. Task specific ILs is also known as functionalised ILs. They are, in effect, designer ILs. ILs

with imidazolium or triphenylphosphine cations functionalised with sulphonic acid ($-\text{SO}_3\text{H}$) groups are some of the examples. These Brønsted acidic ILs were first reported by Frobos and co-workers (2002) and used them as dual solvent- catalyst for a range of acid catalysed organic reaction such as esterification. 1-butyl -3-methyl-imidazolium cobalt tetracarbonyl, $(\text{C}_4\text{mim})(\text{Co}(\text{CO})_4^-)$, was one of the first example of a task specific IL with functionalised anion to be synthesised. Dyson et al. (2007) has described its preparation and use as a transition metal carbonyl catalyst for the debromination of 2-bromoketones. Brown et al. (2001) have also reported similar ILs. In 2006, Dyson and colleagues have reported numerous IL with task specific cation; however, less effort have been devoted to the synthesis of IL with task specific anions.

TSILs containing phosphoramidate [16], 2-hydroxybenzylamine [24, 25], diglycolamide [26–29], phosphate [30–32], carboxyl [33], CMPO [34], malonamide [35], hydrogen phthalate [36] etc groups tethered with the ionic moieties have been reported for the extraction of lanthanides and actinides.

1.3.6 Applications of Ionic Liquids

Due to their distinctive properties, room-temperature ionic liquids are employed in various applications such as in synthesis, catalysis [147-151], separations [152], and electrochemistry [153-155]. The physical as well as chemical properties of the room temperature ionic liquid can be tuned by careful choice of cation/anion. Therefore, they are also referred to as designer solvents. Recent advancements in ionic liquids research provide another route for achieving task-specific ionic liquids (TSILs) in which a functional group is covalently attached to the cation or anion part of the ionic liquid. Growing interest in ILs has been observed in chromatographic method such as gas chromatography (GC), capillary electrophoresis (CE) and liquid chromatography (LC).

1.3.6.1 Application of Ionic Liquids in Nuclear Fuel Cycle

Room temperature ionic liquids are used in nuclear industries both as solvent for extraction studies and as electrolyte for the non-aqueous reprocessing. Excellent reviews on the application of room temperature ionic liquids in the area of nuclear fuel reprocessing and waste management [156-162] are available in the literature. Consequently, there has been a significant increase in the studies related to the use of RTILs in aqueous and non-aqueous reprocessing applications. As this thesis is aimed the aqueous reprocessing application of RTILs, a detailed literature report is given below. Essentially, RTILs are investigated as possible substitute to the molecular diluents in solvent extraction procedures and as an alternative to high temperature molten salt in non-aqueous reprocessing applications [156-162]. Some of the remarkable features of RTILs that make them promising for nuclear fuel cycle application are:

- i) Selectivity of target metal ion can be easily designed by the changing the cation-anion combinations of RTIL diluent, rather than redesigning the structure of extractant
- ii) Presence of ionic diluent in organic phase facilitates a new mode of recovery of metals by direct electrodeposition from the extracted phase
- iii) RTILs can be designed to be completely incinerable, which would simplify the management of spent organic waste
- iv) Ionic liquids can be functionalized with organic moieties for selective separation of actinides from fission products
- v) Fire hazard is almost insignificant, due to negligible vapour pressure of RTILs.

In addition, unusual extraction of metal ions has been observed when traditional extractants are used in RTIL based diluents. Broadly, the application of RTILs in nuclear fuel cycle can be categorized into:

- a) RTIL as diluents

b) Functionalized or Task specific ionic liquids (TSIL)

i) **As Diluents**

RTILs are used as suitable alternate to the conventional diluents such as aromatic and paraffinic diluents in the nuclear industries since more than a decade. A systematic study of the extraction of actinides (mostly U(VI), Pu(IV) and Am(III)) and lanthanides in ionic liquid medium has been reported elsewhere [128-142]. Giridhar et al. [152] have studied the extraction of U(VI) from nitric acid medium by a solution of TBP in C₄mimPF₆ or C₄mimNTf₂. The distribution ratios are compared with those obtained using 1.1 M TBP/n-DD. The mechanistic aspects of U(VI) extraction in TBP dissolved in ionic liquid (C_nmimNTf₂) was investigated in detail by Dietz [154] and later on by Billard et al.[155] wherein the occurrence of ion exchange mechanism during metal ion transfer in to the ionic liquid phase is highlighted. Ikeda et al.[163] have studied the extraction of uranyl ion in the solution of TBP and quaternary ammonium based ionic liquid diluents. The extraction of Pu(IV) from nitric acid medium by a solution of CMPO in C₈mimPF₆ was reported by Lohithakshan et al.[164].

Visser et al.[165] have reported a preliminary investigation on extraction of f-block elements using a solution of 0.1 M CMPO -1.0 M TBP in C₄mimPF₆. The distribution ratios of Am(III), Pu(IV), Th(IV) and U(VI) were found to be an order higher in ionic liquid system than those obtained in n-DD under similar conditions. Nakashima et al. [166, 167] have studied, in detail, the extraction of trivalent lanthanides in CMPO/C₄mimPF₆ and highlighted the diluent property of C₄mimPF₆ over n-DD.

The extraction behavior of UO₂²⁺, Am³⁺, Nd³⁺, Eu³⁺ in a solution of dialkylphosphoric or dialkylphosphinic acid (HA) present in C₁₀mimNTf₂ was reported by Cocalia et al. [158] and proposing the analogous extraction behavior for metal ions both in ionic liquid as well as n-DD. The liquid-liquid extraction of lanthanides (Ln³⁺) from aqueous medium by a solution

of TODGA/C_nmimNTf₂ (n =2, 4, 6) was investigated by Shimojo et al.[168]. Jensen et al. [169] have studied the extraction of Eu(III) in HTTA/C₄mimNTf₂ and proposed the existence of anion exchange mechanism during the extraction.

ii) As Extractants

Nockemann et al. [170] have prepared several TSILs made up of imidazolium, pyridinium, pyrrolidinium, piperidinium, morpholinium, and quaternary ammonium bis(trifluoromethylsulfonyl) imide salts, functionalized with a carboxyl group for the dissolution of several rare earth and transition metal metal oxides and hydroxides. The synthesis of 2-hydroxybenzylamine (LH2) FIL and the extraction of ²⁴¹Am(III) from aqueous medium was reported by Ouadi et al.[171]. Ouadi et al. [172] have also synthesized a few TSILs containing phosphoryl moiety attached to the quaternary ammonium ion. The extraction of U(VI) from 3 M nitric acid medium was reported using these TSILs. The preliminary extraction data indicate the potential use of these FILs for applications related to uranium separation.

A general approach for the synthesis of diphenyl carbamoylmethyl phosphine oxide moiety functionalized on imidazolium ion was reported by Odinet et al. [173]. Using this TSIL, they have studied the extraction of actinides. Recently, Oliver et al. [174] have reported a new β-diketonate functionalized ionic liquid and studied the extraction of lanthanides using silica support (solid – liquid extraction). Recently, the application of these types of ionic liquids for the extraction of lanthanides has been appeared in the literature [175, 176].

1.4 Scope of the Work

The work presented in this thesis was conducted to address the application of ionic liquids in the electrochemical separations and recovery of actinides with respect to the nuclear fuel cycle. The first part of the research effort focused on the use of bis (trifluoro methyl sulphonyl imide) $[\text{NTf}_2^-]$ anion based ionic liquids as diluents in conjunction with the various ligands for the extraction of actinides. In these studies, the extraction of various actinides (U, Pu and Np) using conventional ligand CMPO and some newly prepared bifunctional ligands like NOSCO and DoHyA were carried out. Studies were also carried out to find out the electrochemical and thermodynamic parameters required for understanding some of the basic concepts such as: how the extracted actinide species behave in ionic liquids, what are its transport properties in ILs, possible speciation of extracted complexes and corresponding kinetic parameters. Since, actinide spectroscopy is not only challenging but recently it has gained renewed interest because of its application in various technological areas. Hence, to understand the photophysical characteristics of actinide species in ionic liquid, spectroscopic investigations were also carried out as there very limited literature available from time resolved florescence perspective in detail.

The most important actinide oxides in nuclear industry are UO_2 and PuO_2 . For minimal generation of radioactive waste, it is anticipated to directly dissolve actinides from their oxides rather than dissolution in an aqueous solution followed by extraction. Due to the weakly coordinating properties of the constituting anions and cations, ionic liquids show poor metal oxide dissolution properties. In order to overcome this problem, the second part of this thesis includes the synthesis of task specific ionic liquid (TSIL), and direct dissolution studies of PuO_2 powder in the synthesised TSIL. It details the use of functionalized ionic liquid for the dissolution of PuO_2 avoiding the use of extractant since TSIL act as extractant as well as solvent/ diluents. DFT calculations were performed to understand the structure of the Pu and

Hbet complex which is facilitating the direct dissolution. Also, electrochemical and thermodynamic properties of Pu(IV) in [Hbet][NTf₂] were performed to understand feasibility of using [Hbet][NTf₂] ionic liquid as electrolyte medium for electrodeposition of plutonium. This direct electrodeposition of plutonium species is a simple approach of recovering actinide species via electrochemical reduction which has two advantages. The first advantage is that the location of reduction is localized to the electrode surface forming a deposit affording easy removal from the waste stream. The second advantage is that the use of electrons as the reducing agent does not add to the waste volume. In this methodology, there is no requirement for elevated temperatures unlike molten salts hence the production of unwanted gases is avoided making the recovery process simpler. This method does not require multiple paths or pyrochemical methods to achieve dissolution or separation of the fission products. This method does not require complexing agents, it is performed in non-aqueous solution, and the direct dissolution is achieved in the same solvent system used for electrodeposition. The present method relates to the electrochemical deposition of an actinide species with simple procedure of providing an actinide ion in a TSIL, an electrode within the actinide and TSIL composition at ambient temperature and a potential such that current passes between the electrode-electrolyte interphase to deposit actinide species. This thesis approaches through another step to the growing interest in nuclear industry related to the applications of room temperature ionic liquid (RTIL) in nuclear fuel reprocessing and waste management.

Chapter 2

**Electrochemical methods
and characterization
techniques**

2.1. Electrochemical Methods

Electrochemistry is the branch of chemistry concerned with the oxidation/reduction of chemical species and the corresponding rate of electron transfer. A large part of this field deals with the study of chemical changes caused by the passage of an electric current and the production of electrical energy through controlled chemical reactions. In addition, the reclamation of select chemical species from aqueous or non-aqueous solutions using electrochemical methods is an attractive method because it is clean, efficient, and inexpensive relative to other methods including extraction, sorption, and refining [177].

2.1.1. Faradaic and Non-Faradaic Processes

Two types of activities can take place at an electrode surface and contribute to the measured current. The first is termed 'faradaic' [178] and involves the transfer of electrons between the metal electrode and electroactive species in solution. Depending on the direction of the flow of electrons, the species can either be oxidised or reduced, and the amount converted by electrolysis is proportional to the amount of charge passed. For one mole of electrons, the charge passed is 96485.4 C, known as the Faraday constant, F . In the absence of any additional processes, one Faraday of charge is passed per one equivalent of reactant consumed (assuming $n=1$).

The second type of process is termed 'non-faradaic' and can be caused by adsorption/desorption processes and changes in the interfacial structure as the potential is varied, resulting in charge and discharge of current. This type of charging current, i_c , (sometimes called capacitative current) can be described by:

$$i_c = AC_{dl} (dE/dt) = AC_{dl} v \quad \dots\dots\dots (2.1)$$

where A is the electrode area, C_{dl} is the double layer capacitance, dE/dt is the variation in potential with time and v is the scan rate. Non-faradaic charging currents can be undesirably

large when the scan rate is high (*e.g.* kV s^{-1} , often used in 'fast scan' voltammetry), so electrodes of small diameter (microelectrodes) are required in such experiments to avoid the faradaic response being swamped by capacitive currents. Although both faradaic and non-faradaic processes contribute to the overall measured current response, experimental conditions are usually designed so that non-faradaic contributions are minimised, and only faradaic processes are recorded. The magnitude of any faradaic current is mainly dependent on the following factors: the rate of mass transport of an electroactive species to and from the electrode surface, any heterogeneous electron transfer between the electrode and solution at the interface, and any homogeneous chemical reactions occurring before or after the electron transfer. These topics will be explained in the following sections.

2.1.2. Overview of Electrode Processes

The overall chemical reaction that takes place in a cell is made up of two independent half-cell reactions which describe the real chemical changes that are occurring at the two electrodes (working and counter electrodes). Each half-reaction responds to the interfacial potential difference at the corresponding electrode because the chemical composition of the system near the electrodes is different.

2.1.2.1. Interfacial Region

Electron transfer is an event in a molecular scale where a negatively charged entity passes through between an electrode and species in solution. The reason for electron transfer to occur is the potential gradient present at the electrode surface, which results from difference in the potential values when two different materials or phases come in contact with each other. For example, if the potential difference between a local electrode and the adjacent solution is 1V, measured over a gap of 1 nm, then the potential gradient shall be of

the order of 10^9 V m^{-1} [179]. When studying the rate of electron transfer, a considerable thought on the potential gradient at the interfacial region is of vital importance. Whenever potential is applied to the electrode surface, a charging characteristic involving the electrostatic effect is observed. Ions and dipoles with opposite charges are most likely attracted to the electrode surface. This eventually results in the formation of “electrical double layer”. Movement of ions to the electrode surface causes changes in the potential field and this factor is indispensable when considering the kinetics of electron transfer.

2.1.2.2. Electrical Double Layer

Suppose there is no electron transfer occurring at the interface of the electrode and the solution, in other words, no chemical changes taking place and so no Faradaic current passes, such an electrode is called ideally polarized electrode as no electrode reactions occurs within a certain range of potential values [180]. Ideally polarized electrode behaves like a capacitor and only capacitive current flows upon change of potential. Lot of electrodes possess this kind of characteristics but only within an electrode potential range called the double-layer range.

As mentioned previously, if a potential is applied to an electrode immersed in a solution, the electrode surface will become charged. The amount of charge on the electrode surface is proportional to the electrode material, the electrolyte and potential applied. If the potential applied is negative, then the electron will flow into the surface eventually turning the surface to be negatively charged. On the contrary, if the applied potential is positive, electron will move out of the surface, gradually making it positively charged. Accompanying this phenomenon is the rational that for every electrode/electrolyte combination, there must be a potential at which the surface shall be neutrally charged. This potential is called zero charge, E_{pzc} . Surface charge on the electrode is in fact balanced by the

movement of counter ions from the bulk solution. Extending the argument above, whenever the electrode potential is negative to E_{pzc} , its surface will become negative. Balancing this, the cations and dipoles such as water molecules begin to be attracted to the electrode surface. Similarly, if the potential applied is positive relative to the E_{pzc} , the electrode surface becomes positively charged thus inviting anions and dipoles to its surface. It may be noted that in this case, the orientation of the dipoles will be reversed. Either way, there shall be an organized layer consisting of cations or anions formed very close to the electrode surface resulting from the potential changes. Higher is the applied potential, the stronger is the electrostatic forces produced. As a matter of fact, competition for sites on the electrode surface does exist between the ions and water dipoles in order to form a well organized double layer. An example of the formation of double layer is depicted in Figure 2.1[179].

Thus when the potential of an electrode in an aqueous electrolyte is negative to E_{pzc} , its surface will be negatively charged and both cations and dipoles, particularly water molecules, will be attracted to the surface. Moreover, the more negative is the applied potential, the stronger are the electrostatic forces leading to the formation of an organized layer of cations adjacent to the electrode surface. Conversely, positive to E_{pzc} , the electrode surface will be positively charged and the anions and dipoles will be attracted with the orientation of the dipole reversed. In practice, there will be competition between the ions and water dipoles for sites on the surface. The electrostatic forces leading to a totally organized structure are opposed by the thermal motion of the ions.

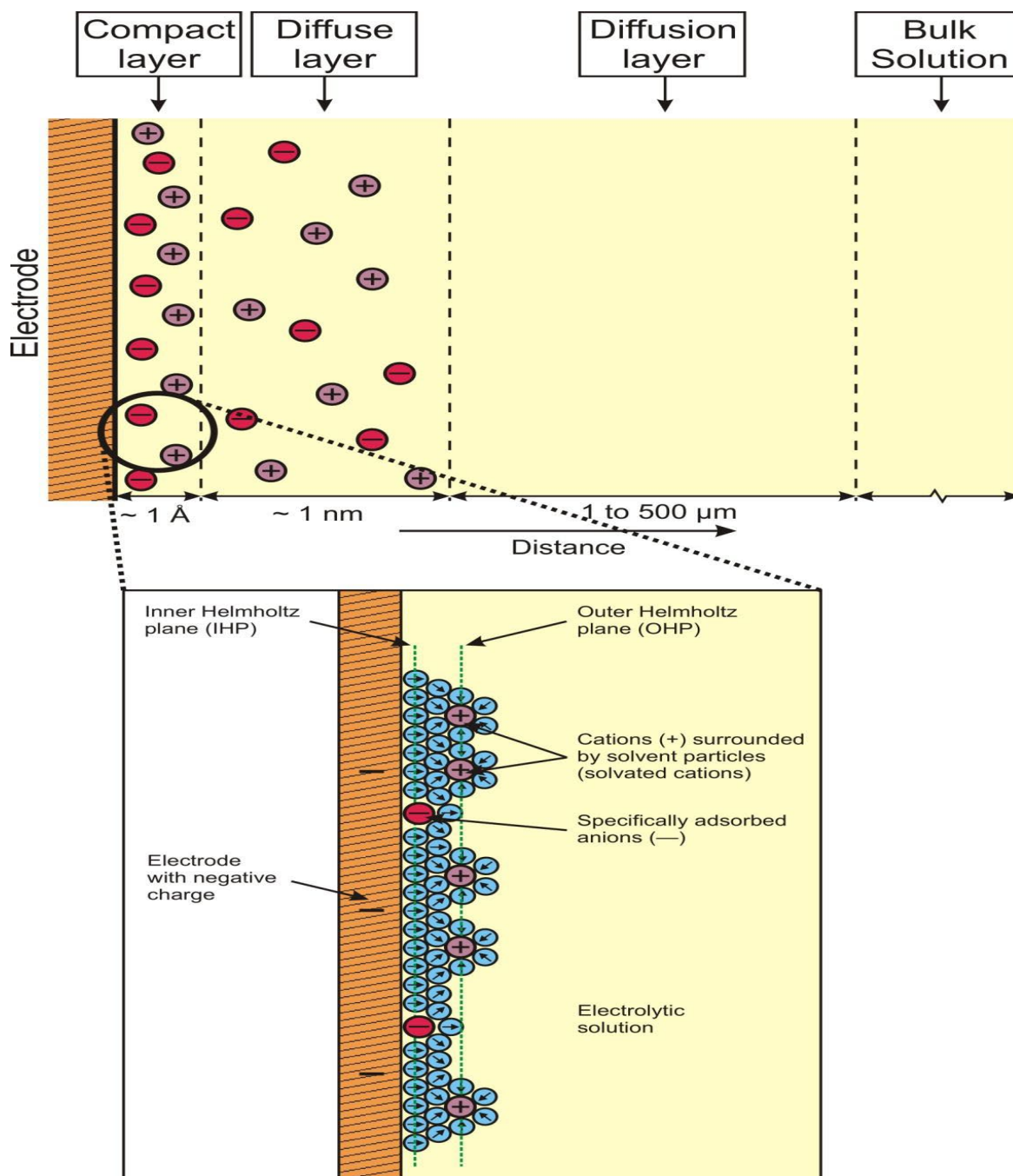


Figure 2.1 Schematic representation of the composition electrical double layer at the interfacial region at the electrode surface (not to scale).

2.1.2.3. Charging Currents

Any change in the potential of an electrode is the driving force for change in the charge on the metal side of the electrode surface. Coupled to this, ions and dipoles reorganization will also occur in the double layer on the solution side. Changing the

potential of the electrode means that there will be electrons flowing into or out of the electrode. In practice, these electrons will eventually pass out through the external circuit and virtually seen as current called “charging current”. This charging current comes from the reactive species present in the cell in addition to the Faradaic current. Its presence is always regarded as “noise” as it complicates the signals produced by the reaction desired in the particular experiment setup. It shall be emphasized that the effect of charging current is only a minor problem for short timescale experiments as reorganization of double layer according to the potential change occurs very fast and once the new structure has been formed, the charging current effect can be totally neglected [179].

For example, in cyclic voltammetric experiment, the charging current may be estimated from the following formula. In general the typical capacitance value is of 0.2 F m^{-2} . Therefore, at scan rates of 0.1 and 100 V s^{-1} , the observed capacitive current density J_{cap} will be 0.02 and 20 A m^{-2} , respectively.

$$J_{\text{cap}} = C \times v \quad \dots\dots\dots (2.2)$$

The current density is expressed by above equation. Here C is the capacitance and v is the potential scan rate. The capacitive current at high scan rate is of the same order of magnitude or higher compared to the Faradaic current for a diffusion controlled reaction.

2.1.3. Electrode Kinetics

Consider the reduction of Fe (III) and the oxidation of Fe (II)



where the rate constants k_{red} and k_{ox} describe the reduction and oxidation respectively. A cathodic process is one at an electrode supplying electrons causing a reduction i.e. cathode

whilst an anodic process is one at an electrode which removes electrons i.e. anode causes an oxidation process.

An example of a reduction for a cation can be taken from Figure 2.1. In order for the electron transfer to occur at a potential negative to E_{pzc} , the cation must be as close as possible to the electrode. Let us say it has to sit on the plane of the closest approach. It is important to note that whether or not the electron transfer occurs at the interface, the structure and properties of the double layer remain the same. Also, it may be emphasized that the resulting structure as well as the behaviour of the double layer originates from the electrostatic effect and not the chemical effect. For these reasons, in a system where the electroactive species exist in a large excess of inert electrolyte, solely the ions will determine the characteristics of the double layer. In practice, the effect of double layer is always minimized by using inert electrolyte.

2.1.4. Mass Transport

The supply of reactant and removal of product to/from the electrode surface are essential to a continuing chemical change. For electron transfer to occur, the reactants have to transport themselves towards the electrode surface, and once the reaction is complete, the product will automatically diffuse away from the electrode surface. Generally, there are three different modes (Figure 2.2) of transportations i.e. diffusion, convection, and migration.

i) **Diffusion.** The difference of concentration between two points in a solution normally ends up with the movement of a more concentrated species to the area of lower concentration. This will last until the concentration between them becomes equal. This phenomenon which originates from the concentration gradient is called diffusion [179]. It plays an important role

when considering reaction on the electrode. Often, the electron transfer process occurs in the vicinity of an electrode.

For example, when an oxidised species undergoes a reduction process at a considerable rate to become reduced at the electrode, the concentration of the former at the electrode surface will be lower than in the bulk solution. In other words, the concentration of the reduced species at the electrode surface will be higher than that in the bulk solution. Fick's first law defines diffusion as diffusional flux which represents the number of moles diffusing per unit area. Fick derived his second law which applies to cases where the change of concentration within a specific area occurs [181]. In Fick's equations (see below equations), j_{ox} is the flux, D is the diffusion coefficient, $[Ox]$ is the concentration of the species, and x is the distance of the species from the electrode surface.

$$j_{ox} = -D_{ox} \frac{\partial [Ox]}{\partial x} \quad \dots\dots\dots (2.4)$$

$$\frac{\partial [Ox]}{\partial t} = -D_{ox} \frac{\partial^2 [Ox]}{\partial x^2} \quad \dots\dots\dots (2.5)$$

In most of the electrochemical measurements where the oxidation and reduction of active species occurs due to applied electrical potential, the Fick's second law is preferable as the former processes always result in changes of concentration at the electrode surface with the elapse of time.

ii) **Convection.** The presence of thermal gradient or difference in density within a solution can lead to another form of mass transport namely convection. Convection may occur in nature or is deliberately induced by means of applying external forces such as shaking or sparging the solution in the electrochemical cell where the electrode

reaction occurs. In general, in an unstirred solution, convection is always caused by the chemical reaction in the vicinity of the electrode surface which probably generates slight changes in density or even the temperature. Meanwhile, unnatural convection is always considered as unfavourable as these changes eventually induce the movement within the cell solution. In electrochemical experiments, convection can be controlled by flowing the electrolyte solution over the electrode surface at a known rate or by the usage of rotating disc electrode [182].

iii) **Migration.** Migration is a form of mass transport which originates due to the potential gradient induced by the movement of charged species such as ions in the electrochemical cells. As in all electrochemical experiments, the application of electrical voltages between electrodes allows the passing of current creating potential drop at the electrode /electrolyte solution surface. Migration, which occurs due to electrostatic forces, is an integral part of the electrode reaction since it balances any changes in the charge capacity. However, it is not compulsorily desired in all circumstances of electrochemical reactions. To overcome this problem, very often the addition or usage of supporting electrolyte solution to the electroactive solution is done to minimize the effect of migration. Even though the reactant or product in the electrode cell may be charged species, but they will be enclosed by the ions of the supporting electrolyte solution due to the presence of excess electrolyte solution. Therefore, these ions are the charged species which move and not the electroactive species themselves [179].

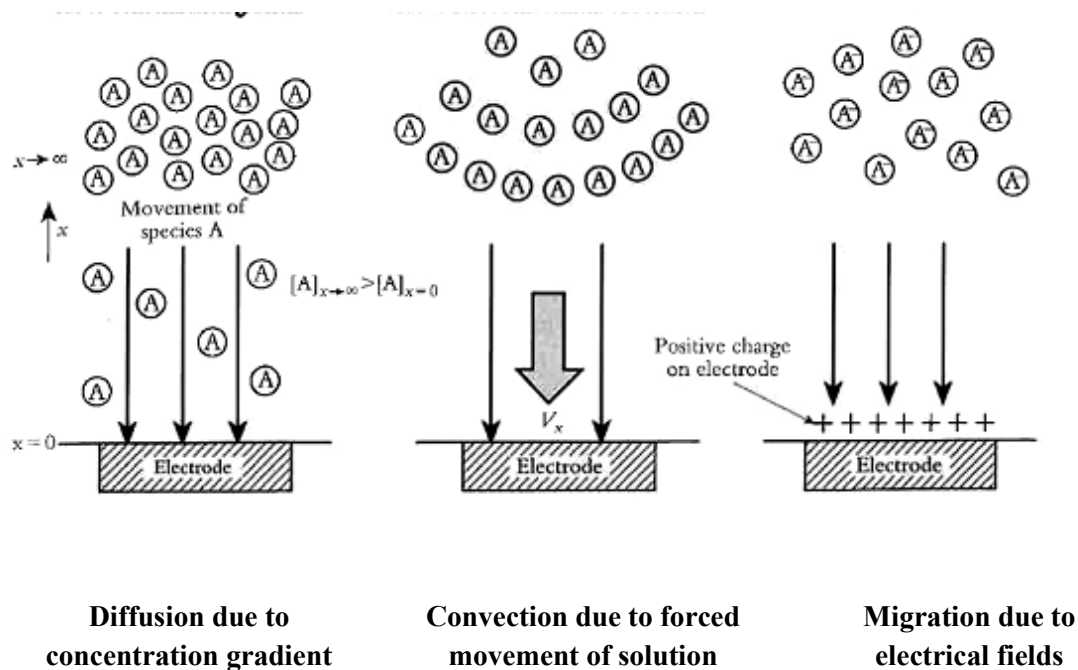


Figure 2.2 Three different forms of mass transport to the electrode surface for electroactive species in solution

2.1.5. Practical Electrochemistry

Usually only one reaction is of interest and the electrode at which it occurs called the working electrode. Therefore, to focus on the reaction at a single working electrode, a reference electrode was used to standardize the other half cell. This electrode is made up of phases having essentially constant composition and potential. For all aqueous measurements performed the silver-silver chloride electrode, Ag/AgCl/KCl (saturated in water) was used. The fixed potential at the reference electrode is predicated on the composition of the electrode not changing as reactions take place at the working electrode. A third electrode, a Pt counter electrode is used to ensure that the potential of the reference electrode does not change as reactions occur at the working electrode. The counter electrode acts as an electron donor and acceptor during the electrochemical reaction without changing the composition

of the reference. Therefore, the potential of the working electrode can be poised versus the reference electrode influencing the energy of the electrons and reactivity at the electrode surface.

Oxidation/reduction at the working electrode occurs as the energy of the working electrode is raised or lowered as a function of the applied potential. When the energy of the working electrode is sufficiently negative of the reduction potential of the chemical species is reduced. When the energy of the working electrode is sufficiently positive of the oxidation potential of the chemical species, the species is oxidized. The critical potentials at which these processes occur are related to the standard potential, E_0 , of the chemical species in solution. A schematic diagram of the electrochemical cell is shown in Figure 2.3.

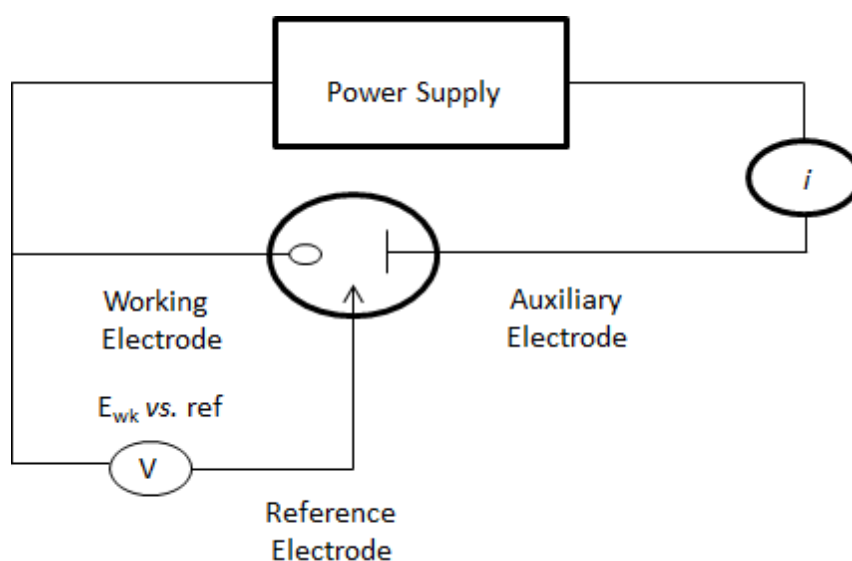


Figure 2.3: Schematic Diagram of the Electrochemical Cell

When considering the overall electrode reaction, defines the conversion of the dissolved oxidized species, O, to a reduced form R, the electrode reaction rate is typically governed by the following:

1. Mass transfer (e.g.: of O from the bulk solution to the electrode surface).

2. Electron transfer at the electrode surface
3. Chemical reactions preceding or following the electron transfer, which might be homogeneous processes or heterogeneous ones on the electrode surface.
4. Other surface reactions, such as adsorption, desorption, or crystallization.

The rate constants for some of these processes (e.g.: electron transfer at the electrode surface or adsorption) are dependent upon the applied potential [177].

2.1.6. Electroanalytical Techniques

As mentioned above, electrochemistry is the study of electron transfer reactions between electrodes and reactant molecules. During the present work, techniques used for the study of these reactions are cyclic voltammetry (CV) and chronoamperometry (CA). There are many experimental set ups that can be used for these measurements but the most commonly used one is the three electrode cell. This involves placing the working electrode, reference electrode and counter electrode in a cell containing solution of the redox system under investigation and an inert background electrolyte. The solution is purged with nitrogen or argon gas to remove dissolved oxygen and the experiment is controlled using a potentiostat and personal computer.

The most important part for conducting voltammetric measurements is called potentiostat. It acts as a potential provider to the electrochemical cell and records the resulting flowing current. The output of a voltammetric scan is called voltammogram, which shows the relationship between the applied potential and the current produced. Typically, a definite potential is applied between the reference and the working electrodes. Since electron transfer occurs at the working electrode, it is of vital importance to ensure that consistent measurements between the electrodes is possible, thus the counter electrode is introduced into the cell. Most fundamental set ups in the electrochemical cell are

designed with an inert gas inlet/outlet. This is required so as to minimize the interference of signals from oxygen during experiments. Nitrogen gas and argon gas are the two most well-known examples of inert gas. Nitrogen is preferred for its low cost, while argon is another option as it is heavier than air. A schematic representation of an electrochemical cell for CV experiments is shown in Figure 2.4.

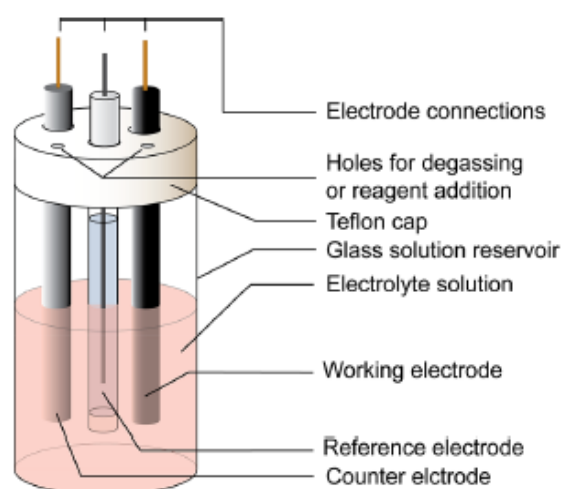


Figure 2.4: Schematic representation of an electrochemical cell for CV experiments.

All potentials are quoted against the Ag/AgCl reference electrode in aqueous solvents. In non aqueous solvents, reference electrodes based on the Ag^+/Ag couple are commonly employed. These consist of a silver wire in a solution containing an Ag^+ salt, typically AgNO_3 . The potential of Ag^+/Ag reference electrode can vary between experiments due to variations in $[\text{Ag}^+]$, electrolyte, or solvent used. So it is important to note the specific details of a non aqueous reference electrode. To circumvent these problems, reduction potentials should be referenced to an internal reference compound with a known E_0' . Ferrocene is commonly included in all measurements as an internal standard, and researchers are encouraged to reference reported potentials vs the ferrocene couple at 0V vs Fc/Fc^+ . Care

should be taken to ensure that the potential window of the analyte's redox processes does not overlap with those of ferrocene and that the analyte does not interact with ferrocene. Since non aqueous reference electrode potentials tend to drift over the course of an experiment, it is recommended having ferrocene present in all measurements rather than adding it at the end of a measurement set.

2.1.6.1. Cyclic Voltammetry (CV)

Cyclic voltammetry (CV) is probably the most widely used technique for studying the electrode processes of all other electrochemical methods. It offers rapid determination of redox potentials of the electroactive species of interest and convenient evaluation of the effect of the medium on the redox process. It is rarely used for quantitative determinations, but is widely used for the study of redox processes, for understanding reaction intermediates, and for obtaining stability of reaction products. CV consists of linearly scanning the potential of stationary working electrode at a particular scan rate in the forward direction (Figure 2.5), and then reversing over the same potential range in the opposite direction.

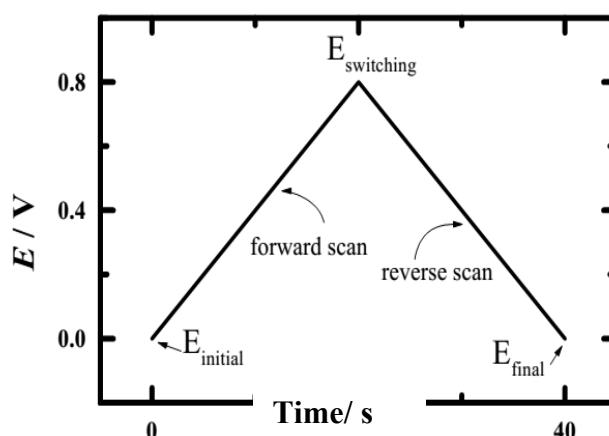


Figure 2.5: Variation of potential with time during a cyclic voltammetry experiment.

For example, the initial scan could be in the negative direction to the switching potential. At that point, the scan would be reversed to run in the positive direction. Depending on the analysis, one full cycle, a partial cycle, or a series of cycles can be performed. The response obtained from a CV can be very simple as shown in Figure 2.6 for the reversible redox system:

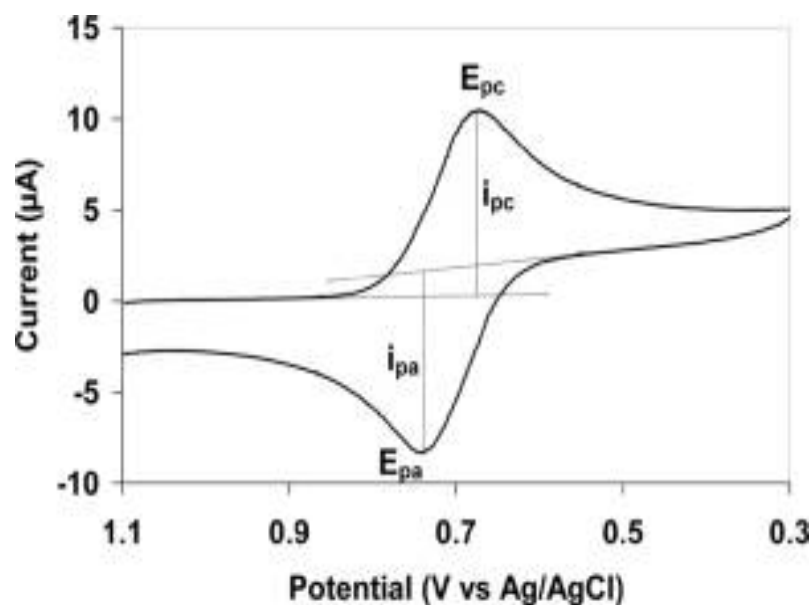


Figure.2.6: Simple reversible cyclic voltammogram

A stationary working electrode in an unstirred solution is employed, and the potential is varied at a definite rate as a linear function of time. Typical sweep rates are in the range of $0.5 - 100 \text{ V s}^{-1}$, and the current potential curves no longer have the S-shape known from techniques with infinitesimally small sweep rates, but exhibit peaks. If a rapid triangular sweep is applied, and an oscilloscope or a fast x-y recorder is used, a cyclic voltammogram is obtained. If, for example, the sweep towards lower potentials produces reduced molecules in the vicinity of the electrode, then they are re-oxidized during the reverse sweep to the same concentration which was initially present in the solution, provided that the rate at which the potential is taken back to its initial value is more rapid

than the diffusion processes needed to establish equilibrium with the bulk of the solution. If the reduced species undergoes irreversible secondary reactions in a shorter period than that of triangular sweep, then new waves may be found in the reverse sweep and the height of the wave corresponding to the forward reaction is reduced.

The peak current i_p in the voltammogram is given by Randles-Sevcik formula

$$i_p = (2.69 \times 10^5) n^{3/2} A D^{1/2} \nu^{1/2} C \quad \dots\dots\dots (2.6)$$

Here i_p is the peak current (in amperes), n is the number of electrons passed per molecule of the analyte oxidized or reduced, A is the electrode area (in cm^2), D is the diffusion coefficient of analyte (cm^2s^{-1}), ν is the potential sweep rate (Vs^{-1}), and C is the concentration of analyte in bulk solution (mol cm^{-3}). The midpoint potential of the two peaks in the voltammogram is given by:

$$E_{mid} = \frac{E_{red} + E_{ox}}{2} \quad \dots\dots\dots (2.7)$$

Here, E_{red} is the reduction potential and E_{ox} is the oxidation potential. The maximum potential E_p in the current-potential curve in the linear scan voltammetric experiment for a reversible electron transfer is given by (where n is number of electron per molecule)

$$E_p = E_{1/2} - \frac{28.5}{n} \quad \text{mV at } 25^\circ\text{C} \quad \dots\dots\dots (2.8)$$

Finally, the separation between the two peaks of the voltammogram is given by

$$\Delta E_p = E_{ox} - E_{red} = 2.303 RTnF = 59 \text{ mV}/n \text{ at } 25^\circ\text{C} \quad \dots\dots\dots (2.9)$$

Hence, depending on what is already known about a given system, one can determine the concentration, the diffusion coefficient, the number of electrons per molecule of the analyte oxidized or reduced, and the redox potential for the analyte.

On the reverse scan, the position of the re-oxidation peak is not identical with the potential of the forward scan and depends on the switching potential, if the reverse sweep starts at less than 100 mV/n cathodic of the reduction peak. If the switching potential however, is set further apart, the separation of the two peaks will be 59 mV/n and is independent of the scan rate of the potential scan. These two criteria along with the equal height of the steps in the forward and reverse reactions, are commonly taken as diagnostics for reversible, purely diffusion controlled charge transfer. Cyclic voltammetry has been used to obtain potentials which could also have been measured by slow techniques, and at the same time to demonstrate reversibility of the electron transfers.

If the scan rate in cyclic voltammetry is increased to values greater than 0.1 V s⁻¹, then the redox couples do not behave like ideal reversible systems because electron transfer rates are not infinitely large and the current is controlled by a combination of diffusion and charge transfer kinetics. This is called the quasi-reversible case and cycling at varying scan rates can be used to measure electron transfer rates.

Reversible and Irreversible Reactions

The term reversible can be misleading and sometimes can be confusing in chemistry as it has different meanings depending on the context of the reaction. In general, reversibility can be divided into two categories; chemical and electrochemical. In order to explain the term 'reversible' clearly, the following simple reaction is considered.



The reaction scheme shows that the reactant, in the reduced form, is being transformed into a product by means of having "n" number of electrons on the time scale of the voltammetric experiment. From the chemical point of view, this Ox/Red couple can be reproduced chemically as represented by the double-sided arrow. Therefore, the oxidation reaction can then be expressed as:



Meanwhile, the heterogeneous process taking place between a working electrode and an electroactive species at the vicinity of the electrode surface results in electron transfer. In electrochemical experiments, electron transfer can be affected by the potential applied and the concentration of the electroactive species at the electrode. Therefore, the rate constants play very important role in determining the electrochemical reversibility of a reaction. Using the same chemically reversible reaction scheme given above, electrochemical reversibility can be explained in the following way. Suppose that the rate constants for reduction and oxidation are k_{red} and k_{ox} respectively. When the applied potential is equal to E^0 of the redox couple at equilibrium, the standard electrochemical rate constant can be represented as k^0 and will have the units of $cm\ s^{-1}$, derived from the concentration of the electroactive species shown in $mol\ cm^{-3}$ and electron transfer to the electrode surface with surface area in cm^2 . Here rate constant for electron transfer in both the forward and backward directions of the above reaction scheme can be represented as :

$$k_{red} = k^0 \exp\left(\frac{-\alpha_{red}nFE}{RT}\right) \quad \dots\dots\dots (2.12)$$

$$k_{ox} = k_{red} \exp\left(\frac{\alpha_{ox}nFE}{RT}\right) \quad \dots\dots\dots (2.13)$$

Here the rate constants for both the reduction and oxidation processes driven by the potential difference or overpotential, $\eta = E - E^0$, from the applied electrical potential, E , can be shown by

$$k_{red} = k^0 \exp\left(\frac{-\alpha_{red}nF(E - E_0)}{RT}\right) \dots\dots\dots (2.14)$$

$$k_{ox} = k^0 \exp\left(\frac{-\alpha_{ox}nF(E - E_0)}{RT}\right) \dots\dots\dots (2.15)$$

k^0 is the rate constant at the electrode surface at equilibrium, α_{red} is the cathodic transfer coefficient, α_{ox} is the anodic transfer coefficient, and R is the gas constant [8.314 (VC) / (mol K)]. α is defined as the fraction of the interfacial potential at the electrode-solution interface that helps in lowering the activation energy barrier for electron transfer process.

Electrochemical reversibility of reaction can be determined by cyclic voltammetric experiments. This method has proven to be extremely helpful when voltammetric responses are being measured within a wide range of scan rates as it is a common practice to record voltammograms over a wide potential window so as to determine the reversibility of a reaction. In practice, there are three parameters which can be used.

(a) Peak to peak separation (ΔE_p)

In a reversible voltammogram, the magnitude of the peak to peak separation, ΔE_p , shall be approximately 59 mV at room temperature (298 K) for one electron process regardless of scan rate values. On the contrary, in the case of quasi and irreversible conditions, the ΔE_p will depend on the potential sweep rate.

(b) Peak current (I_p)

In both the reversible and the irreversible conditions, the peak current generated is proportional to the square root of the scan rate values. However, for quasi-reversible, scan rate does not hold any effect. At room temperature (at 298 K), simple one electron reduction of O to R can be given as

Reversible,

$$I_p = 0.446FA[O]_{bulk}\sqrt{\frac{FDv}{RT}} \dots\dots\dots (2.16)$$

$$= 2.69 \times 10^5 AD^{1/2}[O]_{bulk}\sqrt{v} \dots\dots\dots (2.17)$$

Irreversible,

$$I_p = 0.49\sqrt{\alpha}FA[O]_{bulk}\sqrt{\frac{FDv}{RT}} \dots\dots\dots (2.18)$$

$$= 2.99 \times 10^5 \alpha D^{1/2}[O]_{bulk}A\sqrt{v} \dots\dots\dots (2.19)$$

For room temperature experiments, following assumptions apply: electrode surface area, $A = 1 \text{ cm}^2$, concentration of species O, $[O] = 10^{-3} \text{ M}$, charge transfer coefficient, $\alpha = \beta = 0.5 \text{ cm s}^{-1}$, diffusion coefficient for species O and R, $D^O = D^R = 10^{-5} \text{ cm}^2 \text{ s}^{-1}$.

c) Wave shape of the forward peak

The difference between the peak current potential, E_p , and half peak current potential, $E_{1/2}$, comes in handy when distinguishing a reversible voltammetric signal from an irreversible one as discussed below. All the values for the parameters used in the equations correspond to those at room temperature (at 298 K). Under reversible condition,

$$E_p - E_{1/2} = 2.218 \frac{RT}{F} \quad \dots\dots\dots (2.20)$$

Whereas, under irreversible reduction

$$E_p - E_{1/2} = 1.857 \frac{RT}{F} \quad \dots\dots\dots (2.21)$$

or

$$E_p - E_{1/2} = \frac{44.7}{\alpha} \text{mV} \quad \dots\dots\dots (2.22)$$

and under irreversible oxidation

$$|E_p - E_{1/2}| = 1.857 \frac{RT}{(1-\alpha)F} \quad \dots\dots\dots (2.23)$$

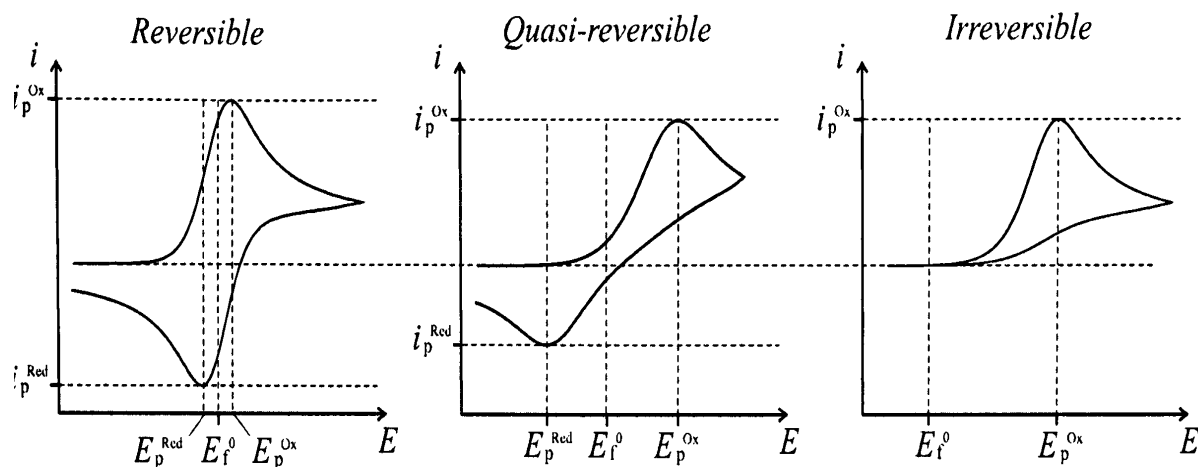


Figure 2.7: A comparison of cyclic voltammetric wave-shapes representing planar diffusion at an electrode

Figure 2.7 shows the cyclic voltammetric wave shapes under reversible, quasi reversible and irreversible conditions.

2.1.6.2 Chronoamperometry (CA)

Chronoamperometry involves applying a fixed potential to a working electrode for a defined period of time. This technique is often used in electrocatalytic applications, where the potential is fixed at a value which will maximise the production of the desired species over an extended period of time while maintaining the activity of the electrode surface. Chronoamperometry is also used in electroanalysis, where it can be used to monitor the presence of a known species by recording the current passed as a function of time.

The Faradaic component of this current for a planar electrode at time t is described by the Cottrell equation: [183]

$$i = \frac{nFAD^{1/2}C_0}{\pi^{1/2}t^{1/2}} \quad \dots\dots\dots (2.24)$$

Chronoamperometry is also used extensively in the electrochemical formation of a variety of materials. This material synthesis aspect is generally performed once the electrochemical behaviour of the working electrode/plating solution interface has been determined through the use of other electrochemical techniques such as cyclic voltammetry. These supporting techniques allow the parameters to be determined for the chronoamperometry. These include the initial potential and the appropriate potential range required for electrodeposition to occur. The deposition time can then be varied in consideration of the initial electrode surface as well as the desired size, shape and coverage of the electrodeposit.

2.2. Materials & Chemicals

2.2.1. Radiotracers

The radiotracers ^{233}U , ^{239}Pu , ^{237}Np tracers were used from laboratory stock solutions and after purification prior to their use by ion-exchange methods as reported earlier [94]. The experiments were carried out with <1% counting statistics errors.

2.2.2. Ionic liquids

Room temperature ionic liquid (RTIL) such as 1-butyl-3-methylimidazolium bis[(trifluoromethyl)sulphonyl] imide ($[\text{C}_4\text{mim}][\text{NTf}_2]$), 1-hexyl-3-methyl-imidazolium bis[(trifluoromethyl)-sulphonyl] imide ($[\text{C}_6\text{mim}][\text{NTf}_2]$) and 1-octyl-3-methyl-imidazolium bis[(trifluoromethyl)sulphonyl] imide ($[\text{C}_8\text{mim}][\text{NTf}_2]$) with purities >99% were procured from Iolitec, Germany and were used as obtained.

2.2.3. Solvents and materials

All other reagents used in this study were of AR grade and were used as received. Betaine hydrochloride and lithium bis(trifluoromethanesulfonylimide) were purchased from Sigma Aldrich. Suprapure nitric acid (Merck, Germany) was used for preparing the aqueous feed solutions.

2.2.4. Extractants

The synthesis of CMPO, NOSCO, DoHyA, Betaine are explained in the respective chapters.

2.3 Characterization techniques

2.3.1 Radiation Detectors

All methods for detection of radiation are based on the interaction of charged particles or electromagnetic radiation with matter. A detection system consists of a detector and a measuring unit. A particular group of detectors are called ionization detectors. These include ionization chambers, proportional counters, Geiger Muller counters and semiconductor detectors. The phenomenon in combination with ionization, which produces luminescence, is involved in scintillation counters.

2.3.2 Alpha Liquid Scintillation Counter

For the distribution ratio measurements, a liquid scintillation counter was used to determine the concentration of the alpha emitting actinides in aqueous and organic solutions offering the following advantages over the other radioactivity assay methods.

- i) Liquid scintillation counting has an efficiency of 100% leading to higher sensitivity.
- ii) Salts and acids normally used in small quantities do not interfere during alpha counting. While using alpha liquid scintillation counting, it should be ascertained that there is no quenching effect while aqueous aliquots are taken into the scintillator solution for counting. The scintillation vial that contains alpha activity was placed in the well of the counter, which was coupled to a single noise low noise photo multiplier tube (EMI 9514) and the associated electronic counting assembly. When alpha particles pass through the scintillator, excited states are produced, which during return to the ground states produce light emission or scintillations. The intensity of light produced is proportional to the incident energy. These light emissions pass through photo multiplier tube and results in current pulses. The resulting charge is proportional to the energy lost by the ionizing particles.

2.3.3 Gamma Counting

The gamma activity of ^{239}Np was determined by a 3" X 3" well-type Sodium iodide – Thallium, NaI (Tl) gamma scintillator detector, coupled to a single channel analyser. The NaI (Tl) scintillation counter detects gamma rays with higher efficiency compared to semiconductor detector. The principle of the counter is same as described above in the case of alpha liquid scintillation counter. Generally crystal scintillations are used here.

2.3.4 Alpha Spectrometry

The alpha spectrum was recorded by a PC-based 8K-MCA and the spectral analyses were carried out using PCA3 software using PIPS alpha detectors (PIPS Canberra PD-300-16-100AM detector having 300 mm² surface area, 100 mm active thickness, 16 KeV FWHM at 5.4 MeV energy of alpha particles emitted by ^{241}Am).

2.3.5 Ultraviolet and Visible (UV-VIS) Spectroscopy

UV-VIS spectroscopy involves the measurement of the absorption of near-ultraviolet and visible light as a function of wavelength for a sample. The visible region of the spectrum comprises of photon energies of 36 to 72 kcal/mole, and the near ultraviolet region extends this energy range to 143 kcal/mole. These energies are sufficient enough to promote outer electrons to higher energy levels. UV-VIS spectroscopy is usually applied to molecules and inorganic ions or complexes in solution. The UV-VIS spectra have broad features that are of limited use for sample identification but are very useful for quantitative measurements. The concentration of an analyte in solution can be determined by measuring the absorbance at a particular wavelength and applying the Beer-Lambert Law:

$$A = \epsilon c l \quad \dots\dots\dots (2.25)$$

(Where A= absorbance, c = sample concentration in moles/litre & l = length of light path through the sample in cm.)

2.3.6 Fourier Transfer Infra-red Spectrometer

The FTIR spectra were obtained on ATR-IR platinum Bruker spectrometer for identifying the functional groups in the bifunctional ligands.

2.3.7 NMR spectrometer

¹H and ¹³C NMR spectra were recorded with a 500 MHz Varian NMR spectrometer, and FIDs were processed using MestReNova v1.13 software multi nuclei solution was used for structure analysis of synthesized ionic liquids and DMSO-d₆ was used as solvents. For bifunctional ligands the ¹H NMR in CDCl₃ for ligands and compounds were recorded on Bruker 300 or 500 MHz spectrometers.

2.3.8 Thermal studies

The thermal stability of ionic liquid was studied using thermogravimetry- differential scanning calorimeter (TG-DSC) model No: DSC-2 and the low temperature phase transition was studied using a differential scanning calorimeter (DSC 823e). Both the instrument was supplied by M/s Mettler Toledo Pvt Ltd, Switzerland. The experiments were carried out at a heating /cooling rate of 5K/min. Reversible run was carried out in DSC, however, only heating run was carried out in TG-DSC.

2.3.9 Luminescence studies

Emission and excitation spectra were recorded on Edinburgh F-900 fluorescence spectrometer in the 200–750 nm regions with a Xe lamp as the excitation source, M-300 monochromators, and a Peltier cooled photomultiplier tube as detector. The acquisition and analysis of the data were carried out by F-900 software supplied by Edinburgh Analytical Instruments, UK. A micro second (Xe) flash lamp with 10–100 Hz frequency range was used as the excitation source. The PL decay time (lifetime) measurements were carried out using time-correlated single-photon counting (TCSPC) technique with the help of a Quantel semiconductor diode LASER with $\lambda_{\text{ex}} = 375$ nm.

2.3.10 Computational Details

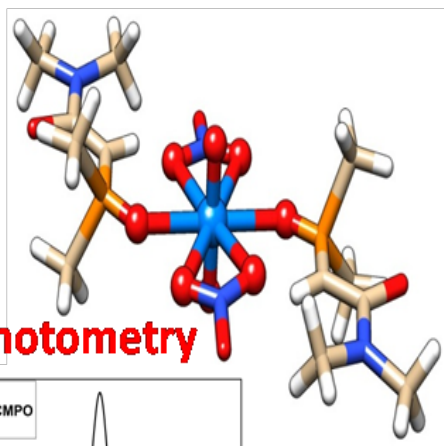
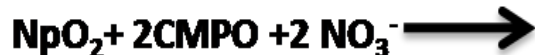
The geometry optimizations and total energy calculations have been performed using the density functional theory (DFT) based electronic structure programs, as implemented in ORCA-4.0[184] programs by employing the GGA based Perdew-Burke-Ernzerhof (PBE) [185] exchange–correlation functional. Initially all the geometries were optimized by PBE functional in conjunction with the def2-TZVP basis set. For plutonium, segmented all-electron relativistically contracted basis sets (SARC-TZVP) has been employed [186]. Scalar relativistic all-electron calculations have been performed with the ZORA Hamiltonian. The resolution of identity approximation has also been applied along with the appropriate auxiliary basis sets. The atomic charge distributions between the plutonium ion and betain IL groups have been calculated by the Mulliken population method, as implemented in the ORCA-4.0 programs.

For Neptunium BP86 functional [187, 188] in conjunction with def-SV (P) basis set for Np and def2-SV (P) basis set for all other atoms was used [189]. The core electrons of Np are treated with def-ECP small core relativistic pseudo potential (60 electrons). All structures

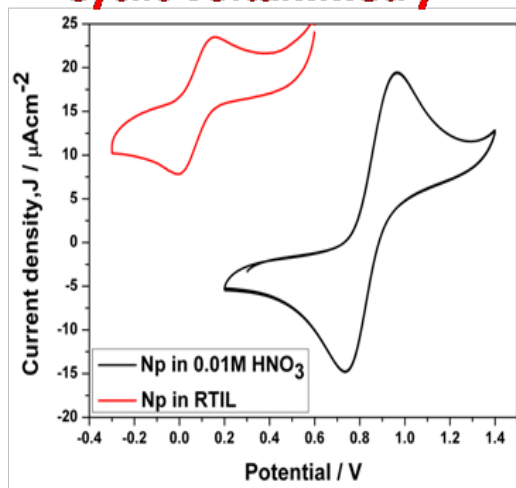
are optimized in gas phase using TURBOMOLE 6.3 [190], and their energies are computed using COSMO continuum solvation model using ORCA 3.0.3 [191]. For the computation of energetics, we have used segmented all electron TZVP basis set (SARC basis set) [192] as implemented in ORCA. Further, scalar relativistic effects are incorporated using ZORA [193].

Chapter 3

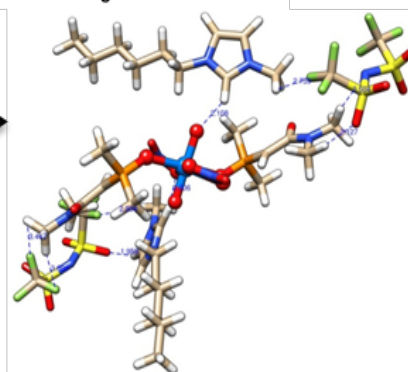
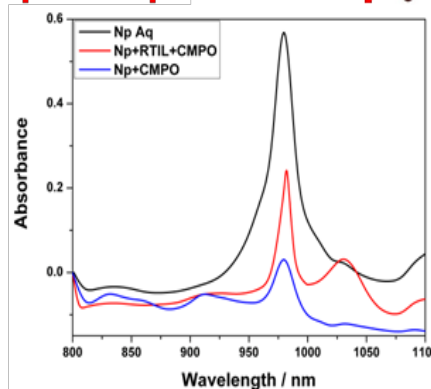
Electrochemical and spectroscopic studies of neptunium in $[C_n \text{mim}][\text{NTf}_2]$ based ionic liquids using CMPO as extractant



Cyclic voltammetry



Spectrophotometry



3.1. Introduction

Neptunium is an important actinide element and its separation from used nuclear fuel is a desirable target, because of the issue of its long-term radiotoxicity and valuable potential application in the production of the Pu-238 radionuclide. Approximately 0.05–0.1% of the mass of SNF contains Np. At present, PUREX process is employed for reprocessing of SNF [194–199]. This method is based on the selective liquid-liquid extraction of uranium and plutonium from other elements in the nitric acid solution of dissolved SNF using 30% tri-n-butylphosphate (TBP) in kerosene. The process starts with the dissolution of spent fuel rods in hot concentrated (8 M) nitric acid. The various nitrogen oxide compounds produced during the dissolution process and the high radiolysis rate in the spent fuel solution result in neptunium existing in several different oxidation states, primarily as Np(V) and Np(VI), possibly as Np(IV). Due to vastly different extractability of its oxidation states, complicating the purification of the uranium and plutonium products, Np can be distributed in both aqueous and organic product streams. Therefore, a better understanding of the kinetic and radiolytic aspects of the redox chemistry of neptunium is needed in order to effectively control the destination of Np. Apart from this; generation of hazardous volatile organic solvent waste is an issue which cannot be ignored in the employed reprocessing methods.

Room temperature ionic liquids (RTIL) have attracted considerable attention as possible replacements for conventional molecular organic solvents in biphasic liquid-liquid extraction systems for the separation of metal ions. The potential advantages of using a water-immiscible ionic liquid (IL) in such separations include exceedingly low volatilities and low flammabilities, the efficient extraction of metal ions that are difficult to extract with molecular organic solvents [79, 80], and the possibility of easily coupling liquid-liquid extraction and electrorefining [82]. In addition, the physico-chemical properties (in particular, polarity, polarizability, and molar volume) of individual ILs can be tuned over wide ranges

by varying the constituent cations or anions. They are known to possess high electrical conductivity and good charge transport properties. Combined with their distinctive solvation ability to a wide variety of inorganic, organic, and organometallic species, ILs have inherent advantages for various electrochemical applications [83- 85, 200].

Arijit et al. have also studied the complexation of Np(IV) with task specific ionic liquid based on CMPO [201]. Although there have been numerous experimental studies on extractabilities of Np by CMPO, many unclear scientific issues still remain. For example (i) how is the extracted Np species behaves in ionic liquids? (ii) what are its transport properties in ILs, (iii) possible speciation of extracted complexes, (iv) what are the photophysical characteristics? and the corresponding kinetic properties. In this context, electrochemical investigations were employed to establish the redox behaviour of Np-CMPO complex in RTIL. There are only limited reports available on the electrochemistry of Np in ILs [202-204].

The [NTf₂] based ionic liquids are less moisture sensitive. Also [C_nmim] [NTf₂] types of ionic liquids have lower viscosity reasonably higher conductivities compared to ionic liquids containing different type of cations and anions [200]. Previously, we have studied the electrochemical aspects of some of the lanthanide ions in this class of ionic liquid [204, 205]. So the present study was carried out employing [C₆mim] [NTf₂]. Furthermore, actinide spectroscopy is not only challenging but recently it has gained renewed interest because of its application in various technological areas [206]. Although lots of reports exists in literature where fluorescence spectroscopy of uranyl compound in solid as well as in solution is discussed [207], however the fluorescence properties of neptunyl ion is not investigated from time resolved fluorescence perspective in detail. Taylor and Hindman [39, 40] have discussed the electronic spectroscopy of neptunyl ions. However, recently some work has been initiated wherein solid and solution state luminescence spectroscopy of neptunyl (VI) has been studied

[41, 42]. In present work the emission and lifetime spectroscopy of Np-CMPO complex in [C₆mim] [NTf₂] ILs are studied in detail.

To gain further insights on the possible speciation of neptunium complexes at the molecular level, the quantum chemical calculations at the density functional theory level is also carried out. Such electronic structure calculations can reveal the possible structural details which were seen in experimental conditions. The speciation of several heavy metal ions such as uranium [208-210], plutonium [211], palladium [212], and platinum ions [213] in different conditions using density function theory (DFT) based calculations is reported from our lab already. The motive of this study is to examine the possible interaction of neptunium in RTIL which are proposed as alternative non-conventional solvents for nuclear waste treatment, due to their potential to reduce the volume of organic solvent waste. Also, generation of basic data is needed for applications of Np which is a strategic element in industries based on nuclear energy while using these new solvents. In view of the paucity of data, electrochemistry, DFT based calculations and photoluminescence spectroscopy were carried out in the present work to understand the complete interactions of NpO₂⁺-CMPO complex in [C₆mim][NTf₂] ionic liquid. The extraction of NpO₂⁺ was carried out from acidic feed solutions using an Octyl-(phenyl)-N, N-diisobutylcarbamoyl methyl phosphine oxide (CMPO) in 1-hexyl-3-methylimidazolium bis (trifluoro-methylsulfonyl) imide ([C₆mim][NTf₂]). The electrochemical and spectroscopic properties of NpO₂⁺-CMPO complex in [C₆mim] [NTf₂] IL were also investigated. Transport properties and kinetics were also studied using cyclic voltammetry and chronoamperometry.

3.2. Experimental

All the chemicals used in this study were of guaranteed reagent grade. 1-hexyl-3-methyl imidazolium bis (trifluoro methyl sulfonyl) imide ([C₆mim] NTf₂) was procured

from Iolitec (99% pure) and was used as received. Octyl(phenyl)-N, N-diisobutylcarbamoyl methyl phosphine oxide (CMPO) was synthesized and purified as reported elsewhere [228]. Cyclic voltammograms and chronoamperograms of the solutions were recorded using CHI 760D electrochemical workstation. All the solutions were prepared in Millipore Milli-Q water ($\sim 18 \text{ M}\Omega \text{ cm}$). NpO_2^+ from 0.1 M nitric acid was transferred to $[\text{C}_6\text{mim}][\text{NTf}_2]$ ILs phase by employing 30% CMPO as an extractant. 30% CMPO in $[\text{C}_6\text{mim}][\text{NTf}_2]$ ILs and 0.1 M aqueous nitric acid containing NpO_2^+ were equilibrated for 30 minutes in a shaker bath. The phase was allowed to settle and the RTIL phase containing NpO_2^+ was taken for voltammetric and spectroscopic studies. ^{237}Np ($t_{1/2} = 2.14 \text{ M yrs}$) is an alpha emitter with three different alpha energies, viz. 4788 KeV (47.6%), 4771 KeV (23.2%) and 4766 KeV (9.3%). The alpha activity of the aqueous phase, before and after solvent extraction, was measured by alpha spectrometry. The alpha source was prepared by drop evaporation method. 10 μL aliquot from the aqueous phase was added on a polished stainless steel planchette, evaporated to dryness under IR lamp and ignited in flame to red-hot. The planchette was placed at a distance of about 4 cm from the PIPS alpha detector in a vacuum chamber and pressure inside the chamber was reduced to -10^{-6} bar. The concentration of NpO_2^+ in $[\text{C}_6\text{mim}][\text{NTf}_2]$ ILs was kept at $\sim 3.7 \text{ mM}$. All voltammetric studies were carried out at room temperature. A glassy carbon disk working electrode (area, $A = 0.07 \text{ cm}^2$) was used as a working electrode. Two Pt wires acted as counter and quasi-reference electrodes. Platinum quasi reference electrode was calibrated with respect to the ferrocene/ ferrocenium redox couple in ionic liquid and E^0 was observed as $= 0.21 \text{ V}$ ($E_{\text{Fc}^+/\text{Fc}} = 0.31 \text{ vs. SCE}$) [177]. The internal standard Fc/Fc^+ was added to $[\text{C}_6\text{mim}][\text{NTf}_2]$ ILs and all the redox potentials are referred against the Fc/Fc^+ redox couple. All solutions were deoxygenated using high purity nitrogen prior to electrochemical experiments. Each measurement was repeated thrice and the average numerical value of each parameter is quoted for discussion (relative error $< \pm 0.1\%$). PL

excitation and emission data of the aqueous as well as the RTIL complexes of NpO_2^+ were recorded. For each spectrum, adequate multiple spectral scans (at least five) were taken so as to get a better S/N ratio. To understand the experimental observations, quantum chemical calculations for a series of neptunium complexes with different equatorial ligands in hexa and penta oxidation states were also carried out. Doublet and triplet spin states of Np are used for VI and V oxidation states respectively.

3.3. Results and Discussions

3.3.1. Extraction of Np by CMPO

Although ^{237}Np has three different alpha energies, a single peak at 4788 KeV was observed in the alpha spectrum since the detector resolution is insufficient to resolve such close energies ($\Delta E < 16 \text{ KeV}$). From the alpha spectra given in Figure 3.1, it is evident that the Np activity left in the aqueous phase after solvent extraction is considerably low. The alpha count rate in 10 μL of the aqueous phase, before and after solvent extraction, was found to be 293 and 8 cpm respectively, which corresponds to about 97% extraction in a single cycle.

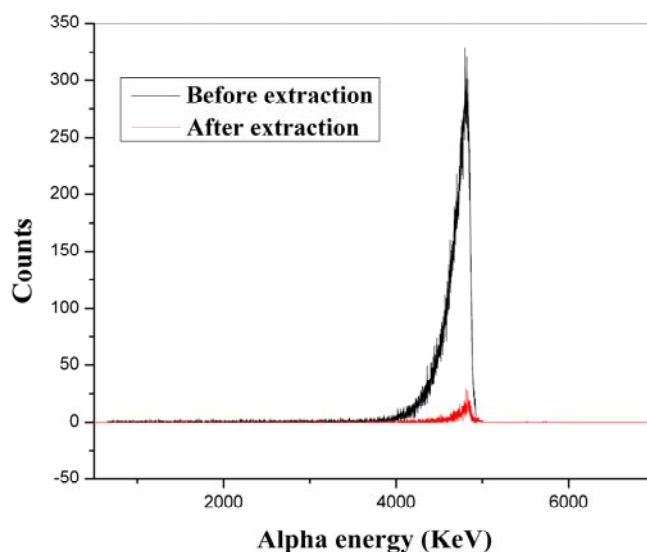


Figure 3.1: Alpha spectra of the Neptunium solutions before and after extraction

3.3.2. Electrochemical Investigations

3.3.2.1. Cyclic Voltammetry

The cyclic voltammogram of $[\text{C}_6\text{mim}][\text{NTf}_2]$ IL recorded at glassy carbon working electrode is shown in inset of Figure 3.2. Reduction of $[\text{C}_6\text{mim}]^+$ cation occurs at a potential of -2.2 V (vs. Fc/Fc^+) and the oxidation of $[\text{NTf}_2]^-$ anion occurs at ~ 1.91 V (vs. Fc/Fc^+). Therefore, the electrochemical window of $[\text{C}_6\text{mim}][\text{NTf}_2]$ IL is ~ 4.1 V, which may be sufficient for permitting the oxidation of $\text{NpO}_2^+/\text{NpO}_2^{2+}$ redox reaction. The cyclic voltammogram of NpO_2^+ in $[\text{C}_6\text{mim}][\text{NTf}_2]$ IL recorded at glassy carbon working electrode at a scan rate of 20 mVs^{-1} is shown in Figure 3.2.

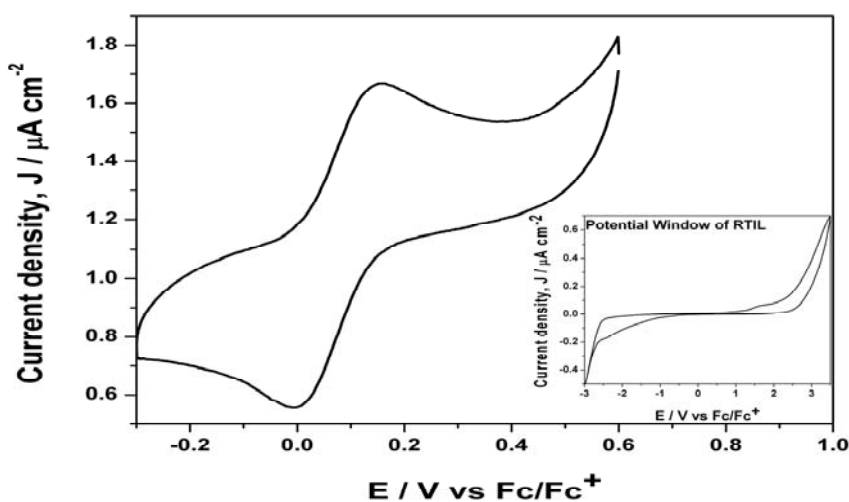


Figure 3.2: Cyclic voltammogram of NpO_2^+ in $[\text{C}_6\text{mim}][\text{NTf}_2]$ ILs recorded at glassy carbon working electrode at a scan rate of 20 mVs^{-1} . Inset shows the cyclic voltammogram of $[\text{C}_6\text{mim}][\text{NTf}_2]$ IL recorded at glassy carbon working electrode.

Cyclic voltammogram of 70% $[\text{C}_6\text{mim}][\text{NTf}_2]$ IL+ 30% CMPO recorded at glassy carbon working electrode at scan rate of 0.1 Vs^{-1} is shown in Figure 3.3. It consists of an anodic wave occurring at a peak potential of 0.15 V which is attributed to the oxidation of NpO_2^+ to NpO_2^{2+} .

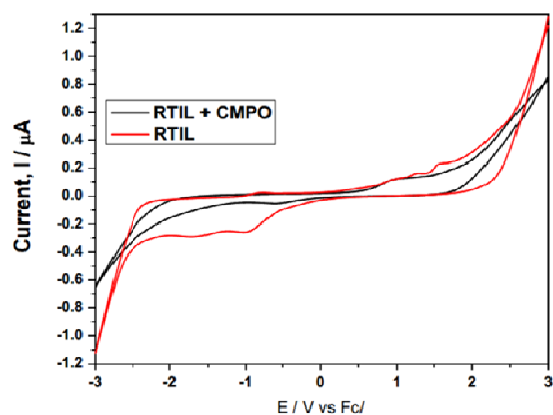


Figure 3.3: Cyclic voltammogram recorded for 70% HmimNTf₂ IL+ 30 % CMPO at glassy carbon working electrode at scan rate of 0.1Vs⁻¹

The voltammogram showing the redox behavior of ferrocene is also shown in Figure 3.4.

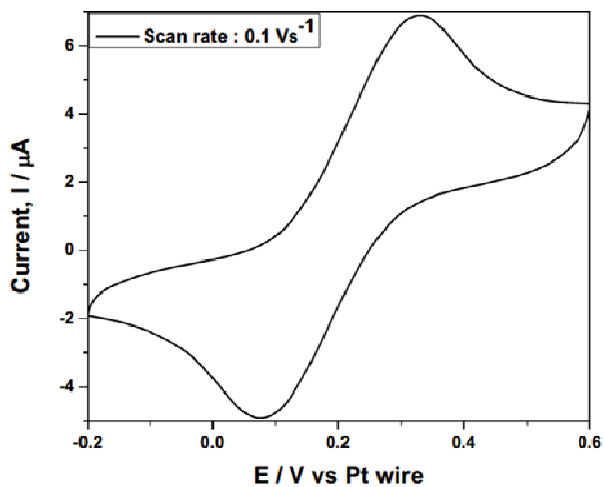


Figure 3.4: Cyclic voltammogram of Fc/Fc⁺ redox couple recorded in C₆mimNTf₂ IL at glassy carbon working electrode at scan rate of 0.1Vs⁻¹

Figure 3.5 shows the cyclic voltammograms of NpO₂⁺ in [C₆mim][NTf₂]ILs recorded at different scan rates at glassy carbon electrode. It is observed that the cathodic and anodic peak current increases with increase in scan rate. The cathodic and the anodic peak potential

(E_{pc} and E_{pa}) shifts cathodically and anodically respectively with increase of scan rate. The value of ΔE_p is quite large (157 mV) than the value expected for a reversible process (60 mV) indicating that NpO₂⁺/ NpO₂²⁺ redox reaction in [C₆mim][NTf₂] IL at glassy carbon electrode is quasi-reversible [177, 214]. It means that this redox reaction is not only controlled by diffusion but also by charge transfer kinetics.

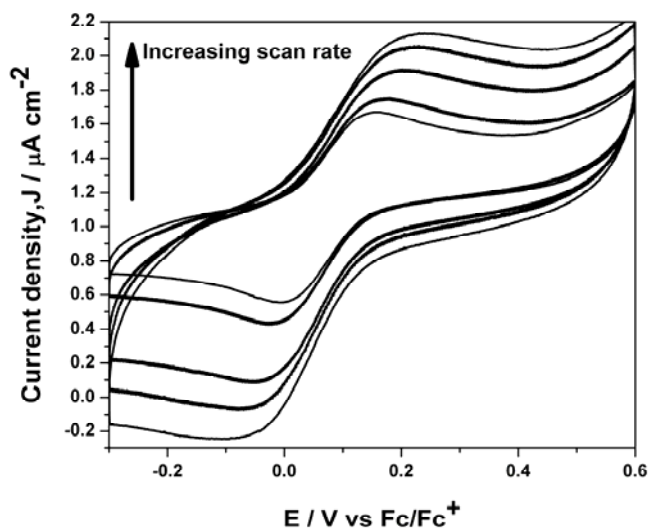


Figure 3.5: Cyclic voltammograms of NpO₂⁺ in C₆mimNTf₂ ILs recorded at different scan rates at glassy carbon electrode

The linear dependence of I_{pc} on square root of scan rate (v^{1/2}), shown in Figure 3.6 confirms the reduction of NpO₂²⁺ to NpO₂⁺ in [C₆mim][NTf₂]IL is diffusion controlled [177]. The cathodic peak current (I_{pc}) and the scan rate for a quasi-reversible reduction reaction for a soluble-soluble couple are related to each other by following expression [177].

$$I_{pc} = 0.496 nFACD^{1/2} \left(\frac{(\alpha n_{\alpha})Fv}{RT} \right)^{1/2} \dots\dots\dots(3.1)$$

where C is the neptunium concentration in mol cm⁻³, D is the diffusion coefficient in cm² s⁻¹, F is the Faraday constant, n is the number of exchanged electrons, v is the scan rate in Vs⁻¹, α is the charge transfer coefficient, n_α is the number of electrons transferred in the rate determining step, A is the geometric area of electrode and T is the absolute temperature in K.

The value of αn_{α} can be determined from following formula, Where, $E_{pc/2}$ is the half-peak potential. The value of αn_{α} is found to be 0.57 for the scan rate of 0.02 Vs^{-1} . By substituting this value in above expression, the diffusion coefficient of NpO_2^+ in $[\text{C}_6\text{mim}][\text{NTf}_2]$ ILs is calculated to be $1.8 \times 10^{-9} \text{ cm}^2 \text{ s}^{-1}$.

$$|E_{pc} - E_{pc/2}| = \frac{1.857RT}{F\alpha n_{\alpha}} \quad \dots\dots\dots(3.2)$$

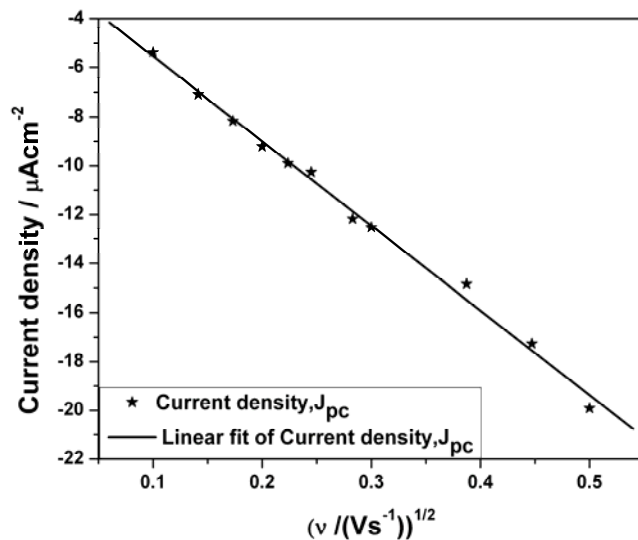


Figure 3.6: The linear dependence of j_{pc} on square root of scan rate ($v^{1/2}$)

The cyclic voltammograms obtained in ionic liquid were much broader with reduced j_{pc} and j_{pa} as compared to the one obtained with aqueous solution as shown in Figure 3.7.

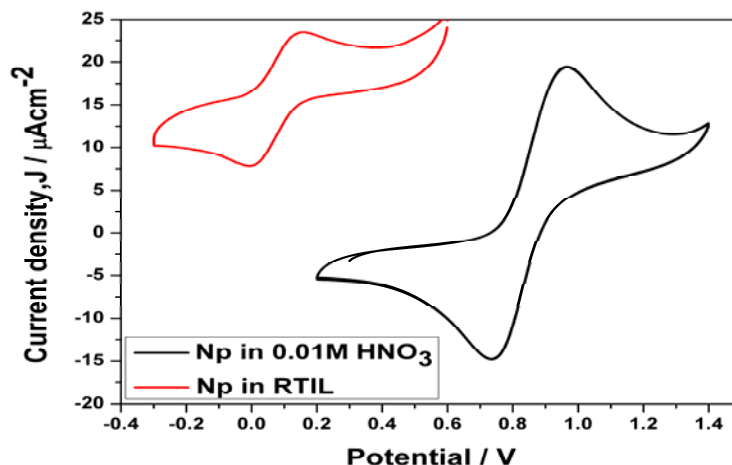


Figure 3.7: Comparison of cyclic voltammograms obtained in ionic liquid versus Fc/Fc^+ and aqueous solution versus Ag/AgCl as reference electrodes

3.3.2.2. Chronoamperometry

The chronoamperogram for the $\text{NpO}_2^+/\text{NpO}_2^{2+}$ redox reaction in $[\text{C}_6\text{mim}][\text{NTf}_2]$ IL at 298K are shown in Figure 3.8. The Cottrell equation given below describes the current density against time for the reduction of electroactive species.

$$j = \frac{nFD^{1/2}}{\pi^{1/2}t^{1/2}} \quad \dots\dots\dots(3.3)$$

The linearity obtained from the plot of j vs. $t^{-1/2}$ (Cottrell plot, Figure 3.8 inset) indicates the validity of simple diffusion controlled reduction and the value of diffusion coefficient can be determined using above equation. Inset of Figure 3.8 shows the Cottrell plots in $[\text{C}_6\text{mim}][\text{NTf}_2]$ IL where, j is the current density at time t , D is the diffusion coefficient, C is the concentration, n is the number of electrons transferred and F is the Faradays constant. The diffusion coefficient of NpO_2^+ was calculated to be $2.23 \times 10^{-9} \text{ cm}^2 \text{ s}^{-1}$ at 298K, which is close to the value obtained by cyclic voltammetry experiments.

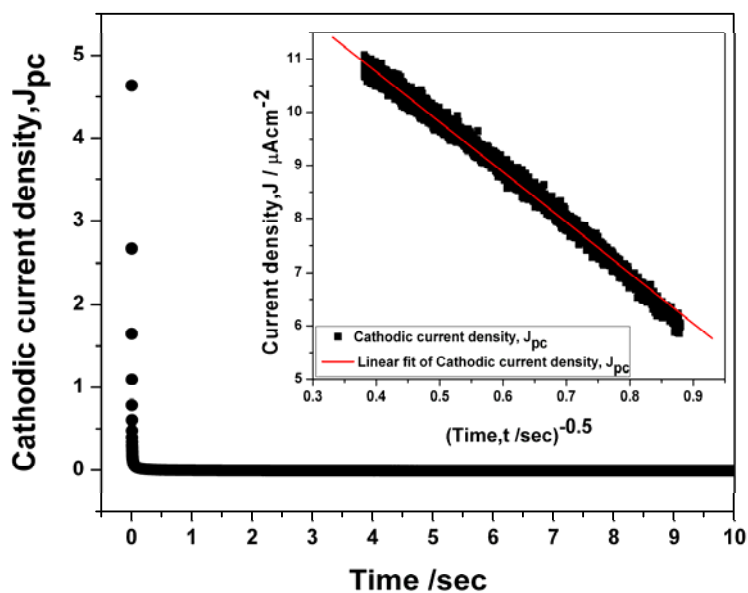


Figure 3.8: Chronoamperograms for the $\text{NpO}_2^+/\text{NpO}_2^{2+}$ redox reaction in $[\text{C}_6\text{mim}][\text{NTf}_2]$ ILs at 298K . Inset shows the Cottrell plot of Np in $[\text{C}_6\text{mim}][\text{NTf}_2]$ ILs

Since $\text{NpO}_2^+/\text{NpO}_2^{2+}$ redox reaction in $[\text{C}_6\text{mim}][\text{NTf}_2]$ IL is quasi-reversible and controlled by diffusion as well as charge transfer kinetics, as discussed above, the rate constant for the charge transfer reaction, k_s (cm s^{-1}), can be determined using following equation [214].

$$k_s = 2.18 \left[D(\alpha n_\alpha) \frac{vF}{RT} \right]^{1/2} \exp \left[\frac{\alpha^2 n F}{RT} (E_{pc} - E_{pa}) \right] \quad \dots\dots\dots (3.4)$$

By putting all the parameters in the above equation, the value of charge transfer rate constants k_s , was found to be $7.71 \times 10^{-6} \text{cm s}^{-1}$ for the scan rate 0.02Vs^{-1} .

3.3.3. UV-Vis Spectroscopy

The absorption spectrum of NpO_2^+ is dominated by a band in the near-IR region with a fairly high intensity at 980.2 nm and a weaker band at 1024 nm, which is attributed to 5f-5f electric dipole transition forbidden by Laporte's rule. The intensity of these transitions

depends on the symmetry of the Np(V) species. The position and intensity of these bands are also affected by the coordination environment of NpO_2^+ and are frequently used to study the complexation behavior of NpO_2^+ . The absorption band of the free $[\text{NpO}_2(\text{H}_2\text{O})_n]^+$ ion at 980.2 nm is usually shifted to longer wavelengths when NpO_2^+ forms complexes with ligands that replace the water molecules in the primary hydration sphere. In the present study, a sharp peak observed at 980 nm corresponding to Np(V) species predominantly present in the solution (Figure 3.9). After the extraction with CMPO the peak at 980 nm is still present but there is an appearance of a broad peak at 1030 nm. The intensity and sharpness of this peak further increase as $[\text{C}_6\text{mim}][\text{NTf}_2]$ IL added into it. UV-Vis absorption spectra of Np in different media are shown in Figure 3.9.

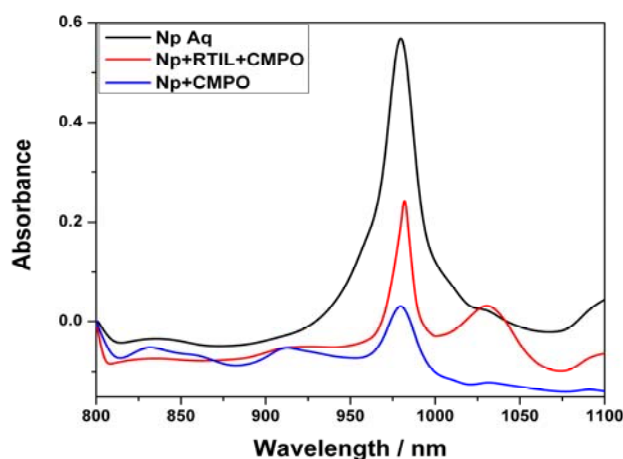


Figure 3.9: UV-Vis Absorption spectra of Np in different media

3.3.4. Time resolved fluorescence spectroscopy:

Np(V) is the most stable oxidation state of neptunium where it mostly exists as the monocationic neptunyl ion (NpO_2^+). This species is iso-electronic to plutonyl (PuO_2^{2+}) having electronic configuration $5f^2$ where the two electrons reside in either one or two of the non bonding molecular orbitals made up of both ‘Np’ and ‘O’ atomic orbitals. The presence

of oxygen atoms in the vicinity decreases the effective charge on 'Np' to +1.9. The ground state electronic configuration thus can be represented by $\delta_u^1\phi_u^1$, δ_u^2 or ϕ_u^2 which leads to the creation of many excited energy states for this ion [215]. In fact, NpO_2^+ is known to have 19 excited states originated from the f^2 configuration. The absorption peaks for this ion occur in the visible to NIR region with the most intense peak observed in between 950-1000 nm. Since both the ground and excited states of this species are similar in parity, the transitions are electric dipole forbidden. The emission from this neptunyl species is known to occur at NIR regions [206]. However, in the visible region, the electronic spectroscopy for this moiety is dominated by the ligand to metal charge transfer bands (LMCT) from either the oxygen or other electron rich ligands. This phenomenon has also been observed in other actinyl (both +5 and +6 oxidation state) ions.

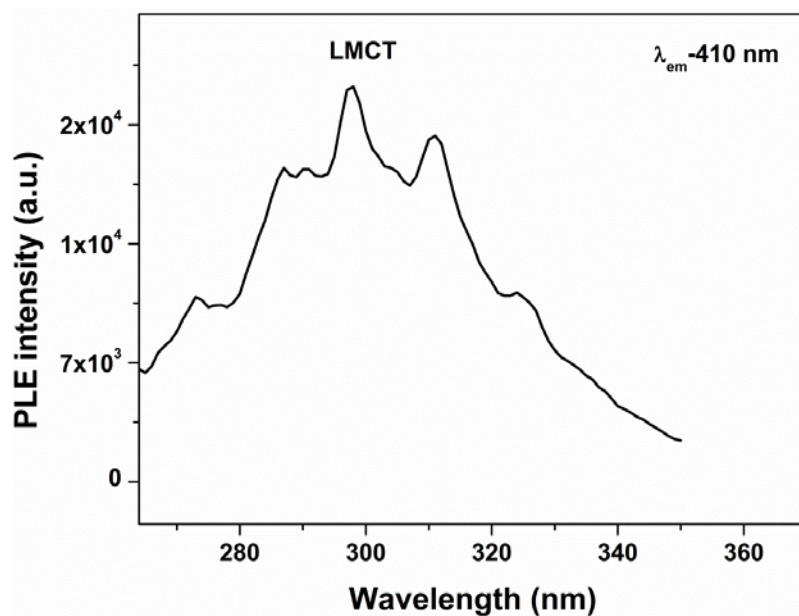


Figure 3.10: Excitation spectrum of Np-CMPO complex aqueous solution

Excitation spectrum of Np-CMPO complex in aqueous solution recorded under emission wavelength of 410 nm is shown in Figure 3.10. The spectrum depicts a broad

excitation band from 280–340 nm peaking at 300 nm. This is attributed to ligand to metal charge transfer from filled 2p orbital of oxygen to empty 5f orbital of neptunium. There is not much change in the excitation pattern on RTIL addition.

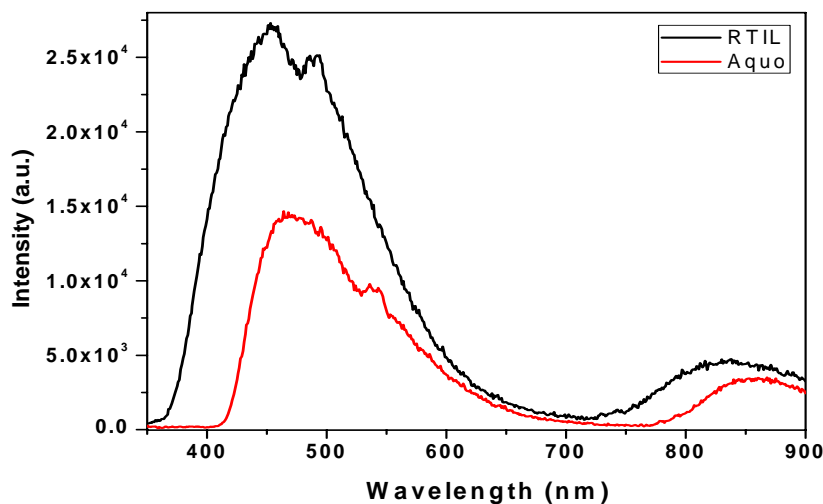


Figure 3.11: Emission spectra of Np-CMPO complex in RTIL as well as in aqueous solution

Figure 3.11 shows the emission spectra of Np-CMPO complex in RTIL (room temperature ionic liquid) and aqueous media with 390 nm excitation from Xenon lamp. Both the spectra are marked by a broad emission band ranging from 430 to 650 and peaking at around 500 nm. This is a characteristic feature arising from LMCT in neptunyl (V). Therefore, it can be revealed from emission spectroscopy that neptunium stabilizes as NpO_2^+ in Np-CMPO complex in RTIL as well as in aqueous solution. The data is similar to that of reported by Bradshaw et al. for the neptunyl (V) ion and its complexes in solution [216].

In addition, a relatively weak band is also seen at ~850 nm in both the samples which is attributed to f-f transition neptunium ion. As compared to the aquo spectrum, the RTIL emission peak is blue shifted by 20-25 nm which can probably be interpreted in two ways: (a) slight change in electronic energy level when Np-CMPO is extracted in RTIL and (b) equatorial bonding/coordination of the metal ion in the basal plane. Further, it may be noted

that the emission spectrum of NP-CMPO in RTIL spectrum is higher in intensity than the corresponding aqua complex. This indicates reduction in the non radiative pathways for the RTIL system as compared to the aqua one. This shows clearly that the hydroxyl group is responsible decreasing the emission intensity of Np-aqua complex, since OH is known fluorescence quencher due to its high oscillation frequency.

To further confirm this observation, time correlated single photon counting (TCSPC) was used to establish the emissive lifetimes of Np-CMPO complex in aqueous solution as well as RTIL media. The decay profile for both the systems followed bi-exponential behaviour (Figure 3.12) and their respective lifetimes values are given in Table 3.1.

Table 3.1: Decay time values for Np-CMPO complex in RTIL as well as in aqueous solution

Sample	τ_1 (in ns)	τ_2 (in ns)	χ^2	τ_{avg} (ns)
Np-Aqua	2.85	0.40	0.962	1.649
Np-RTIL	2.93	0.83	0.965	1.860

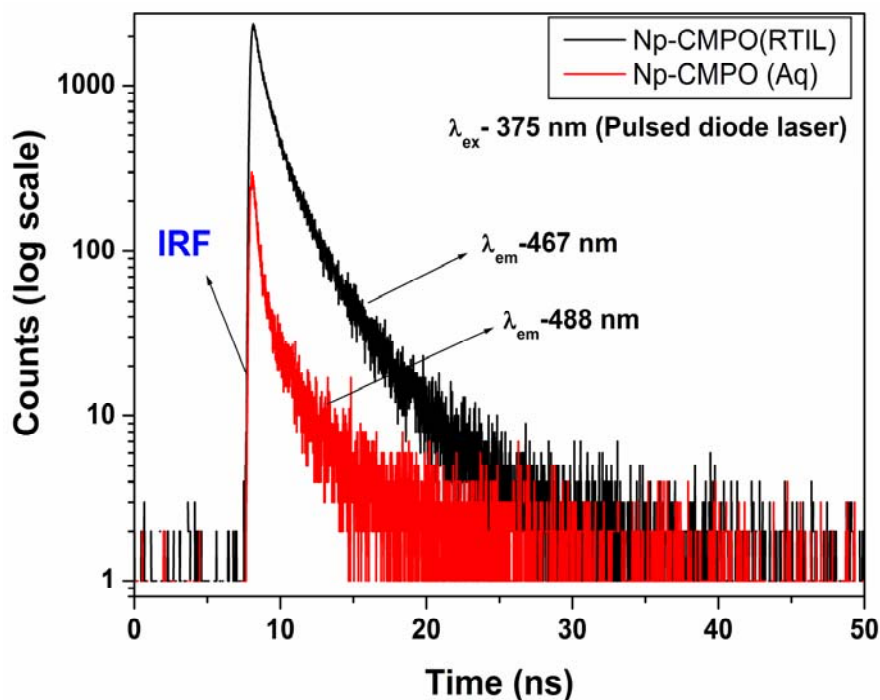


Figure 3.12: Luminescence lifetime of Np-CMPO complex in RTIL as well as in aqueous solution

The raw data obtained from the spectrometer were fitted with an iterative program using the following equation.

$$I(t) = I(t) = A_0 + A_1 \exp(-t/\tau_1) + A_2 \exp(-t/\tau_2) \quad \dots\dots\dots (3.5)$$

The decay time values with best parameters of fitting (χ^2) were taken as the true life time values for the system. All the decay time curves showed bi-exponential fitting which was attributed to the slow exchange of bound and bulk water molecules in the system vis-à-vis the experimental time scales. The decay time values and its bi-exponential nature are in accordance with the reported literature values for neptunyl (V) [206, 216]. It is evident from the decay time data that each component has high lifetime value for Np-CMPO in RTIL compared to that in water. This confirms the presence of lesser non-radiative pathways in the RTIL sample which was also evidenced by the emission data.

3.3.5. Computational Results

Nitrates can coordinate to Np ion in either mono-dentate or bi-dentate fashion. Both binding motifs are considered and found that the binding preferences are very similar, thus the bi-dentate nitrate coordinating motif (Figure 3.13) is chosen for calculation. Further, the optimized structures of Np (VI) and (V) with one and two nitrates reveal that binding is very strong through favourable electrostatic interactions. Further, the binding of nitrates leads to the elongation of axial Np=O bond by 0.015 to 0.025 Å in both oxidation states. In addition to this, the negative charge on the axial oxygens (from 0.55 a.u (for Np-aqua complex) to 0.64 a.u (for Np-(NO₃)₂(H₂O)₂) are also increased. The increased negative lead to the elongation of Np=O as indicative from Mayer bond order analysis.

The optimized several neptunium complexes at the DFT level in V oxidation state is shown in Figure 3. 13.

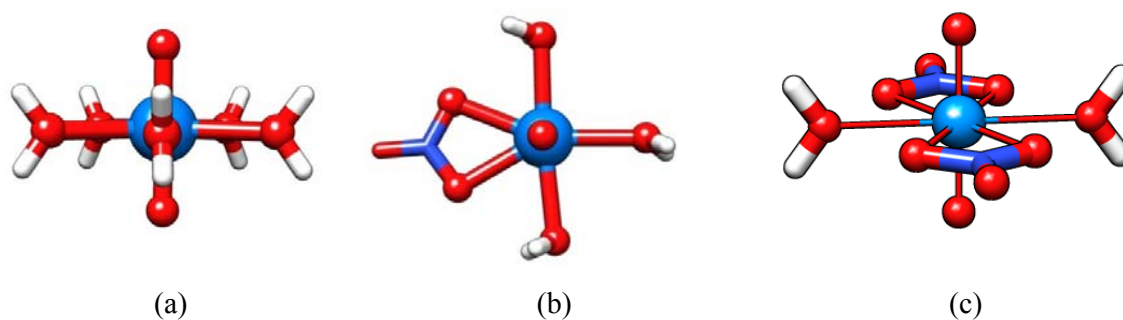


Figure 3.13: Optimized Np(V) complexes with water and nitrates

The optimized structures of penta-aqua neptunium complexes in VI and V oxidation states are in good agreement with earlier reported values of Shamov and Schrechenbach [217] and those of Austin et al. [218]. The computed geometric parameters and the redox potential for the neptunium aqua complex is 1.47 eV which is in reasonable agreement with the experimental value of 1.14 eV [217]. To mimic the experimental conditions; the binding of nitrate, CMPO extractant and the ionic liquid to Np(VI) and Np(V) species are considered. It should be noted that Wang et al. have investigated the structures, possible binding modes and binding free energies of UO_2^{2+} and NpO_2^+ ions in CMPO ligands [219]. For computational ease, the alkyl chain is replaced by methyl group in CMPO ligand. The choice of Np(V) nitrate structures are discussed in Figure 3.13.

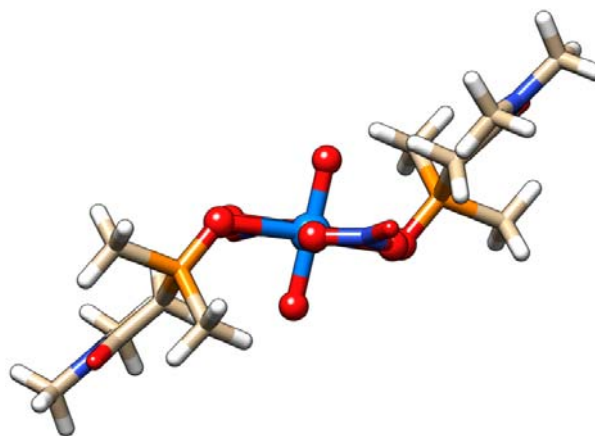


Figure 3.14: Optimized $[\text{Np}(\text{CMPO})_2(\text{NO}_3)_2]^{1-}$

The CMPO ligand can bind to Np in either mono-dentate or bi-dentate coordination motif. It is found that CMPO extractant replaces two water molecules of the Np-nitrate species and binds via oxygen atom of phosphine oxide group (mono-dentate mode) to Np. It is observed that in the presence of two nitrates, the mono-dentate CMPO binding is more favorable as compared to bidentate CMPO binding with two nitrates in mono-dentate motif to Np^{V} by $\sim 10 \text{ kcal mol}^{-1}$, a value close to those reported by Wang et al. [219]. The change in $\text{Np} = \text{O}$ bond lengths in VI and V oxidation states are 1.79 Å and 1.84 Å respectively. This change in bond lengths ($\Delta \text{Np} = \text{O}$) is reduced in the CMPO bound structure (0.04–0.05 Å) as compared to aqueous structure (0.06 Å). Further, the charges on Np in both oxidation states are also very similar. These variations suggest that both geometric and electronic structures are surprisingly similar in both oxidation states which may be responsible for the observed $\text{Np}(\text{VI})$ and $\text{Np}(\text{V})$ species in the experimental ABS spectrum. Further, unlike the studies of Runde and co-workers [220], the ionic liquid cannot directly coordinate to the metal centre. It should be noted that Wipff et al. [221] have carried out MD simulations of UO_2 binding to ionic liquid. Off the several possible binding, it is found that the cationic part of the IL can interact with the axial oxygens of Np strongly and the negative part of the IL interacts with the CMPO methyl hydrogen (Figure. 3.15).

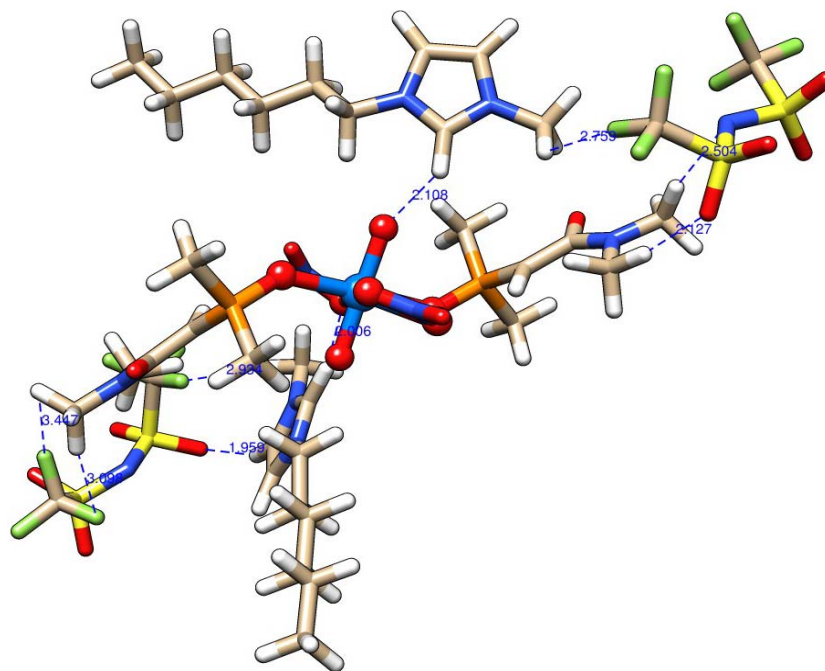


Figure 3.15: Optimized $[\text{Np}(\text{CMPO})_2(\text{NO}_3)_2]^{1-} \cdot (\text{IL})_2$.

Further, due to hydrogen bonding (2.05 Å in VI and 1.84 Å in V), there exist a weakening of Np=O bonds. Nevertheless, the change in axial bond lengths upon oxidation from Np(V) to Np(VI) is even less in the presence of IL (0.04 Å) are very similar. These variations in the geometries lead to multiple signals corresponding to both VI and V oxidation states of Np in the experimental data.

3. 4. Conclusions

A systematic study on redox chemistry, complexation behaviour and optical properties of NpO_2^+ -CMPO complex in aqueous medium and in ionic liquid was carried out using electrochemical measurement, DFT calculations and TRFS studies. This is indeed the only report on where electrochemistry, DFT based calculations and photoluminescence spectroscopy was carried out on to understand the complete interactions of NpO_2^+ -CMPO

complex. The extractability of Np was measured using alpha spectrometry which shows that the Np activity left in the aqueous phase after solvent extraction is considerably low. The cyclic voltammograms obtained in ionic liquid were much broader with reduced cathodic and anodic peak current density compared to the one obtained with aqueous solution. Cyclic voltammetry studies showed that $\text{NpO}_2^+/\text{NpO}_2^{2+}$ redox reaction in ionic liquid is quasireversible. The diffusion coefficient of NpO_2^+ calculated using chronoamperometric study was found to be $2.23 \times 10^{-9} \text{ cm}^2 \text{ s}^{-1}$ at 298 K, which is close to the one obtained by cyclic voltammetry experiments. From cyclic voltammetry studies other kinetic parameter such as charge transfer rate constant were also evaluated. UV-Vis spectrophotometry confirms the stabilization of neptunium ion as Np(V) in Np-Aquo, Np-CMPO as well as in Np-CMPO-RTIL systems. After the extraction with CMPO the characteristic Np (V) absorption band is present with the appearance of a broad peak at 1030 nm. The intensity and sharpness of this particular peak further increased as addition ionic liquid. The complexation behavior of CMPO with Np in aqueous solution as well as in $[\text{C}_6\text{mim}][\text{NTf}_2]$ was studied using density function theory (DFT). Based on these calculations NpO_2^+ forms $[\text{NpO}_2(\text{CMPO})_2(\text{NO}_3)_2]^{1-}$ complexes in aqueous solution whereas $[\text{NpO}_2(\text{CMPO})_2(\text{NO}_3)_2]^{1-} \cdot (\text{IL})_2$ complex in IL. Luminescence spectroscopy also supported the spectrophotometric data and confirms the stabilization of Np as NpO_2^+ in aqueous as well as in ionic liquid. It also brings an important fact into consideration that fluorescence yield of neptunyl ion in aqueous solution is relatively less compared to ionic liquid which is attributed to high frequency oscillation of OH group thereby providing an additional pathway for non-radiative transition. The emission kinetics studies are in complete agreement with emission spectroscopic data. Such complete studies on actinide chemistry and its behavior in ionic liquid provide an exciting and challenging road map not only for actinide researcher but also to those working in the field of nuclear fuel reprocessing.

Chapter 4

Electrochemical studies of actinides in [C_nmim][NTf₂] ionic liquid employing New Bifunctional Ligands

4.1 Introduction

Nuclear energy is trusted to be one of the most feasible options to meet the increasing worldwide demand of energy as the fossil fuel resources are limited [69]. Uranium (U) is one of the actinide elements used as a nuclear fuel in both the research and the power reactors. The uranium resources in India are limited hence the recovery of plutonium from the used nuclear fuel is one of the most important areas of research to be concentrated for the sustainability of nuclear fuel cycle [222]. Plutonium can exist in different oxidation states (III, IV, V, VI, VII). The oxidation and reduction potentials for different oxidation states of plutonium vary significantly with the electronic structure and the properties of the media in which it is studied. Neptunium is also an important actinide element, because of the issue of its long-term radiotoxicity and its valuable potential application in the production of Pu-238 radionuclide, its separation from used nuclear fuel is an attractive target. PUREX process (Plutonium Uranium Reduction EXtraction) is used for the separation of uranium (U) and plutonium (Pu) from the extracted organic medium [72,223, 224]. In PUREX process spent nuclear fuel is first dissolved in concentrated nitric acid which is followed by liquid–liquid extraction. Lot of hazardous chemicals such as concentrated nitric acid, tributyl phosphate, dodecane or kerosene etc. is used in it [225]. Np concentration is 0.05–0.1% of the mass of SNF. During the dissolution process the various nitrogen oxide compounds are produced and the high radiolysis rate in the spent fuel solution result in neptunium existing in several different oxidation states (IV, V, VI). Np can be distributed in both aqueous and organic product streams, due to its vastly different extractability of oxidation states, which complicates the purification of the uranium and plutonium from the product stream.

Despite of the differences in oxidation and reduction chemistry of the actinides, electrochemical techniques have never been applied for considerable nuclear fuel reprocessing. There is a need to develop actinide selective extractants. Researchers have

proposed many ligands with different functional groups for the extraction of actinides from spent fuel [48, 59, 224–230]. The present studies report the extraction and electrochemical behavior of plutonium with a new bifunctional ligand namely (N, N-dialkyl carbamoyl methyl) (2-pyridyl-N-Oxide) sulfide (NOSCO type) [231] in ionic liquid 1-butyl-3-methylimidazolium bis (trifluoromethanesulphonyl) imide ($[\text{C}_4\text{mim}][\text{NTf}_2]$) and N, N-dioctyl, α -hydroxy acetamide (DoHyA) [232] in ionic liquid 1-octyl-3-methylimidazolium bis(trifluoromethanesulphonyl)imide ($[\text{C}_8\text{mim}][\text{NTf}_2]$). Intrinsic characteristics of room temperature ionic liquids (RTILs) like tunable solubilization, high chemical, thermal and radiation stability, negligible vapor pressure have recognized them as novel solvents with exceptional advantages for fundamental research and technological applications [80,233–237]. The use of RTIL for electrochemical investigations and applications has received more attention recently [233-235]. This can be attributed to their unusual solvent properties and beneficial features like suitably large electrochemical window, superior conductivity that evade the need for supporting electrolytes and the interpretable double layer structure of electrode/RTIL interface. These advantageous characteristics of RTILs over the conventional solvents and electrolytes, ensure their use as solvents or supporting electrolytes in electrochemical applications as they are practically easy to work with and theoretically easy to interpret [233, 235–239].

Dialkyl substituted imidazolium cation based ionic liquids are usually air and moisture stable and have been used extensively in the electrochemical investigations [240, 241]. For application in nuclear fuel cycle, the radiolytic stability is a very crucial factor. RTILs, containing imidazolium and pyridinium cation, are fairly stable to radiolytic degradation due to the presence of aromatic rings. For imidazolium cation based ionic liquids, physical properties such as density, surface tension, refractive index, etc. are not considerably affected upon irradiation, but the viscosity is reported to be slightly higher due

to the polymerization of the imidazolium cation [242]. The ligands present in the solvent systems are more stable to radiolysis in the RTIL due to more effective scavenging of the electron by the ionic liquid cation as compared to other molecular solvents [242, 243]. Till now there is still inadequate data for the understanding of the electrochemical activities of actinides in ILs. As part of our multifaceted approach to study the electrochemical, thermodynamic, and kinetic behavior of actinides [204,205,238], the electrochemical studies of plutonium in a new bifunctional ligand (N, N-dialkyl carbamoyl methyl) (2- pyridyl-N-Oxide) sulfide $C_5H_4NOSCH_2CON(C_8H_{17})_2$, (NOSCO) and $[C_4mim][NTf_2]$ ionic liquids (ILs) system was carried out. The redox behaviour of Pu(IV)/Pu(III) couple was investigated in order to find out physical constants and kinetics in this medium. In addition, the electrochemical studies of actinides (U, Pu, Np) in another new bifunctional ligand N, N-dioctyl, α -hydroxy acetamide $(C_8H_{17})_2NCOCH_2OH$ (DoHyA) and $[C_8mim][NTf_2]$ ionic liquids (ILs) system were also carried out.

4.2 Experimental

Pu stock solution was passed through an anion exchange column for the separation of ^{241}Am by employing a method described elsewhere [239]. The valency of Pu was adjusted by adding a few drops of dilute solution of $NaNO_2$ followed by HTTA (2-thenyltrifluoroacetone) extraction from 1 M HNO_3 solution [244]. The HTTA extract contained only Pu(IV) ion, it was subsequently stripped with 8 M HNO_3 to get a fresh aqueous solution of Pu(IV). Pu was assayed radiometrically using a liquid scintillation counting system using commercial dioxane based scintillator cocktail.

Cyclic voltammograms and chronoamperograms of the solutions were recorded using CHI 760D electrochemical workstation. All the solutions were prepared in Millipore Milli-Q water ($\sim 18 M\Omega\text{ cm}$). Glassy carbon disk working electrode (area, $A = 0.07\text{ cm}^2$) was used as

working electrode. Two Pt wires acted as counter and quasi-reference electrodes (vs. ferrocene/ferrocenium $E_0 = 0.31$ V vs. NHE) respectively. The internal standard Fc/Fc^+ was added to ($[\text{C}_4\text{mim}][\text{NTf}_2]$) ILs and all the redox potentials are referred against the Fc/Fc^+ redox couple. All solutions were deoxygenated using high purity nitrogen prior to electrochemical experiments. Each measurement was repeated thrice and the average numerical value of each parameter is quoted for discussion relative error $\pm 0.1\%$).

4.2.1 Synthesis and Characterization of Ligands

(N, N-dialkylcarbamoylmethyl) (2-pyridyl-N-Oxide) sulphide $\text{C}_5\text{H}_4\text{NOSCH}_2\text{CO-N}(\text{C}_8\text{H}_{17})_2$, (NOSCO) and N, N-dioctyl- α -hydroxy acetamide (DoHyA) were synthesized and purified as reported elsewhere [231, 232] and the structure of NOSCO and DoHyA are shown in Figure 4.1 and 4.2.

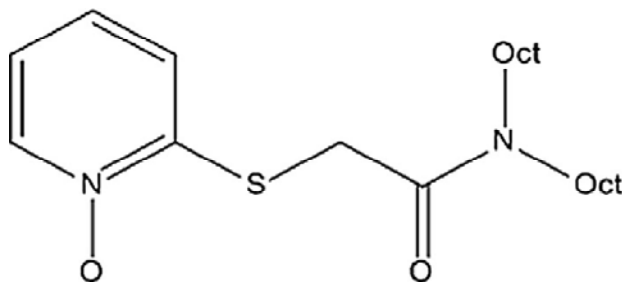


Figure 4.1: Structural formula of (N, N-dioctyl carbamoyl methyl) (2- pyridyl-N-Oxide) sulfide (NOSCO)

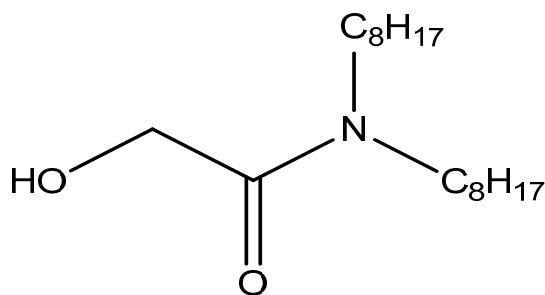


Figure 4.2: Structural formula of N, N-dioctyl- α -hydroxy acetamide (DoHyA)

4.3 Results and discussions

4.3.1 Extraction and Electrochemical investigations of Pu employing N, N-dioctyl carbamoyl methyl (2- pyridyl-N-Oxide) sulfide (NOSCO) in (C₄mim[NTf₂])

4.3.1.1 Extraction Studies

Equal volumes of 0.2 M NOSCO in ([C₄mim][NTf₂]) IL and 3 M HNO₃ containing Pu(IV) were equilibrated for 30 min in a shaker bath. The phase was allowed to settle and the RTIL phase containing Pu(IV) was taken for electrochemical studies. Assay of aqueous phase was analyzed in duplicate by alpha counting using a dioxane based liquid scintillator. The percentage extraction of Pu in organic phase was found to be 84% in single contact. Hence the concentration of Pu which was taken for further studies was 3.1 mM.

4.3.1.2 Effect of Ligand concentration

Distribution studies were performed by using 0.5 mL solution of ligand in ([C₄mim][NTf₂]) (0.005, 0.01, 0.02, 0.05, 0.1, 0.20 M) with the aqueous phase spiked with, ²³⁹Pu tracers and fixed nitric acid concentration as 3 M at 25 ± 0.1 °C. An assay of aqueous phase was done in duplicate by alpha counting using a dioxane based liquid scintillator for ²³⁹Pu. The distribution ratio (D_{Pu}) is calculated as the ratio of the concentration of plutonium in the organic phase to that of the aqueous phase.

Distribution ratios (D_{Pu}) as a function of ligand concentration (Figure 4.3) show clearly that Pu (IV) is extracted significantly from the novel bifunctional ligand. The effect of ligand concentration variation on extraction of metal ions is also important to assess the stoichiometry of ligand in metal complexes.

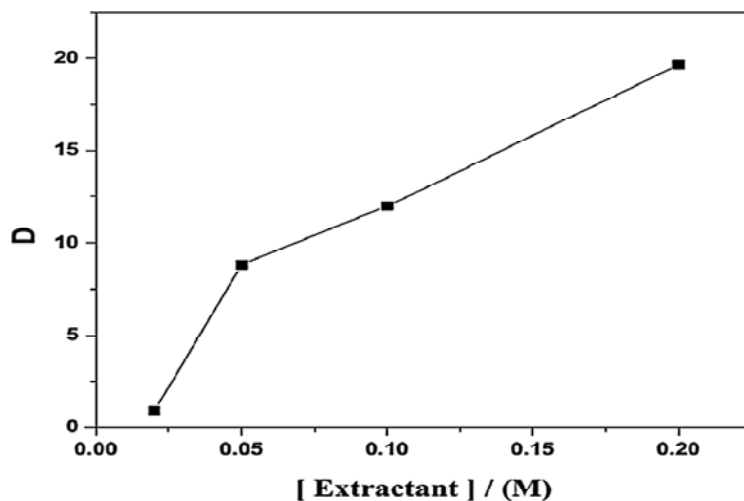


Figure 4.3: Variation of D values with extractant concentration

Distribution ratio (D_{Pu}) values for plutonium were determined at varying concentration (0.005–0.2 M) of ligand at fixed nitrate conc. i.e. 3 M HNO_3 is shown in the Figure 4.4. The log D versus log [Extractant] plot showed a straight line with slope values 1.3 ± 0.09 . It means that predominantly only one ligand is involved per metal ion in extraction process. Pu(IV) from 3M HNO_3 was transferred to ($[C_4mim][NTf_2]$) IL phase by employing 0.2 M NOSCO as extractant.

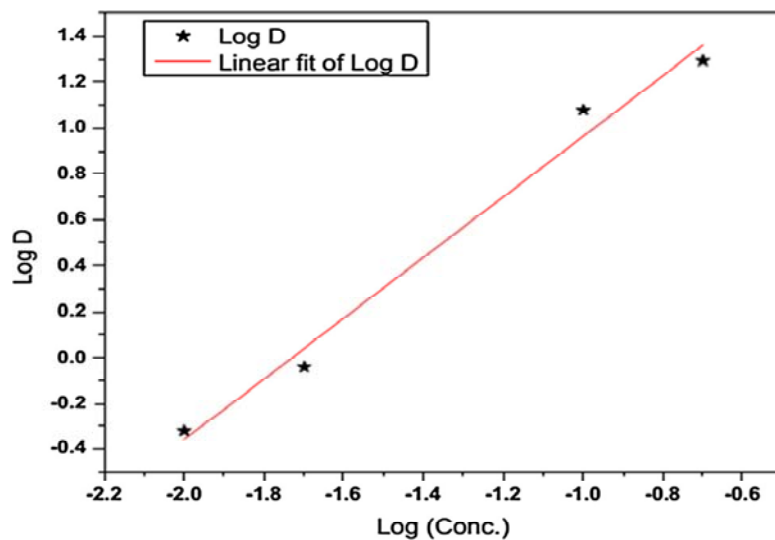


Figure 4.4: Plot of Log log D versus Log of [extractant]

4.3.1.3 Electrochemical Studies

The cyclic voltammogram of ([C₄mim][NTf₂]) IL recorded at glassy carbon working electrode is shown in Figure 4.5. Reduction of [C₄mim]⁺ cation occurs at a potential of ~ -2.0 V (vs. Fc/Fc⁺) and the oxidation of NTf₂⁻ anion starts at 1.3 V (vs. Fc/Fc⁺). Therefore, the electrochemical window of ([C₄mim][NTf₂]) ILs is 3.3 V (vs. Fc/Fc⁺), which may be sufficient for permitting the reduction of Pu(IV) to Pu(III) and vice versa.

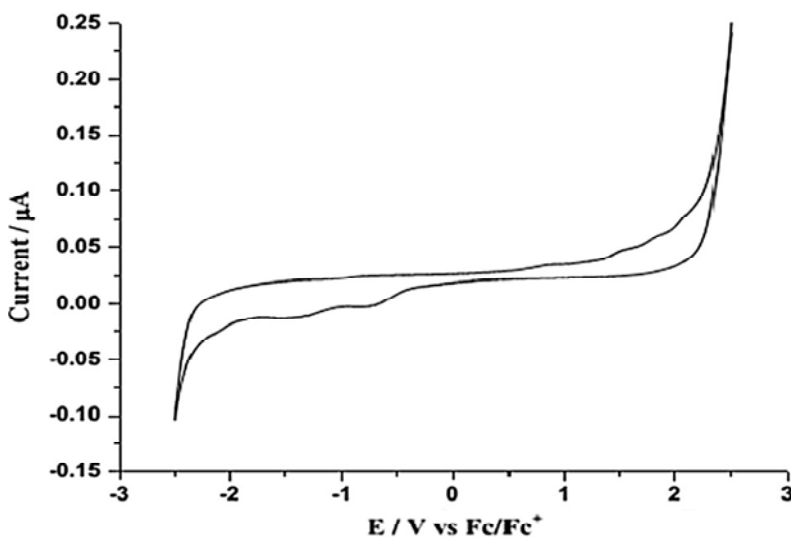


Figure 4.5: Cyclic voltammogram of [C₄mim][NTf₂] at GC electrode at 298 K at a scan rate of 0.1Vs⁻¹

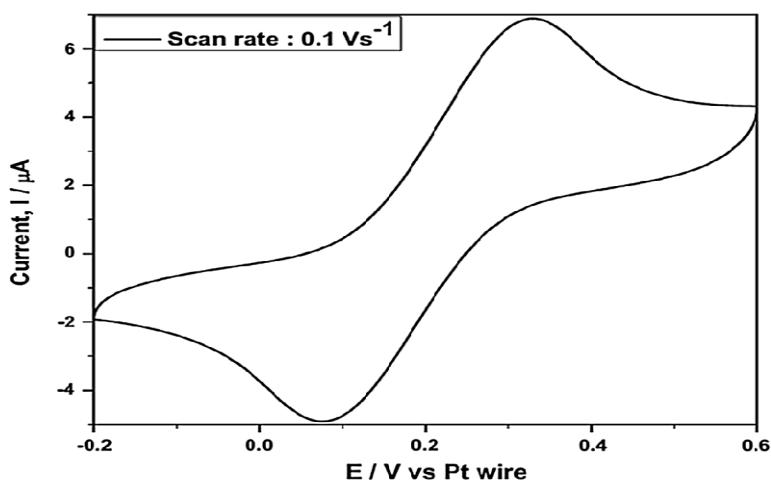


Figure 4.6: Cyclic voltammogram of Fc/Fc⁺ redox couple recorded in [C₄mim][NTf₂] IL at glassy carbon working electrode at scan rate of 0.1Vs⁻¹

The voltammogram showing the redox behavior of ferrocene is given in Figure 4.6. The comparison of the cyclic voltammogram of blank ionic liquid, ionic liquid + ligand and ionic liquid + ligand + Pu are shown in Figure 4.7. It shows two distinctive peaks for Pu(IV)/Pu(III) reduction appears at - 1.02 V and for Pu(III)/Pu(IV) appears at 0.54 V respectively. There is no electroactive species present in this potential range in ionic liquid and mixture of ionic liquid and ligand.

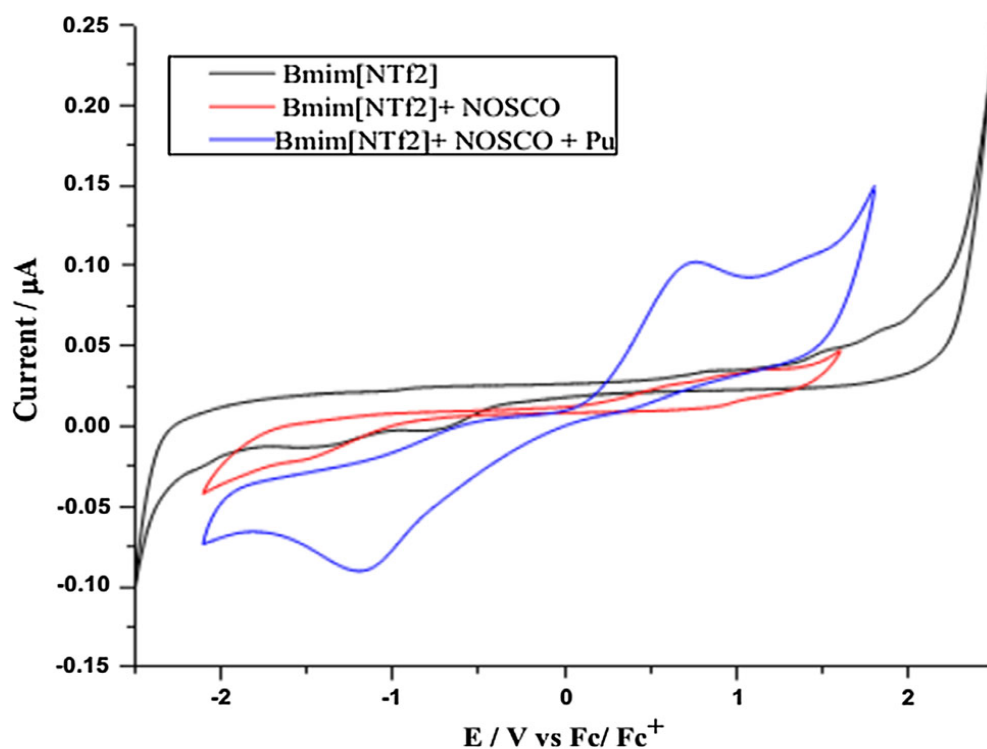


Figure 4.7: Comparison of the cyclic voltammogram of blank $[C_4mim][NTf_2]$, ($[C_4mim][NTf_2] + 0.2$ M NOSCO) and ($[C_4mim][NTf_2] +$ NOSCO + 3.1 mM Pu) solution at a scan rate of 0.02 Vs^{-1} .

The cyclic voltammograms obtained in ionic liquid were much broader with reduced I_{pc} and I_{pa} as compared to the one obtained with aqueous solution as shown in Figure 4.8. A clear shift in the reduction potential of Pu(IV)/Pu(III) system was observed towards positive voltage in 0.1 M HNO_3 solution compared to $[C_4mim][NTf_2]$. This fact suggests that the conversion of Pu(IV) to Pu(III) is more facile in 0.1 M HNO_3 or in other words, Pu(IV) is

more stable in $[C_4mim][NTf_2]$ there by requiring more negative potential for its reduction and hence the shift is more negative in the RTIL.

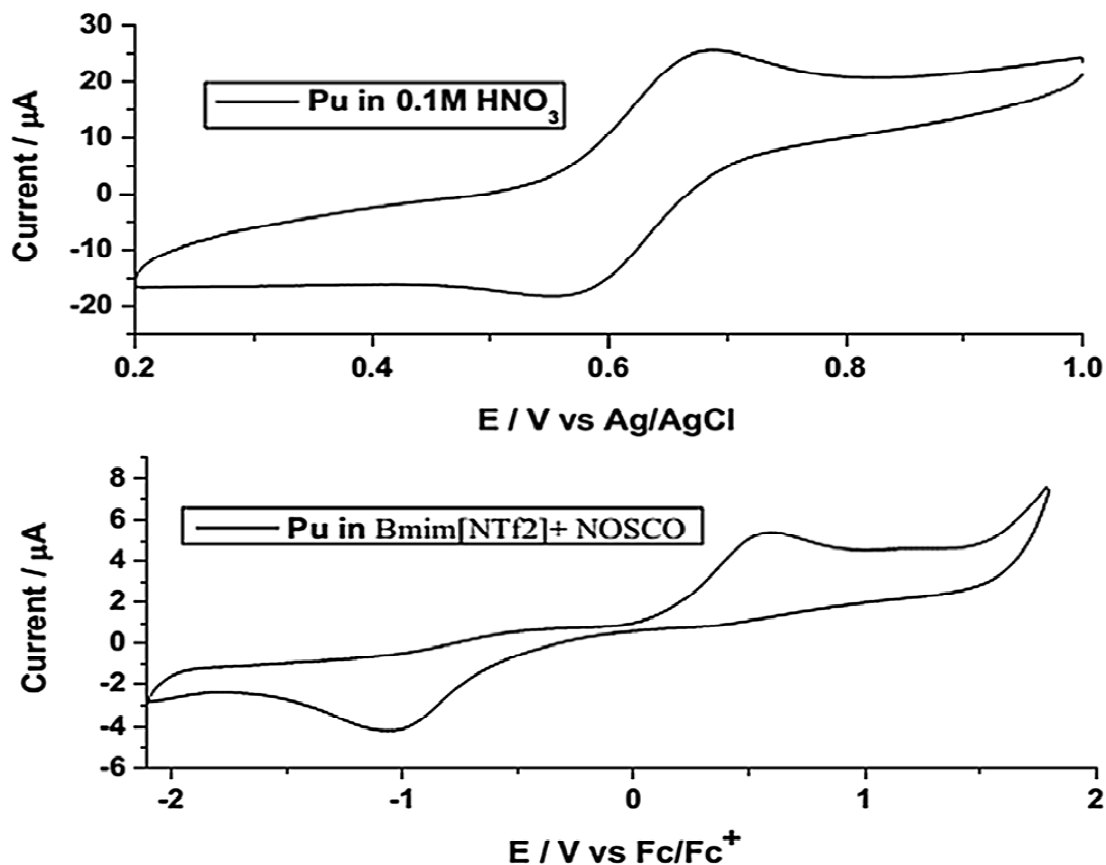


Figure 4.8: Comparison of cyclic voltammograms obtained in ionic liquid and aqueous solution

Figure 4.9 shows the cyclic voltammograms of Pu(IV) in $([C_4mim][NTf_2])$ IL recorded at different scan rates at glassy carbon electrode. It is observed that the cathodic peak current (I_{pc}) increases and the cathodic peak potential (E_{pc}) shifts cathodically with increase of scan rate. The value of peak potential difference ΔE_p ($\Delta E_p = E_{pc} - E_{pa}$) is quite large (480 mV) in comparison to the value expected for a reversible process (60 mV) indicating that the reduction of Pu(IV) to Pu(III) in $(C_4mim[NTf_2])$ IL at glassy carbon electrode is quasi reversible [29, 177].

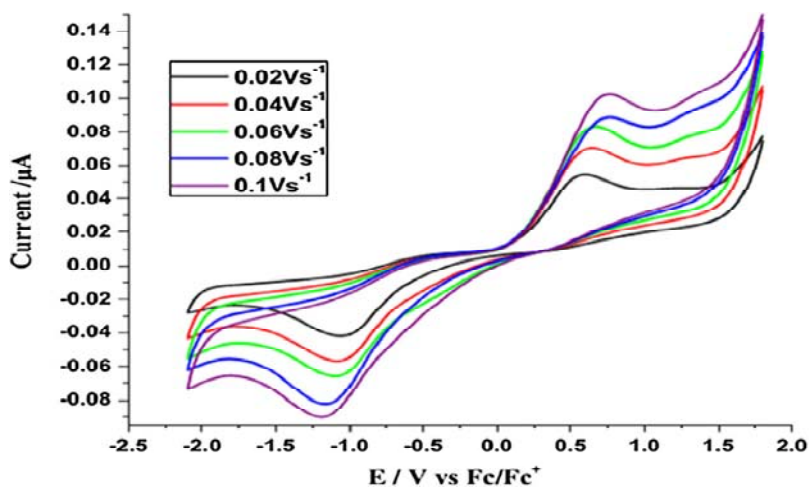


Figure 4.9: Cyclic voltammograms of Pu(IV) in ($[C_4mim][NTf_2]$ + 0.2 M NOSCO) recorded at different scan rates at glassy carbon electrode

The linear dependence of I_{pc} with square root of scan rate ($v^{1/2}$), shown in Figure 4.10 confirms the reduction of Pu(IV) in ($[C_4mim][NTf_2]$ + NOSCO) is diffusion controlled.

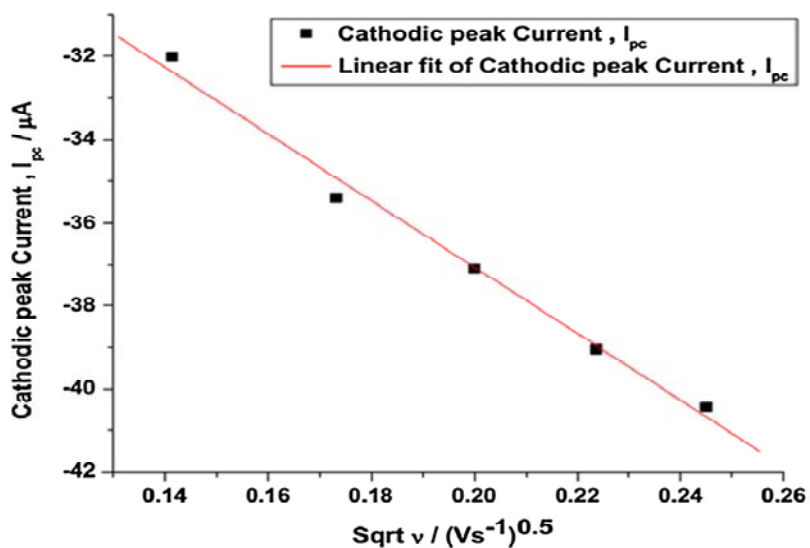


Figure 4. 10: The linear dependence of I_{pc} on square root of scan rate ($v^{1/2}$)

The cathodic peak current (I_{pc}) and the scan rate for a quasi reversible reduction reaction for a soluble–soluble couple are related to each other by following equation [177].

$$I_{pc} = 0.496 nFACD^{1/2} \left(\frac{(\alpha n_{\alpha})Fv}{RT} \right)^{1/2} \dots\dots\dots (4.1)$$

where A is the electrode area in cm², C is the plutonium concentration in mol cm⁻³, D is the diffusion coefficient in cm² s⁻¹, F is the Faraday constant, n is the number of exchanged electrons, m is the scan rate in Vs⁻¹, α is the charge transfer coefficient, n_α is the number of electrons transferred in the rate determining step and T is the absolute temperature in K. The value of αn_α can be determined from the following expression, where E_{p/2} c is the half-peak potential. The average value of αn_α was found to be 0.17. By substituting this value in above expression, the diffusion coefficient of Pu(IV) in ([C₄mim][NTf₂] + NOSCO) was calculated to be 9.38 × 10⁻⁶ cm² s⁻¹.

$$|E_{pc} - E_{pc/2}| = \frac{1.857RT}{F\alpha n_{\alpha}} \dots\dots\dots (4.2)$$

Table 4.1: Electrochemical parameters of the cyclic voltammograms of Pu solution in 0.1M HNO₃ and ([C₄mim][NTf₂]+ NOSCO) system on glassy carbon electrode at different scan rates

Medium	Scan rate(Vs ⁻¹)	E _{pc} (V)	E _{pa} (V)	E _{pc} -E _{pc/2} (V)	αn _α	D (cm ² /s)	k _s (cm/s)
0.1 M HNO ₃	0.02	0.552	0.684	0.09	0.5297	8.37×10 ⁻⁵	3.68 × 10 ⁻³
	0.03	0.553	0.685	0.09	0.5297	8.37×10 ⁻⁵	
	0.04	0.555	0.685	0.087	0.5480	8.09×10 ⁻⁵	
	0.05	0.554	0.686	0.087	0.5480	8.09×10 ⁻⁵	
	0.06	0.555	0.69	0.089	0.5357	8.28×10 ⁻⁵	
C ₄ mim[NTf ₂]	0.02	-1.029	0.542	0.268	0.1779	8.92×10 ⁻⁶	3.58 × 10 ⁻⁴
	0.03	-1.044	0.566	0.275	0.1734	9.15×10 ⁻⁶	
	0.04	-1.05	0.586	0.288	0.1655	9.58×10 ⁻⁶	
	0.05	-1.059	0.597	0.270	0.1766	8.98×10 ⁻⁶	
	0.06	-1.065	0.609	0.308	0.1548	1.02×10 ⁻⁵	

The cyclic voltammograms obtained in ionic liquid were much broader with reduced I_{pc} and I_{pa} in comparison to the one obtained with aqueous solution. Since the reduction of Pu(IV)/Pu(III) in ([C₄mim][NTf₂] + NOSCO) is quasi reversible and controlled by diffusion the rate constant for the charge transfer reaction, k_s (cm s⁻¹), can be determined using following equation [218].

$$k_s = 2.18 \left[D(\alpha n_\alpha) \frac{\nu F}{RT} \right]^{1/2} \exp \left[\frac{\alpha^2 n F}{RT} (E_{pc} - E_{pa}) \right] \quad \dots\dots\dots (4.3)$$

By putting all the parameters in the above equation, the value of charge transfer rate constants k_s , was found to be 3.5×10^{-4} cm s⁻¹, indicating that the reduction of Pu(IV) to Pu(III) in ([C₄mim][NTf₂] + NOSCO) is quasi reversible. According to the value of k_s , the electrode reaction can be summarized to be reversible when $k_s \geq 0.3 \nu^{1/2}$ cm s⁻¹, quasi-reversible when $0.3 \nu^{1/2} \geq k_s \geq 2 \times 10^{-5} \nu^{1/2} \geq$ cm s⁻¹ and irreversible when $k_s \leq 2 \times 10^{-5} \nu^{1/2}$ cm s⁻¹. A quasi reversible electrode reaction of Pu(IV)/ Pu(III) and vice versa is confirmed by the value of k_s obtained from the experimental data. Table 4.1 shows the electrochemical parameters of the cyclic voltammograms of Pu solution in 0.1 M HNO₃ and ([C₄mim][NTf₂] + NOSCO) system on glassy carbon electrode at different scan rates. It clearly suggests that the kinetics is sluggish in case of ([C₄mim][NTf₂] + NOSCO) which is attributed to the retardation of the electron transfer rate at electrode–electrolyte interface due to high viscosity of the system.

4.3.2 Extraction and Electrochemical investigations of U, Pu and Np employing N, N-dioctyl- α -hydroxy acetamide in (C₈mim[NTf₂])

Equal volumes of 0.2 M DoHyA in ([C₈mim][NTf₂]) IL and 3M HNO₃ containing U(VI), Pu(IV) and Np(V) were equilibrated for 30 min in a shaker bath. The phase was allowed to settle and the RTIL phase containing U(VI), Pu(IV) and Np(V) were taken for electrochemical studies. After equilibration, the phases were allowed to settle and the aliquots were drawn from the ionic liquid and aqueous phases. The radioactivity of ²³⁹Pu and ²³³U present in the ionic liquid and aqueous phases were measured by liquid scintillation counting. All the assays of aqueous phase were analyzed in duplicates by alpha counting using a dioxane based liquid scintillator. The radioactivity of ²³⁹Np was measured using alpha spectrometer before and after extraction which is shown in Figure 4.11. The distribution ratio (D_{An}) of actinides in ionic liquid phase was determined using following expression.

$$D_{An} = [D_{An}]_{org} / [D_{An}]_{aq} \quad \dots\dots\dots (4.4)$$

where An = U(VI) or Pu(IV) or Np(V) and % extraction is calculated by using following equation.

$$\% \text{ Extraction} = [D_{An} / (D_{An} + 1)] \times 100 \quad \dots\dots\dots (4.5)$$

The percentage extraction of U(VI), Pu(IV) and Np(V) in organic phase is tabulated in Table 4.2 with single contact. Hence the concentrations of U, Pu and Np which were taken for further studies accordingly.

Table 4.2: Distribution ratios and % of Extraction for U(VI), Pu(IV) and Np(V)

Element	Initial Concentration in aqueous phase mM	Final Concentration in organic phase mM	Distribution Ratio	% Extraction
U(VI)	10	9.7	32	96.97
Pu(IV)	4	3.99	399	99.98
Np(V)	12.14	8.5	2.3	70

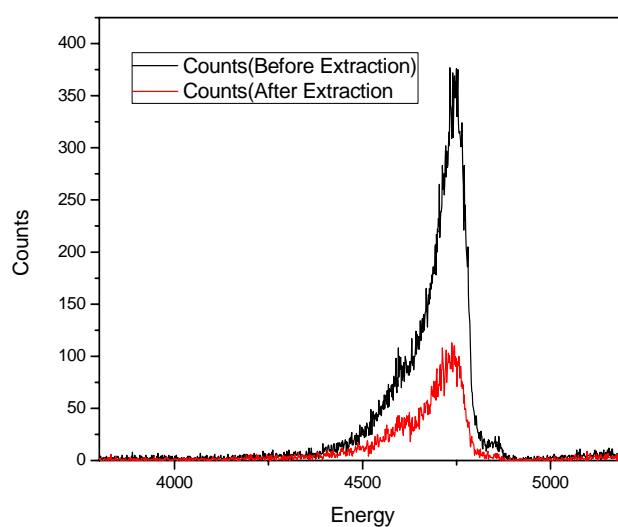


Figure 4.11: Alpha spectra of the Neptunium solutions before and after extraction

4.3.2.1 Electrochemical Studies of Uranium

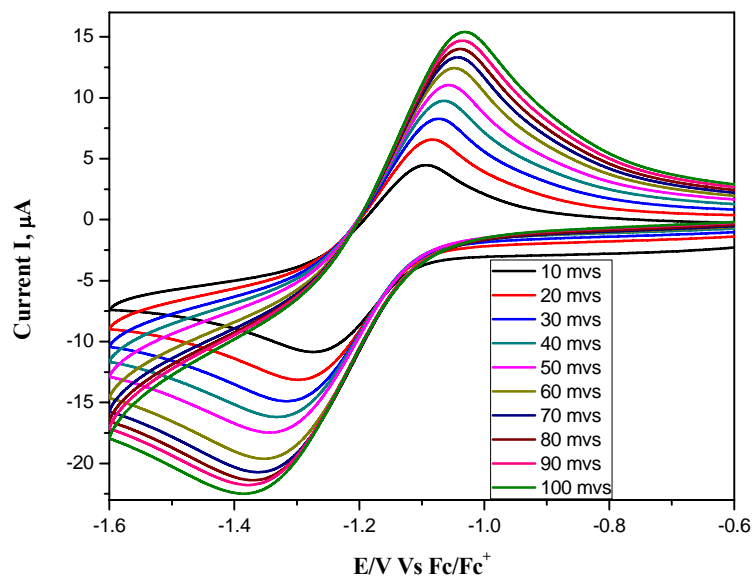


Figure 4.12: Cyclic voltammograms of 9.7 mM U(VI) in ($[\text{C}_8\text{mim}][\text{NTf}_2]$ + 0.2 M DoHyA) recorded at different scan rates at Pt electrode

Figure 4.12 shows the cyclic voltammograms of U(VI) in ($\text{C}_8\text{mim} [\text{NTf}_2]$) IL recorded at different scan rates at platinum electrode. It is observed that the cathodic peak current (I_{pc}) increases and the cathodic peak potential (E_{pc}) shifts cathodically with increase of scan rate. The value of peak potential difference ΔE_p ($\Delta E_p = E_{pc} - E_{pa}$) is large (176 mV) in comparison to the value expected for a reversible process (60 mV) indicating that the reduction of U(VI) to U(IV) in ($\text{C}_8\text{mim}[\text{NTf}_2]$) IL at platinum electrode is quasi reversible.

Table 4.3 shows the electrochemical parameters of the cyclic voltammograms of U solution in 3M HNO_3 and ($[\text{C}_8\text{mim}][\text{NTf}_2]$ + DoHyA) system on platinum electrode at different scan rates.

Table 4.3: Electrochemical parameters of the cyclic voltammograms of U(VI) solution in ([C₈mim][NTf₂]+ DoHyA) system on platinum electrode at different scan rates

Scan Rate	E _{pc} (V)	E _{pa} (V)	I _{pc}	I _{pa}	E _{pa/2}	E _{pc/2}
0.01	-1.2686	-1.0928	-1.0814E-5	4.4852E-6	-1.189	-1.173
0.02	-1.2903	-1.0817	-1.3135E-5	6.5612E-6	-1.184	-1.181
0.03	-1.311	-1.0748	-1.4923E-5	8.3299E-6	-1.178	-1.189
0.04	-1.3277	-1.0655	-1.6199E-5	9.7838E-6	-1.173	-1.196
0.05	-1.3355	-1.054	-1.7511E-5	1.0988E-5	-1.169	-1.201
0.06	-1.3503	-1.0461	-1.9627E-5	1.2442E-5	-1.166	-1.203
0.07	-1.3604	-1.041	-2.0757E-5	1.3319E-5	-1.164	-1.207
0.08	-1.366	-1.042	-2.1386E-5	1.4022E-5	-1.162	-1.211
0.09	-1.3747	-1.0332	-2.163E-5	1.4737E-5	-1.16	-1.215
0.1	-1.3821	-1.0332	-2.2399E-5	1.5382E-5	-1.158	-1.218

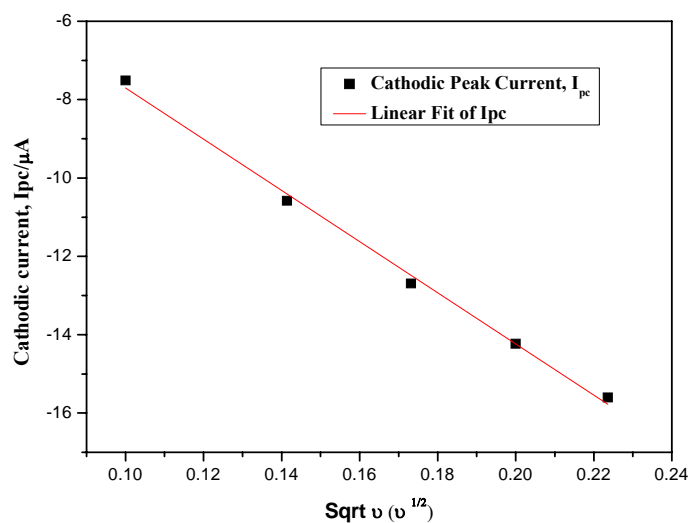


Figure 4.13: The linear dependence of I_{pc} on square root of scan rate (v^{1/2})

The linear dependence of I_{pc} with square root of scan rate (v^{1/2}), shown in Figures 4.13 confirms the reduction of U(VI) to U(IV) in (C₈mim[NTf₂]) IL and ([C₈mim][NTf₂] + DoHyA) are diffusion controlled.

3.2.2. Electrochemical Studies of Plutonium

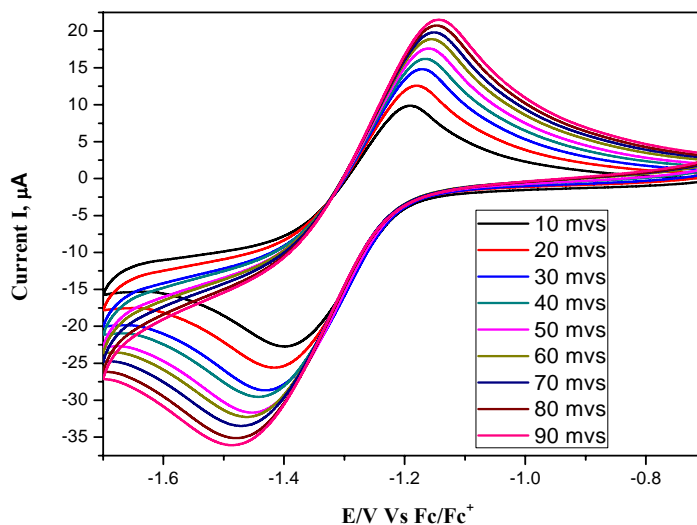


Figure 4.14: Cyclic voltammograms of 3.99mM Pu (IV) in ($[\text{C}_8\text{mim}][\text{NTf}_2]$ + 0.2 M DoHyA) recorded at different scan rates at Pt electrode

Figure 4.14 shows the cyclic voltammograms of Pu(IV) in ($\text{C}_8\text{mim} [\text{NTf}_2]$) IL recorded at different scan rates at platinum electrode. It is observed that the cathodic peak current (I_{pc}) increases and the cathodic peak potential (E_{pc}) shifts cathodically with increase of scan rate. The value of peak potential difference ΔE_p ($\Delta E_p = E_{pc} - E_{pa}$) is large (205 mV) in comparison to the value expected for a reversible process (60 mV) indicating that the reduction of Pu(IV) to Pu(III) in ($\text{C}_8\text{mim}[\text{NTf}_2]$) IL at platinum electrode is quasi reversible.

Table 4.4 shows the electrochemical parameters of the cyclic voltammograms of Pu solution in 3M HNO_3 and ($[\text{C}_8\text{mim}][\text{NTf}_2]$ + DoHyA) system on platinum electrode at different scan rates.

Table 4.4: Electrochemical parameters of the cyclic voltammograms of Pu(IV) solution in ([C₈mim][NTf₂]+ DoHyA) system on platinum electrode at different scan rates

Scan Rate	E _{pc}	E _{pa}	I _{pc}	I _{pa}	E _{pa/2}	E _{pc/2}
0.01	-1.397	-1.1918	-2.2752E-5	9.963E-6	-1.298	-1.268
0.02	-1.4128	-1.1825	-2.5644E-5	1.2661E-5	-1.291	-1.281
0.03	-1.4299	-1.173	-2.8775E-5	1.494E-5	-1.287	-1.29
0.04	-1.4392	-1.1686	-2.9605E-5	1.6153E-5	-1.283	-1.297
0.05	-1.4452	-1.1628	-3.1625E-5	1.7549E-5	-1.277	-1.289
0.06	-1.4589	-1.1562	-3.2285E-5	1.8775E-5	-1.279	-1.309
0.07	-1.469	-1.1496	-3.3605E-5	1.968E-5	-1.276	-1.314
0.08	-1.4732	-1.1469	-3.5246E-5	2.0696E-5	-1.275	-1.319
0.09	-1.4808	-1.1438	-3.5967E-5	2.1555E-5	-1.274	-1.324

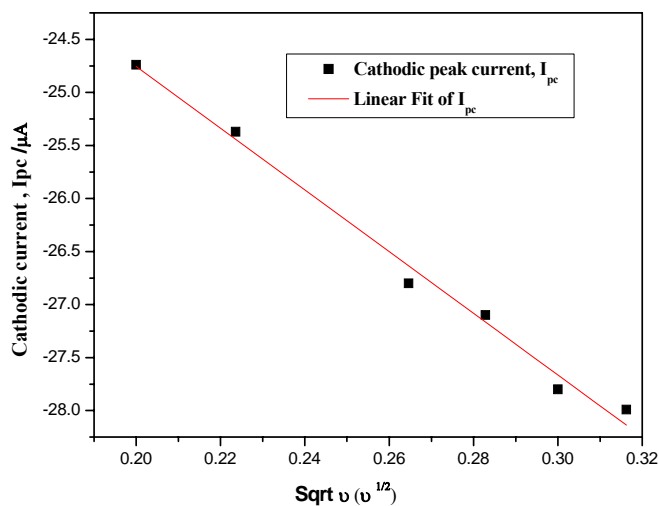


Figure 4.15: The linear dependence of I_{pc} on square root of scan rate (v^{1/2})

The linear dependence of I_{pc} with square root of scan rate (v^{1/2}), shown in Figure 4.15 confirms the reduction of Pu(IV) to Pu(III) in (C₈mim[NTf₂]) ILs in ([C₈mim][NTf₂] + DoHyA) are diffusion controlled.

3.2.3. Electrochemical Studies of Neptunium

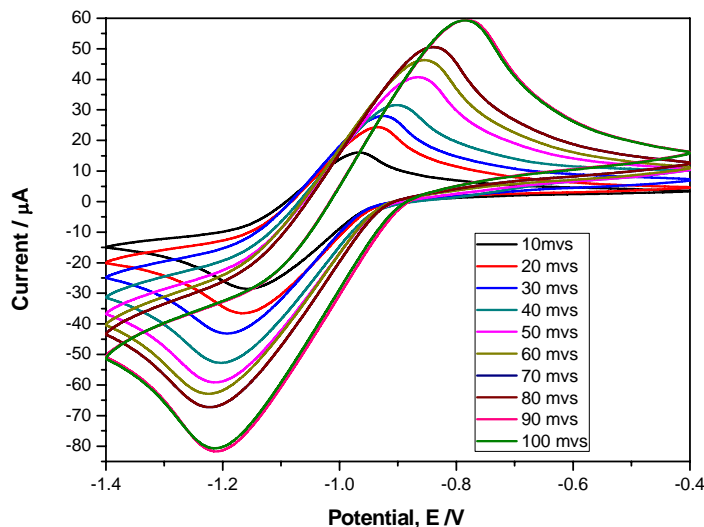


Figure 4.16: Cyclic voltammograms of 12 mM Np (V) in ($[\text{C}_8\text{mim}][\text{NTf}_2]$ + 0.2 M DoHyA) recorded at different scan rates at Pt electrode

Figure 4.16 shows the cyclic voltammograms of Np(V) in ($\text{C}_8\text{mim} [\text{NTf}_2]$) IL recorded at different scan rates at platinum electrode. It is observed that the cathodic peak current (I_{pc}) increases and the cathodic peak potential (E_{pc}) shifts cathodically with increase of scan rate. The value of peak potential difference ΔE_p ($\Delta E_p = E_{pc} - E_{pa}$) is large (194mV) in comparison to the value expected for a reversible process (60 mV) indicating that the reduction of Np(VI) to Np(V) in ($\text{C}_8\text{mim}[\text{NTf}_2]$) IL at platinum electrode is quasi reversible. Table 4.5 depicts the electrochemical parameters of the cyclic voltammograms of Np solution in 3M HNO_3 and ($[\text{C}_8\text{mim}][\text{NTf}_2]$ + DoHyA) system on platinum electrode at different scan rates.

Table 4.5: Electrochemical parameters of the cyclic voltammograms of Np(V) solution in ([C₈mim][NTf₂]+ DoHyA) system on platinum electrode at different scan rates

Scan Rate	E _{pc}	E _{pa}	I _{pc}	I _{pa}	E _{pa/2}	E _{pc/2}
0.01	-1.1576	-0.964	-2.844E-5	1.6073E-5	-1.072	-1.031
0.02	-1.1655	-0.935	-3.6468E-5	2.4406E-5	-1.051	-1.032
0.03	-1.1882	-0.9226	-4.3093E-5	2.8216E-5	-1.054	-1.051
0.04	-1.1996	-0.9026	-5.2919E-5	3.1671E-5	-1.042	-1.049
0.05	-1.2133	-0.867	-5.9413E-5	4.0528E-5	-1.025	-1.048
0.06	-1.2196	-0.8543	-6.2652E-5	4.639E-5	-1.022	-1.051
0.07	-1.218	-0.8425	-6.7161E-5	5.0452E-5	-1.01	-1.046
0.08	-1.218	-0.8388	-6.7365E-5	5.0452E-5	-1.01	-1.046
0.09	-1.2117	-0.7805	-8.1979E-5	5.9158E-5	-0.969	-1.029
0.1	-1.2106	-0.785	-8.0412E-5	5.8845E-5	-0.968	-1.033

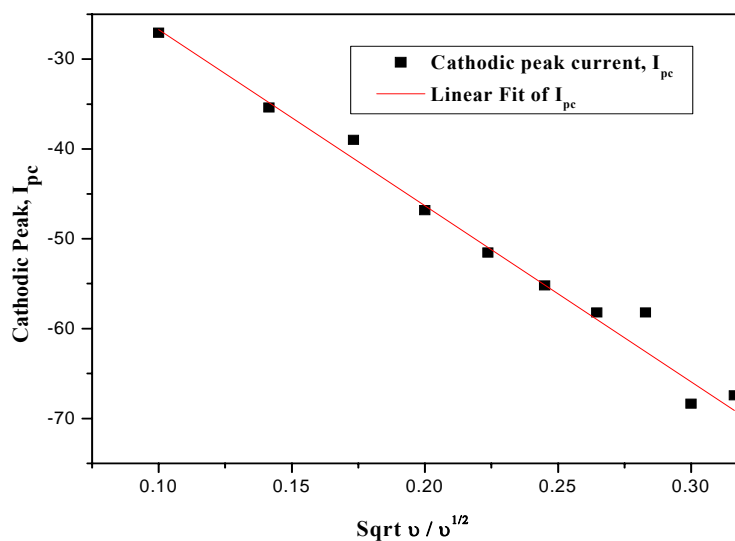


Figure 4.17: The linear dependence of I_{pc} on square root of scan rate (v^{1/2})

The linear dependence of I_{pc} with square root of scan rate (v^{1/2}), shown in Figure 4.17, confirms the reduction of Np(VI) to Np(V) in (C₈mim[NTf₂]) ILs and ([C₈mim][NTf₂] +

DoHyA) is diffusion controlled. The diffusion coefficients of U(VI), Pu(IV) and Np(V) in ([C₈mim][NTf₂]+ DoHyA) were determined and tabulated in Table 4.6. Since the reduction of U(VI), Pu(IV) and Np(VI) in ([C₈mim][NTf₂]+ DoHyA) is quasi reversible and controlled by diffusion, the rate constant for the charge transfer reaction, k_s (cm s⁻¹), was also calculated and given in Table 4.6.

Table 4.6: Electrochemical parameters of the cyclic voltammograms of various actinides in 3M HNO₃ and ([C₈mim][NTf₂]+ DoHyA) system on platinum electrode at different scan rates.

Element	αn_a	D (cm ² /s)	k_s (cm/s)
U	0.4987	2.83×10^{-6}	8.88×10^{-3}
Pu	0.3696	1.00×10^{-4}	2.46×10^{-2}
Np	0.3766	3.38×10^{-5}	1.41×10^{-2}

A quasi reversible electrode reactions of these actinides are confirmed by the k_s value obtained from the experimental data. It clearly suggests that the kinetics are also sluggish in ([C₈mim][NTf₂] + DoHyA) which is attributed to the retardation of the electron transfer rate at electrode–electrolyte interface due to high viscosity of the system.

4.4 Conclusions

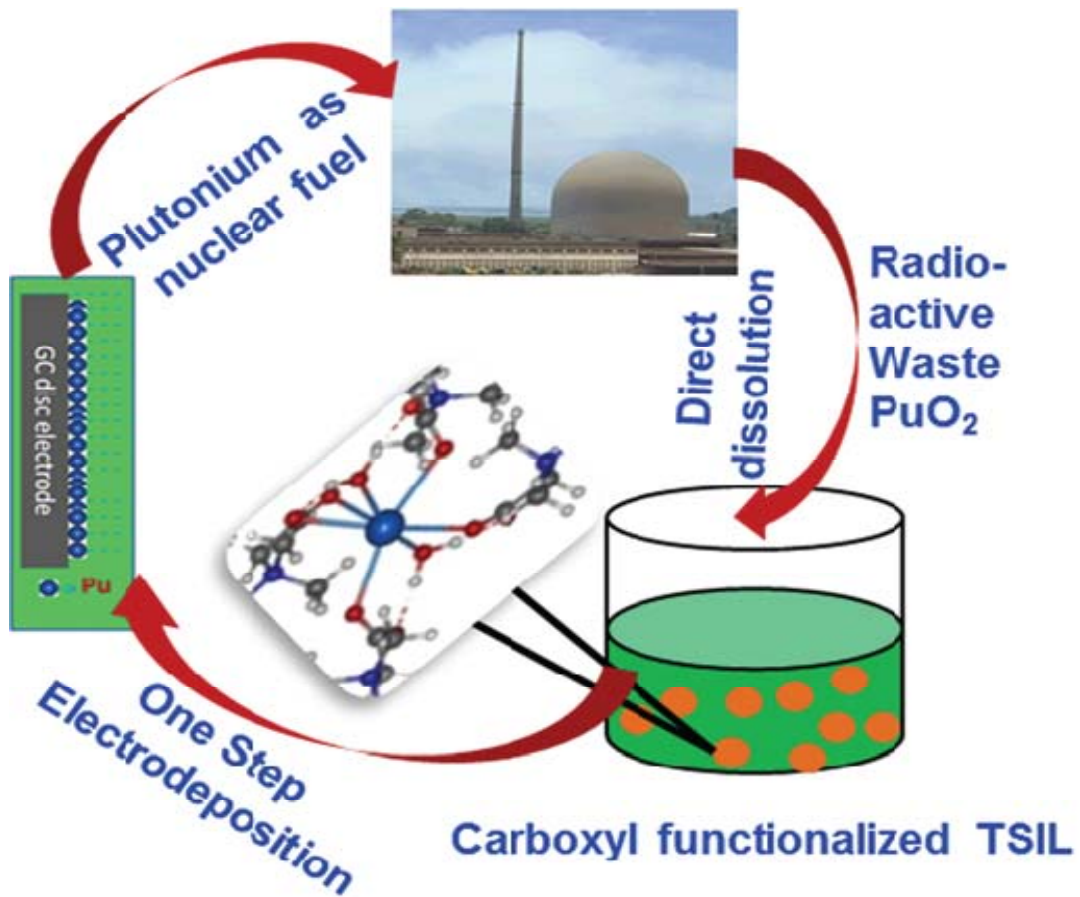
A systematic study on extraction and redox chemistry of plutonium in aqueous medium and in ([C₄mim][NTf₂]+ NOSCO) system was carried out using electrochemical measurements. The extractability of plutonium was measured using alpha counting which shows that the Pu activity left in the aqueous phase after solvent extraction with the new bifunctional ligand, NOSCO is considerably low. The cyclic voltammograms obtained in ionic liquid were much solution. Cyclic voltammetry studies showed that Pu(IV)/ Pu(III) redox reaction in ([C₄mim][NTf₂] + NOSCO) system is quasi reversible. The diffusion

coefficient of Pu(IV) calculated using cyclic voltammetric study was found to be 9.38×10^{-6} $\text{cm}^2 \text{s}^{-1}$ at 298 K. Heterogeneous charge transfer coefficient and rate constants were also evaluated.

A systematic study on extraction and redox chemistry of various actinides (U, Pu, Np) in ($[\text{C}_8\text{mim}][\text{NTf}_2]$ + DoHyA) were also carried out using electrochemical measurements. The extractability of these actinides was measured using alpha counting which shows that the ^{233}U , ^{239}Pu and ^{237}Np activity left in the aqueous phase after solvent extraction with the DoHyA bifunctional ligand is considerably low. The cyclic voltammograms obtained in ionic liquid were much broader with reduced cathodic and anodic peak current density. Cyclic voltammetry studies showed that these redox reactions in ($[\text{C}_8\text{mim}][\text{NTf}_2]$ +DoHyA) systems are quasi reversible. The diffusion coefficient of these actinides is calculated using cyclic voltammetric study at 298K. Heterogeneous charge transfer coefficient and rate constants were also evaluated. Such studies on actinide electrochemistry and its behaviour in ionic liquid provide an exhilarating and demanding road map not only for actinide researcher but also to those working in the field of nuclear fuel reprocessing broader with reduced cathodic and anodic peak current density compared to the one obtained with aqueous system.

Chapter 5

Task Specific Ionic Liquid for Direct Dissolution of Plutonium Oxide



5.1 Introduction

Protonated 1-carboxy-N, N, N-trimethylmethanaminium bis (trifluoromethylsulfonyl) imide trivially known as protonated betaine bis(trifluoromethylsulfonyl)-imide ([Hbet][NTf₂]), is a task specific ionic liquid reported to be a directly dissolving oxides of some lanthanides and actinides [170, 245, 246]. The carboxyl group attached to the cationic moiety of [Hbet][NTf₂] co-ordinates with metal ion through mono or bidentate coordination to facilitate the dissolution of oxides. This ionic liquid has also been used to extract U from UO₃ by forming complexes with zwitter ionic carboxylate ligands and bis-triflate counter anions [247]. Dissolution of UO₂, UO₃ and U₃O₈ was reported at elevated temperature in [Hbet][NTf₂] [248]. The dissolution of plutonium oxide is quiet challenging in terms of the radioactivity associated with it. ²³⁹Pu is an α-active nuclide with a half-life of 2.4×10^4 years which corresponds to the production of 138×10^6 α-particles/min/mg of Pu. Plutonium is notoriously hazardous when it finds its way into the human body. It should be studied exclusively in actinide laboratory equipped with glove boxes and analytical apparatus for actinide research to avoid any health risk caused by the radiation exposure.

Due to this the dissolution of plutonium oxide has never been explored in this ionic liquid. In this work studied were carried out to insights into the prospective of [Hbet][NTf₂] in nuclear fuel cycle following systematic routes. Firstly, the task specific ionic liquid was synthesized and characterized. The dissolution of PuO₂ was carried out directly into the synthesized ionic liquid inside a glove box. Due to the absence of the radioactive set up of physical and chemical characterization to understand the dissolution mechanism DFT calculations were also performed. With the help of these calculations the structure of the Pu and [Hbet][NTf₂] complex which is facilitating the direct dissolution was proposed. Also, electrochemical and thermodynamic properties of Pu(IV) in [Hbet][NTf₂] were performed to

understand feasibility of using [Hbet][NTf₂] ionic liquid as electrolyte medium for electro-deposition of plutonium.

5.2 Experimental Section

All the chemicals used in this study were used as received. Betaine hydrochloride and lithium bis(trifluoromethanesulfonylimide) were purchased from Sigma Aldrich. [Hbet][NTf₂] was prepared by the procedure described elsewhere [170]. In brief, lithium bis(trifluoromethylsulfonyl) imide (0.05 mol, 14.4 g) was dissolved in 50 mL of H₂O, and an aqueous solution (25 mL) of betaine hydrochloride (0.05 mol, 7.7 g) was added to it under stirring. After 2 h of stirring, the ionic liquid phase was separated, washed with H₂O (3 × 15 mL) to remove any traces of chloride impurities, and finally dried under vacuo to obtain pure [Hbet][NTf₂] (Yield 12.3 g, 62%). ¹H NMR (500 MHz, DMSO-d₆): δ 3.21 (s, 9H), 4.31 (s, 2H); ¹³C NMR (125 MHz, DMSO-d₆): δ 53.3, 63.0, 115.9, 118.4, 121.0, 123.6, 166.4. ¹H and ¹³C NMR spectra are shown in Figure 5.1 and 5.2 respectively.

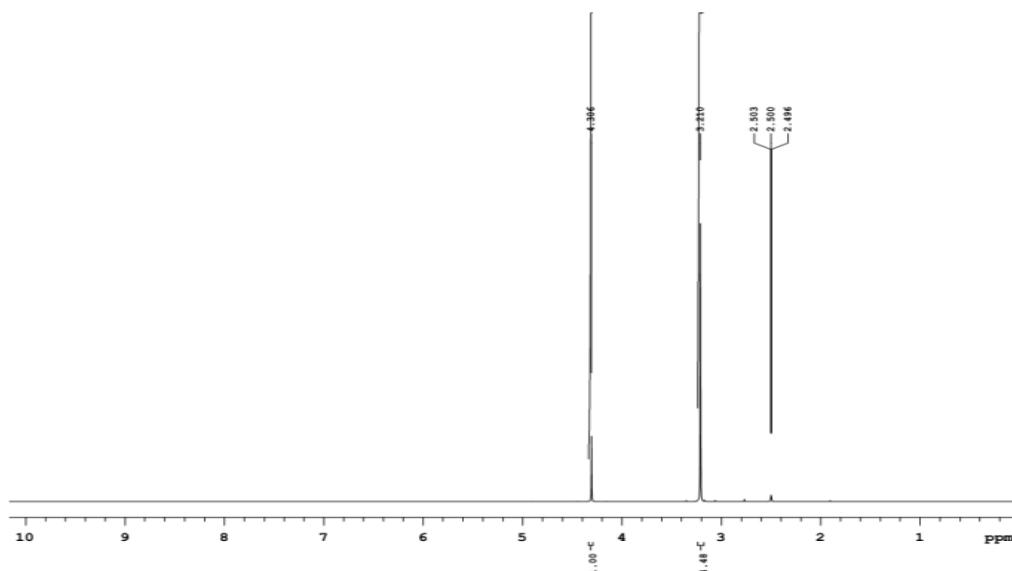


Figure 5.1: ¹H NMR of [Hbet][NTf₂]

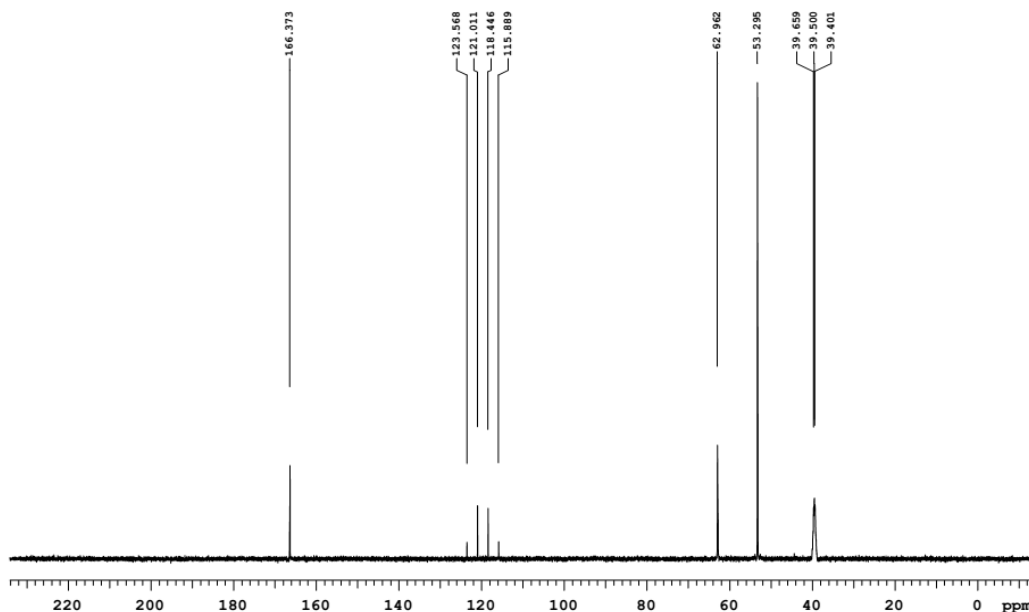


Figure 5.2: ^{13}C NMR of [Hbet][NTf₂]

The water content in the ionic liquid was found to be insignificant as evident from thermogravimetric studies discussed later. Pure PuO₂ is obtained / processed from Pu-analysis waste solution by first passing through anion exchange column to get Pu-nitrate solution, and then it is precipitated as Pu-oxalate. This oxalate is heated in a furnace under flowing oxygen at 450°C to get PuO₂ powder. All the experiments were performed with great care inside a glove box with negative pressure under safe condition. Known and accurately weighed PuO₂ (equivalent to 9 mM) powder was transferred to [Hbet][NTf₂] RTIL taken in a round bottom flask fitted with Liebig condenser. This flask was immersed in a silicone oil bath heated by an electromagnetic mantle setup at 50-100 rpm at ~400 K, which was housed in a Glove Box maintained at 1" negative pressure. The set up for PuO₂ dissolution is shown in Figure 5.3.

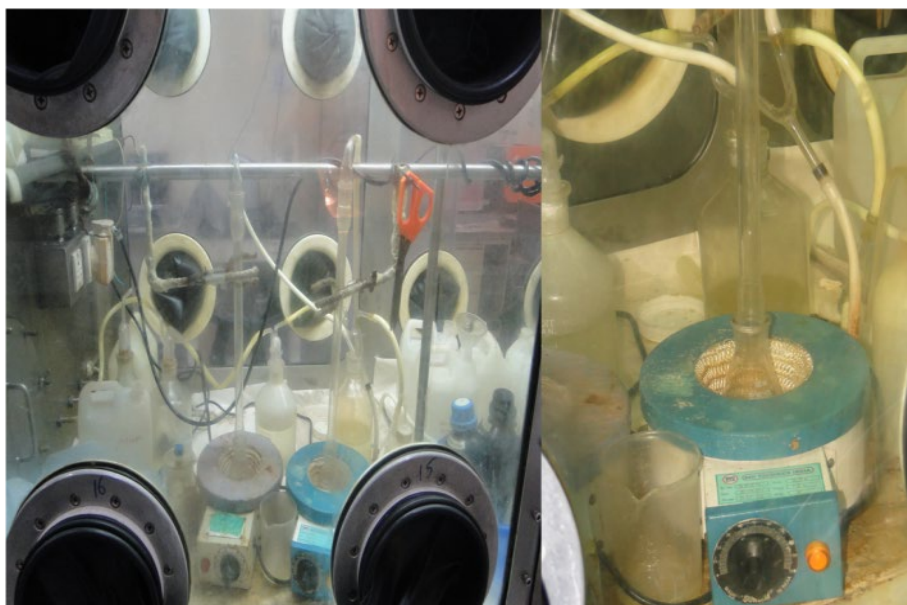


Figure 5.3: Set up for PuO_2 dissolution inside glove box.

The reflux process was continued till all the PuO_2 powder gets dissolved into RTIL. The aliquot of $[\text{Hbet}][\text{NTf}_2]$ containing plutonium, in the present study, was also equilibrated with 1M HNO_3 to strip the plutonium from the ionic liquid aliquot and the amount of plutonium in nitric acid was estimated by alpha counting. The alpha activity of the aqueous phase, before and after solvent extraction, was measured by alpha spectrometry.

Voltammetric studies of the solutions were done in the temperature range 298–351 K. A glassy carbon disk working electrode (area, $A = 0.07 \text{ cm}^2$) was used as a working electrode. Two Pt wires acted as counter and quasi-reference electrodes. Platinum quasi reference electrode was calibrated with respect to the ferrocene/ferrocenium (Fc/Fc^+) redox couple in ionic liquid and E^0 was observed as = 0.21 V. The internal standard Fc/Fc^+ was added to ($[\text{Hbet}][\text{NTf}_2]$) ILs and all the redox potentials are referred against the Fc/Fc^+ redox couple.

All solutions were deoxygenated using high purity argon prior to electrochemical experiments. Each measurement was repeated thrice and the average numerical value of each parameter is quoted for discussion with a relative error $< \pm 0.1\%$. The electrochemical cell had a single leak-tight compartment and all the electrodes were placed in the same compartment. The cell was kept under argon atmosphere during entire study. The thermal stability of ionic liquid was studied using thermogravimetry-differential scanning calorimeter (TG-DSC). The experiments were carried out at a heating /cooling rate of 5K/min. Reversible run was carried out in DSC, however, only heating run was carried out in TG-DSC. The alpha spectrum of Pu electrodeposited on a polished stainless steel planchette was recorded using a passivated ion-implanted planar silicon detector. The electrodeposited alpha source was placed at a distance of about 1 cm from the PIPS detector in a vacuum chamber and pressure inside the chamber was reduced to 10^{-6} bar. In order to achieve good counting statistics, the spectrum was recorded for a time to accumulate minimum 10,000 counts at the characteristic alpha energies of Pu isotopes. The analyses of peak area at the characteristic alpha energies of $^{238,239,240}\text{Pu}$ were carried out. The geometry optimizations and total energy calculations have been performed using the density functional theory (DFT). Initially all the geometries were optimized by BP86 function and then, B3LYP has been used further calculations.

5.3. Results and Discussion

5.3.1. DSC and TG studies

DSC curve of [Hbet][NTf₂] showed a glass transition around -56°C as explained in literature [249]. Later at -16.8°C, there is a probability of cold crystallization which appears as exothermic peak. The melting of IL occurred at 28.6°C, which is quite broad and two peak merging with each other. In the cooling curve again the crystallization of ILs occurred as a

sharp peak with onset at 4°C due to the super-cooling effect. The thermogram of [Hbet][NTf₂] (Figure 5.4.(b)) showed two weight losses due to decomposition of IL at 310°C and 426°C, respectively. Hence IL is predicted to be stable upto temperature of 300°C. The loss processes are reflected as endothermic peak in Figure 5.4 (a).

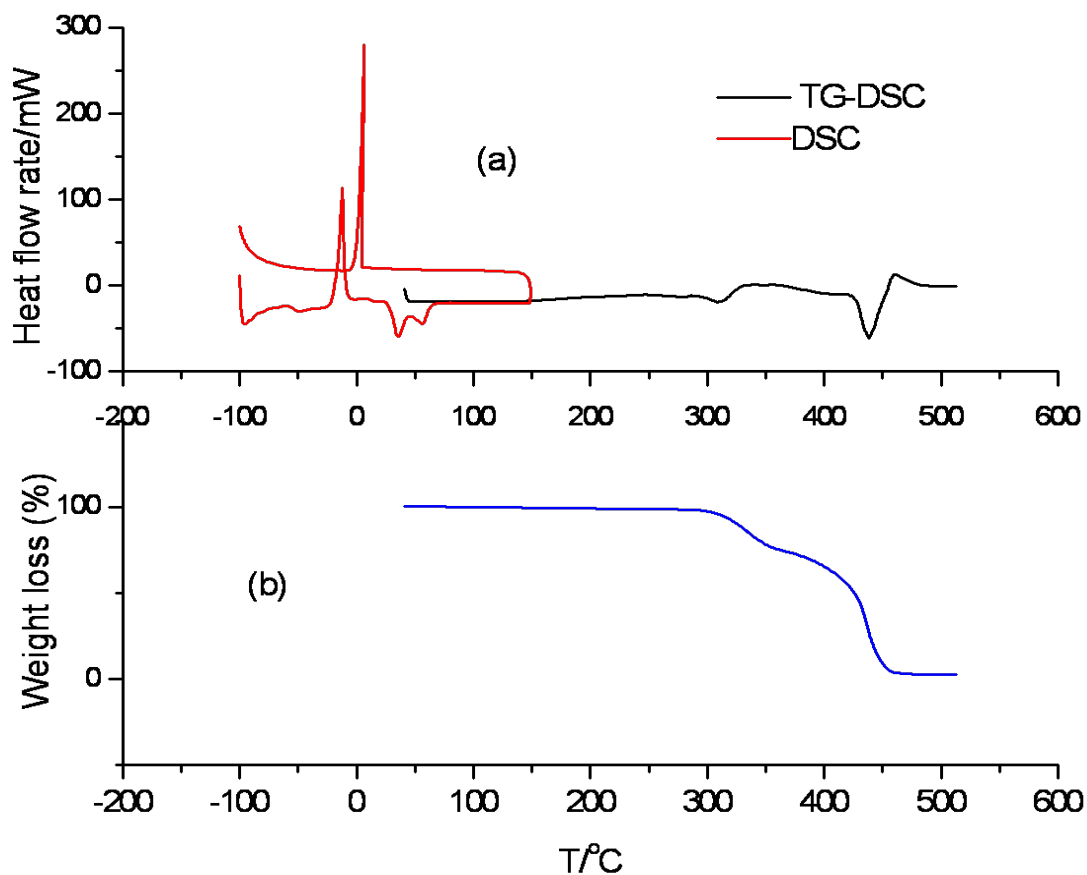


Figure 5.4: The DSC and Thermograms of synthesized ([Hbet][NTf₂]) ionic liquid

5.3.2 UV-VIS spectroscopy

After complete dissolution of PuO₂ in ionic liquid, UV-Vis spectroscopy was undertaken to see the predominant oxidation state in the resulted solution. Figure 5.5 presents the UV-Visible spectra of plutonium in [Hbet][NTf₂]. The most prominent peak observed at

476 nm in [Hbet][NTf₂] was attributed to Pu(IV). Also, no peak corresponding to Pu(III) and Pu(VI) was observed [250].

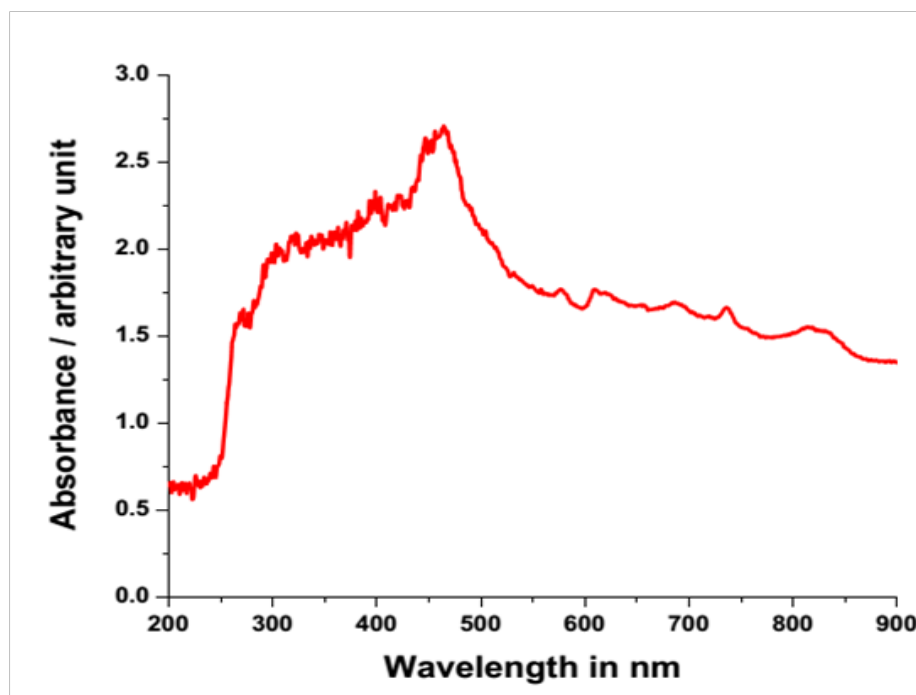


Figure 5.5: UV-Visible spectra of plutonium directly dissolved in Hbet][NTf₂]

5.3.3 Electrochemical Studies

The cyclic voltammogram of [Hbet][NTf₂] recorded at glassy carbon working electrode is shown in Figure 5.6. The result showed reductive and oxidative limits of -2.8 and 1.4 V, respectively, relative to a Fc/Fc^+ reference, which gives an electrochemical potential window of 4.2 V. This potential window may be adequate for investigating the reduction of Pu(IV) to Pu(III) and vice versa. The cyclic voltammogram of 9 mM Pu(IV) in [Hbet][NTf₂] recorded at glassy carbon working electrode at a scan rate of 0.2 Vs⁻¹ is also shown in Figure 5.6. It can be seen that the cathodic wave occurring at the onset of -0.8 V, leading to a prominent cathodic wave at the peak potential of -1.15 V is due to the reduction of Pu (IV) to Pu(III).

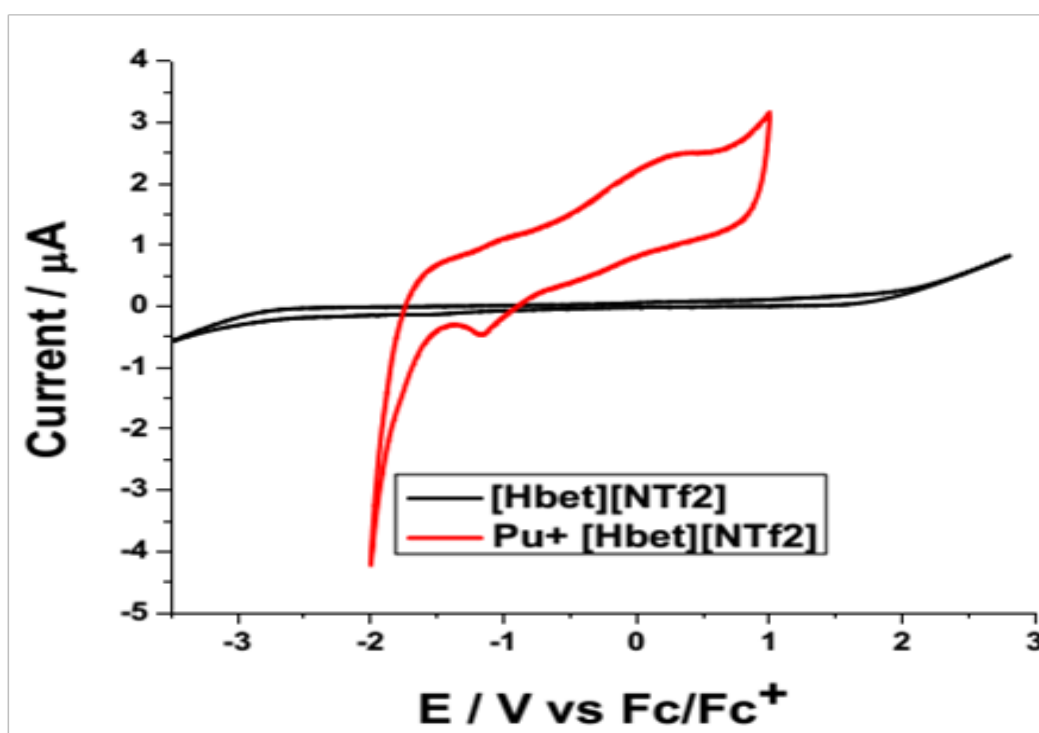


Figure 5.6: Cyclic voltammogram of [Hbet][NTf₂] in absence and presence of 9 mM Pu (IV) recorded at glassy carbon working electrode at a scan rate of 0.2 V s⁻¹

The oxidation wave occurs at the peak potential of 0.3 V vs. Fc/Fc⁺. It can be seen that in absence of Pu, there is no other significant redox peak present in the system confirming the absence of any other electroactive species in the TSIL. The difference in peak potential, ΔE_p ($E_{pa} - E_{pc}$) is quite significant than the value required for a reversible one electron transfer process. The cyclic voltammograms of Pu(IV) in [Hbet][NTf₂] recorded at various scan rates at glassy carbon electrode at 298K are shown in Figure 5.7. It can be seen that the cathodic current (I_{pc}) increases and the cathodic peak potential (E_{pc}) is shifted cathodically with increase of scan rate.

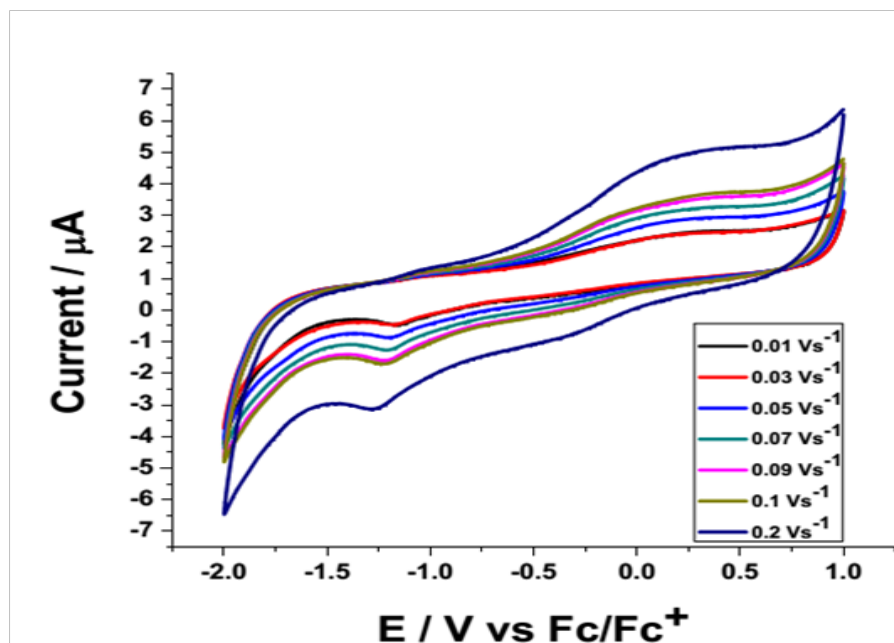


Figure 5.7: Cyclic voltammograms of Pu(IV) in [Hbet][NTf₂] recorded at various scan rates at glassy carbon electrode at 298K.

These findings indicate that the reduction of Pu(IV) to Pu(III) in [Hbet][NTf₂] at glassy carbon electrode is not reversible but quasi-reversible. Hence, it can be presumed that the reduction is controlled not only by diffusion of Pu(IV) ion in [Hbet][NTf₂] medium, but also by the kinetics of the charge transfer reaction occurring at the electrode-electrolyte inter phase. Figure 5.8 shows the cyclic voltammograms of 9 mM Pu(IV) in [Hbet][NTf₂] at various temperatures. Temperatures were well controlled and selected as 298 K, 313 K, 328 K, 348 K and 373 K, respectively. For Pu(IV) in [Hbet][NTf₂], the current densities increased along with the rise of temperature. This feature is associated with the mass transition caused by the viscosity of [Hbet][NTf₂], which depends on temperature closely. Thus, the transport properties of IL, including conductivity, diffusion coefficient, and charge transfer rate are also temperature-dependent for the variation of viscosity.

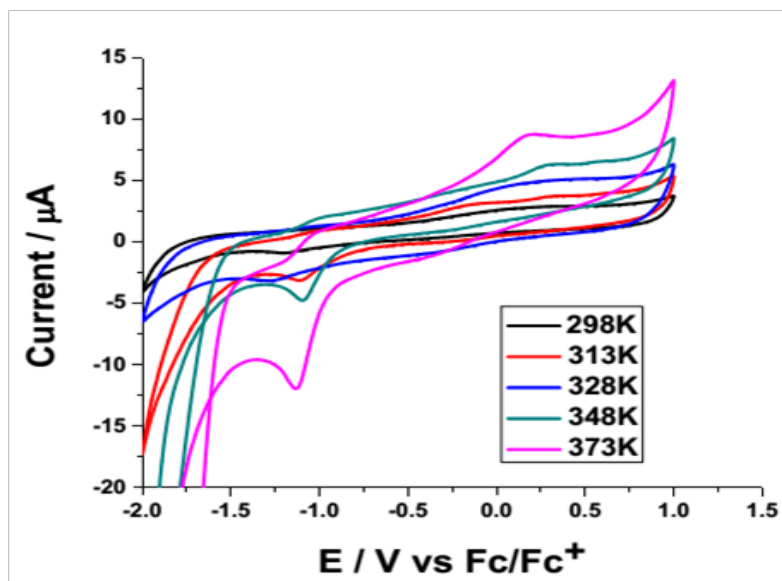


Figure 5.8: Cyclic voltammograms of 9 mM Pu(IV) in [Hbet][NTf₂] at various temperatures.

For [Hbet][NTf₂] ionic liquid, its viscosity decreased and the conductivity increased at higher temperature, which would facilitate the diffusion of Pu(IV). The diffusion rate also enhances as the temperature is increased. Both current intensity and peak potential were changed, along with the change of scan rate. The anodic peak potentials were shifted to anodic direction with increase in temperature and the cathodic peak potential also shifted to more anodic direction and the anodic peaks were less sharp than the cathodic ones as the temperature reached 348K. The plots of cathodic peak current densities (I_{pc}) against the square-root of the potential scan rate ($v^{1/2}$) are shown in Figure 5.9 at different temperatures.

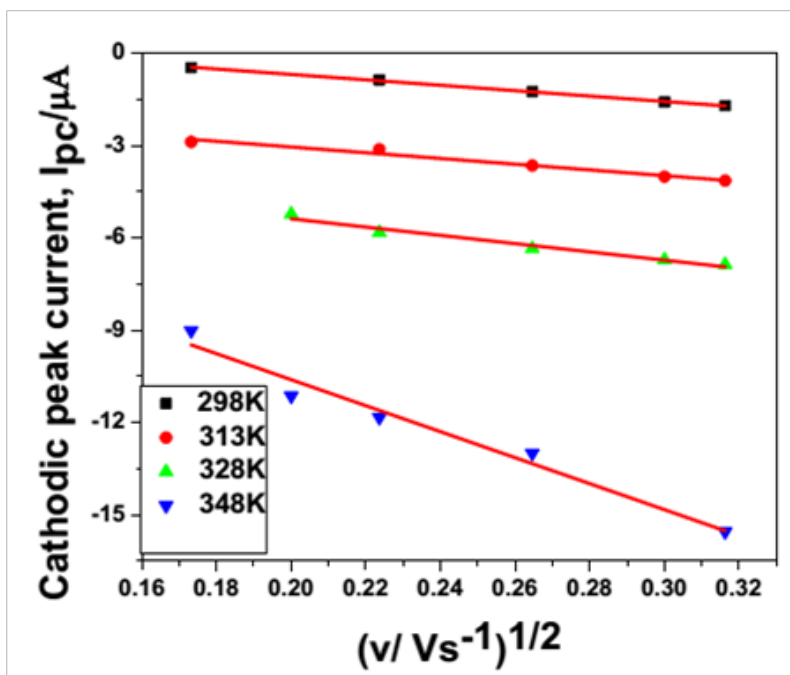


Figure 5.9: The plots of cathodic peak current (I_{pc}) against the square-root of the potential scan rate ($v^{1/2}$) at different temperatures.

The linear dependence of I_{pc} on square root of scan rate ($v^{1/2}$), shown in Figure 5.9 also confirms the reduction of Pu(IV) to Pu (III) in [Hbet][NTf₂] IL is diffusion controlled. A positive correlation of the current intensity with the square root of scan rate was also seen. The cathodic peak current (I_{pc}) and the scan rate for a quasireversible reduction reaction for a soluble-soluble couple are related to each other by following expression [177].

$$I_{pc} = 0.496 nFAcD^{1/2} \left(\frac{(\alpha n_{\alpha})Fv}{RT} \right)^{1/2} \dots\dots\dots (5.1)$$

where C is the plutonium concentration in mol cm⁻³, D is the diffusion coefficient in cm² s⁻¹, F is the Faraday constant, n is the number of exchanged electrons, v is the scan rate in Vs⁻¹, α is the charge transfer coefficient, n_α is the number of electrons transferred in the rate determining step, A is the geometric area of electrode and T is the absolute temperature in K. The value of αn_α can be determined from following equation. Where, E_{pc/2} is the half-peak potential. The value of αn_α was found at different temperatures for the scan rate of 0.02Vs⁻¹. By substituting the αn_α value in above expression, the diffusion coefficient of Pu(IV) in [Hbet][NTf₂] was determined at different temperatures and are given in Table 5.1.

$$|E_{pc} - E_{pc/2}| = \frac{1.857RT}{F\alpha n_{\alpha}} \quad \dots\dots\dots (5.2)$$

Since the reduction of tetravalent plutonium is not only controlled by diffusion but also by charge transfer kinetics, the rate constant of charge transfer reaction, k_s can be determined using the equation below [218].

$$k_s = 2.18 \left[D(\alpha n_{\alpha}) \frac{\nu F}{RT} \right]^{1/2} \exp \left[\frac{\alpha^2 n F}{RT} (E_{pc} - E_{pa}) \right] \quad \dots\dots\dots (5.3)$$

The electrode reaction can be classified as reversible when $k_s \geq 0.3\nu^{1/2} \text{ cm s}^{-1}$, quasi-reversible when $0.3\nu^{1/2} \geq k_s \geq 2.0 \times 10^{-5} \nu^{1/2} \text{ cm s}^{-1}$ and irreversible when $k_s \leq 2.0 \times 10^{-5} \nu^{1/2} \text{ cm s}^{-1}$. The k_s values for the reduction of Pu(IV) to Pu(III) at different temperatures in ionic liquid media are summarized in Table 5.1.

Table 5.1: Diffusion coefficients and charge-transfer coefficients of Pu(IV) in [Hbet][NTf₂]

Temperature (K)	D (cm ² /s)	k _s (cm/s)
298	3.92 × 10 ⁻⁹	4.62 × 10 ⁻⁴
313	4.40 × 10 ⁻⁹	3.89 × 10 ⁻⁴
328	8.09 × 10 ⁻⁹	4.06 × 10 ⁻⁴
348	6.14 × 10 ⁻⁸	8.06 × 10 ⁻⁴

The reduction was found to be quasi reversible as suggested by the k_s values in all the cases. With increase in temperature, the k_s value increased indicating the increase in

reversibility and can be attributed to the facilitated electron transfer at electrode–electrolyte interface at high temperatures. k_s values were found to be less in ionic liquid phase as compared to aqueous phase indicating the increase in irreversibility in RTIL which is attributed to the retardation of the electron transfer at electrode – electrolyte interface due to high viscosity.

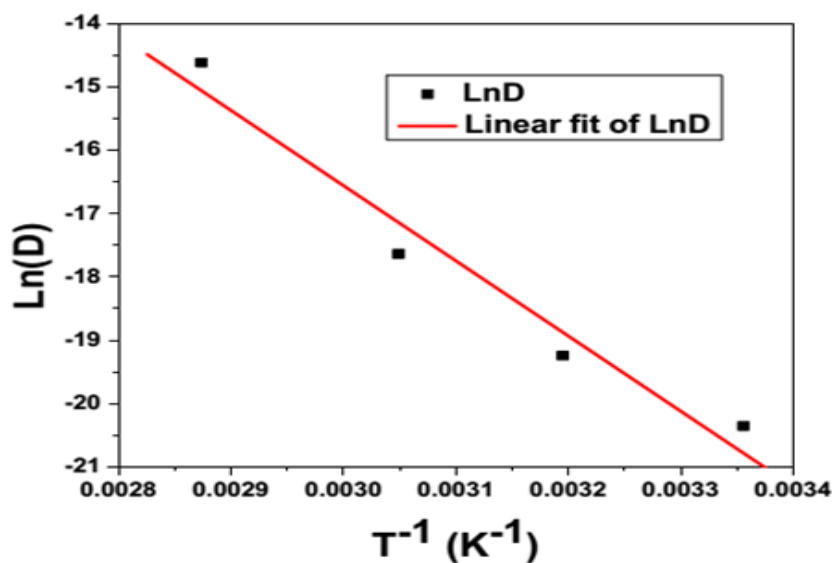


Figure 5.10: A plot of $\ln D$ versus $1/T$

The activation energy for the diffusion of the metal ion can be evaluated using Arrhenius equation given below:

$$D_0 = A \exp(-E_a/RT) \quad \dots\dots\dots (5.4)$$

Where A is the pre-exponential factor and E_a is the corresponding activation energy. A plot of $\ln D$ versus $1/T$ gave a straight line as shown in Figure 5.10 with a slope of $(-E_a/R)$. From the slope, the activation energy for the diffusion of Pu(IV) was found to be 98.3 KJ/mol for [Hbet][NTf₂]. This signifies that 98.3 KJ/mol of energy are required for the diffusion of Pu(IV) ion at electrode–electrolyte inter-phase in [Hbet][NTf₂] medium.

5.3.4 Computational Details

The structures of [Hbet][NTf₂] and its complex with Pu(IV) ions are determined using density functional theory (DFT) based calculations by employing the electronic structure programme ORCA 25 and the optimized structures are shown in Figure 11 and 12 respectively. The structure of the IL shows that there is weak hydrogen bonding between the betaine (cationic) and bis(trifluoromethylsulfonyl) imide (anionic) groups, mostly governed by the C–H...X (X = N and O) interactions. The calculated shortest distance between these two units and the longest hydrogen bonding distance is found to be ~2.3 and 3 Å, respectively. More interestingly, the dipole moment of this ionic liquid is calculated to be very large, 12.82 Debye, and it can be attributed to the presence of highly electronegative trifluoro groups bonded to the sulfonyl group.

The dissolution of PuO₂ in ionic liquid has been assumed to follow a equation as given below:

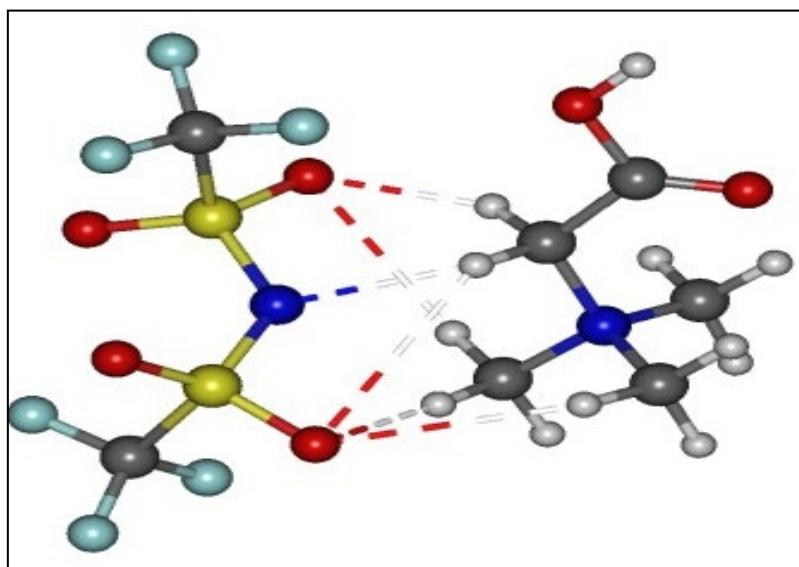
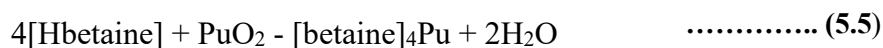


Figure 5.11: Optimized Structure of TSIL

The structure of the Pu(IV) complex shows that the Pu(IV) is surrounded by four betaine units and two water molecules in an octahedral geometry. After losing one proton from the carboxyl group of the betaine unit, it acts as a monodentate anionic ligand and satisfies the positive charge of the Pu(IV) ion. Thus, the four betaine units bind through one of the oxygen atoms of the carboxylate (COO⁻) group to the metal centre. The two water molecules formed during the reaction not only satisfy the coordination of the metal centre but also significantly stabilize the whole molecule by intra-molecular hydrogen bonding interaction with one of the carboxylate oxygen atoms of the betaine group. The distances between Pu(IV)–(H₂O) (2.77 Å) and Pu(IV)–O(COO⁻) (2.56 and 2.62 Å) are found to be in good agreement with experimental reports. The dipole moment of the Pu-dissolved in IL complex is around 5.29 Debye and the Mulliken gross atomic population on Pu shows the negative charge with the value of -0.75 a.u. The additional charge on the Pu ion unambiguously suggests that the Pu ion has a very strong affinity towards the carboxyl groups.

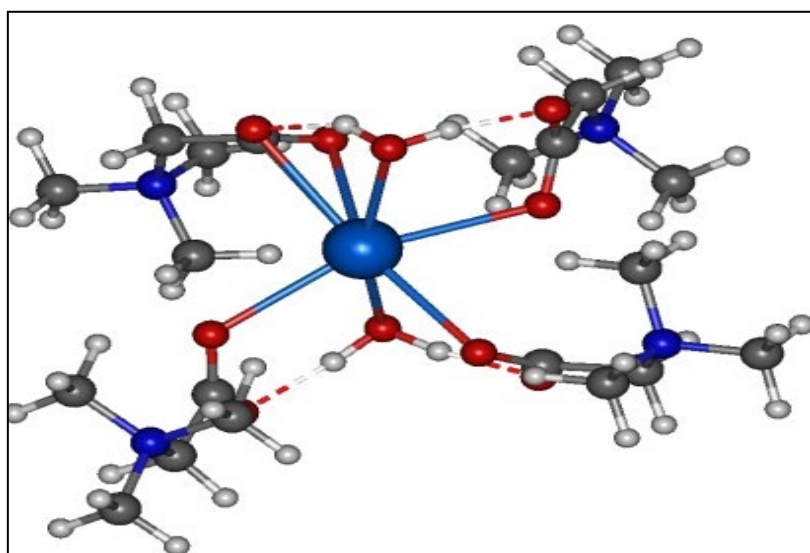


Figure 5.12: Optimized Structure of Pu-(betaine)₄.2H₂O complexes.



Different colorful spheres refer to the atoms H, C, N, O, F, S, Pu respectively

The enthalpy of formation of the complex is calculated to be $-51.28 \text{ kcal mol}^{-1}$ which signifies that the proposed mechanism of dissolution is a favorable process. It may be noted that the structure of the complex is found to be very stable only when two water molecules are directly bonded to the plutonium (IV) ion, without which, the complex is found to be unstable. Similarly, attempts to find other suitable structures with different numbers of betaine units resulted in mostly unstable complexes. Thus, it can be confirmed that the stronger binding affinity of the carboxyl group of the betaine group towards the plutonium ion followed by the insitu formation of two water molecule facilitates the dissolution of PuO_2 in $[\text{Hbet}][\text{NTf}_2]$. More interestingly, it has been reported that very little extraction of trivalent and tetravalent plutonium has been achieved through the usage of amine-containing organic media in acetate solution. This can be very well correlated with our results, i.e. the betaine group, which consists of the amine as well as acetate functional groups, could be responsible for the successful dissolution process for plutonium.

5.3.5 Alpha Spectrometry

The electrochemical deposition of Pu metal/oxide was attempted from its solution in $[\text{Hbet}][\text{NTf}_2]$ medium by applying cathodic potential of -1.5V employing controlled potential coulometry at stainless steel planchette. The alpha spectrum of the stainless steel planchette recorded after the deposition of plutonium is given in Figure 5.13. The alpha spectrum shows that there are two characteristic peaks at energies 5.157 MeV and 5.499 MeV , respectively for $^{239,240}\text{Pu}$ and ^{238}Pu isotopes. No other peaks corresponding to other actinides viz. U, Th or Np were seen in the spectrum. There is a possibility of spectral interference of ^{241}Am ($E_\alpha = 5.486 \text{ MeV}$) at 5.499 MeV alpha energy, however, the observed gamma spectrum of the sample confirms the absence of ^{241}Am (the 59.54 keV peak is absent). The tailing of the alpha energy in Figure 5.13 is attributed to the deposition of a higher concentration of plutonium on

the planchette, which leads to the loss of kinetic energy of alpha particles within the source itself. The outcome of the above results clearly reveals that the dissolved plutonium can be quantitatively recovered from the ionic liquid medium via electrochemical reduction.

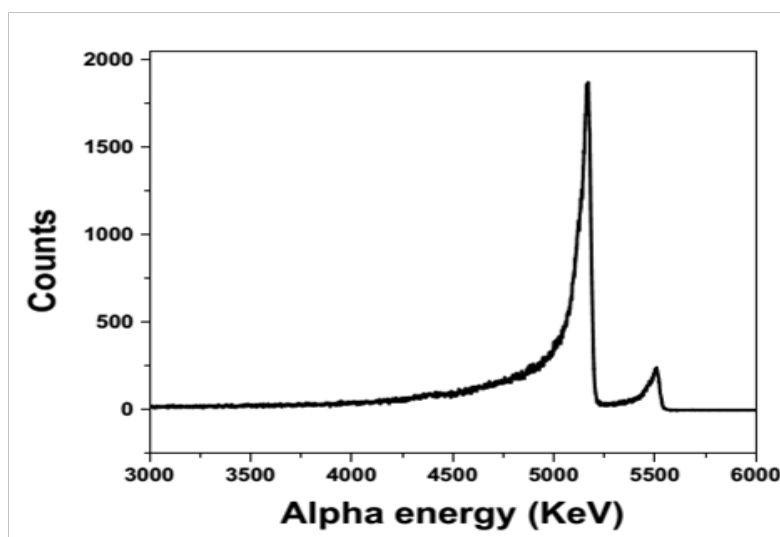


Figure 5.13: Alpha spectra of stainless steel planchette after the electrochemical deposition of plutonium

5.4 Conclusions

Direct dissolution of plutonium oxide (PuO_2) in protonated 1-carboxy-N, N, N-trimethylmethanaminium bis (trifluoromethylsulfonyl)imide ($[\text{Hbet}][\text{NTf}_2]$) task specific ionic liquid (TSIL) will open a new gateway for the nuclear researchers for RTIL based non aqueous reprocessing/ waste management and an attractive possibility to electro-deposit actinides. The electrochemical behavior of Pu(IV) in $[\text{Hbet}][\text{NTf}_2]$ was studied at glassy carbon working electrode. The cyclic voltammogram of Pu(IV) exhibited a quasi-reversible redox behaviour. The diffusion coefficient of Pu(IV) was determined at various temperatures and it was in the order of $\sim 10^{-9} \text{cm}^2/\text{s}$. Increase in the experimental temperature increased the diffusion coefficient. In this work, a new approach through another step to the growing

interest in nuclear industry related to the applications of room temperature ionic liquid (RTIL) in nuclear fuel reprocessing and waste management.

In addition, the direct dissolution of plutonium oxide through the usage of TSIL [Hbet][NTf₂] followed by electrodeposition of plutonium from the dissolved solution is achieved. Theoretical studies reveal that the carboxyl group attached to the cationic moiety of [Hbet][NTf₂] co-ordinates strongly with the plutonium(IV) ion in a monodentate coordination mode, facilitating the dissolution of oxides. The two water molecules generated during the dissolution reaction play a key role in satisfying the coordination sphere and also stabilizing the complex in solution via intra-molecular hydrogen bonding. On the contrary to the conventional dissolution process in an aqueous solution followed by several extraction steps through severe acidic/basic media, the present approach is a very simple and elegant one-step approach, which will open up a new avenue for the dissolution of actinides, especially nuclear fuels, by using TSIL-based green solvents.

REFERENCES

1. J.F. Facer Jr; K. M. Harmon; *USAEC Rept. HW-31186 (Del)*, **1954**.
2. O.J. Wick; “*Plutonium Handbook -A Guide to the Technology*”, Gordon and Breach Science Publishers, New York, **1967**, 1, 6.
3. S.K. Patil; *International Symposium on Artificial Radioactivity*, Pune, **1985**, 231.
4. K.M. Harmon; W.H. Reas; *Symposium on the Reprocessing of Irradiated Fuels, Belgium, USAEC Report TID- 7534 (Bk.1)*, **1957**, 332.
5. J.J. Katz; L.R. Morss; G.T. Seaborg; “*The Chemistry of Actinide Elements*”, Chapman and Hall, NewYork, **1986**.
6. S. Ahrland; “*Comprehensive Inorganic Chemistry*”, (Ed.) J.C.Bailer et al., Pergamon Press, **1973**, 5, 465.
7. L.H. Jones; R.A. Penneman; *J. Chem. Phys.*, **1953**, 21, 542.
8. L.H. Jones; *J. Chem. Phys.*, **1955**, 23, 2105.
9. .H. Zachariasen; *Acta. Crystallogr.* **1948**, 1, 277.
10. S.W. Rabideau; *J. Am. Chem. Soc.*, **1957**,79, 6350 .
11. A.J. Zielen; D. Cohen; *J. Phys. Chem.*, **1970**, 74, 394.
12. C.K. Jorgensen; *Chem. Phys. Lett.*, **1968**, 2, 549.
13. W.M. Latimer; “*The Oxidation States of Elements and their Potentials in Aqueous Solutions*”, *II edition*, Prentice-Hall Inc., NJ, USA, **1952**, 296.
14. C.A. Hempel; “*Encyclopedia of Electro Chemistry*”, (ed.), Reinhold Publishing Corporation, New York, **1964**, 415.
15. J.M. Cleveland; “*Plutonium Hand Book*”, (ed.) O.J. Wick, Gordon and Breach Science Publishers, New York, **1967**, 419.
16. R.E. Connick; “*Actinide Elements*”, *National Nicl. Engg. Series*, (Ed.) G.T.Seaborg; J.J. Katz; NNEs- IV, 14 A McGraw-Hill Book Co., New York, **1954**, 221.

17. T.W. Newton; F.B. Baker; "Lanthanide/ Actinide Chemistry", *ACS Adv. Chem. Ser.*, American Chemical Society, Washington DC, **1967**, 71, 268.
18. T.W. Newton; ERDA Critical Review Series, TID-26506, NTIX: Spring field VA, **1975**.
19. K. L. Nash; J.C. Sullivan; *Adv. Inorg. Bioinorg. Mech.*, **1988**, 4, 185.
20. R.E. Connick; *J. Am. Chem. Soc.*, **1949**, 71, 1528.
21. P.I. Artyukhin; V.I. Medvedouskii ; A.D. Gelman; *Russ. J. Inorg. Chem. (Eng. Trans.)*, **1959**, 4, 596.
22. R.D. Jones; G.R. Choppin; *Actinides Rev.*, **1969**, 1, 311.
23. S. Ahrland; *Structure and Bonding*, **1968**, 5, 118.
24. R.G. Pearson; *J. Am. Chem. Soc.*, **1963**, 85, 3533.
25. C.F. Baes; R.E. Mesmer, "*Hydrolysis and Cation*", Wiley, New York, **1976**.
26. J. Burgers; "*Metal Ions in Solution*", Wiley, NewYork, **1978**.
27. G.W. Kanffman; J.F. Baxter Jr.; *J. Chem. Ed.*, **1981**, 58, 349.
28. K.A. Kraus; *Proc. 1st U.N. Inst. Conf. Peaceful Uses of At. Energy*, **1956**, 7, 245.
29. J.M. Cleveland; "*Plutonium Hand Book*", (ed.) O. J. Wick, Gordon and Breach Science Publishers, New York, **1967**, 436.
30. A. Brunstan; *Ind. Eng. Chem.* **1959**, 51, 38.
31. D.W. Ockenden; S.A. Welch; *J. Chem. Soc.*, **1956**, 3358.
32. R.H. Rainey; *USAEC Report Cf-59-12-95*, **1959**.
33. D.J. Savage; J. W. Kyffin; *Polyhedron*, **1986**, 5, 743.
34. H. Irving; *Q. Rev. (London)* **1951**, 5, 200.
35. E. P. Horwitz; D. G. Kalina; *Solvent Extr. Ion Exch.* **1984**, 2, 179.
36. S. Yang ; Y. Zhao ; G. Tian ; *Dalton Trans.* **2016**, 45, 2681.
37. S.A. Ansari; A. Bhattacharyya; A. Zhang; L. Rao; *Inorg. Chem.* **2015**, 54, 8693.

38. D. Cohen; B. Taylor; *J. Inorg. Nucl. Chem.* **1961**, 22, 151.
39. R. Joblom; J.C. Hindman; *J. Amer. Chem. Soc.* **1951**, 73, 1744.
40. M.P. Wilkerson; J. M Berg; T. A. Hopkins; H. J. Dewey; *J. Solid State Chem*, **2005**, 178, 584.
41. C. Talbot-Eeckelaers; S. J. A. Pope; A. J .Hynes; R .Copping; C. J. Jones; R.J. Taylor; S . Faulkner; D. Sykes; F. R. Livens; *J. Am. Chem. Soc.* **2007**, 129, 2442.
42. H. A. C. McKay; The PUREX process. In Science and technology of tributyl phosphate, **1990**.
43. E. A. Puzikov; B. Y.Zilberman; Y. S. Fedorov; I. V. Blazheva; A. S. Kudinov; N. D Goletskiy; D. V. Ryabkov; A New Approach to Simulation of Extraction Equilibria in the PUREX Process. *Solvent Extr. Ion Exch.* **2015**, 33, 362.
44. A. P. Paiva; P. Malik; Recent advances on the chemistry of solvent extraction applied to the reprocessing of spent nuclear fuels and radioactive wastes. *J. Radioanal. Nucl. Chem.***2004**, 261, 485.
45. P. B. Ruikar; M. S. Nagar; M. S. Subramanian; K. K.Gupta; N .Varadarajan; R. K. Singh; Extraction behavior of uranium (VI), plutonium (IV), zirconium (IV), ruthenium (III) and europium (III) with γ -pre-irradiated solutions of N, N'-methylbutyl substituted amides in n-dodecane. *J. Radioanal. Nucl. Chem.***1995**, 201, 125.
46. C. Musikas; H. Hubert; Extraction by N, N'-Tetra AlkylMalonamides II. *Solvent Extr. Ion Exch.* **1987**, 5, 877.
47. T. H. Siddall; Effects of Structure of N, N-Disubstituted Amides on their Extraction of Actinide And Zirconium Nitrates And of Nitric Acid. *The J. Phys. Chem.* **1960**, 64, 1863.

48. B. N. Laskorin; D. I. Skorovarov; E. A. Philipp; I.I. Volodin; Extraction of uranium and plutonium by tertiary aliphatic phosphine oxides. *J. Radioanal. Nucl. Chem.* **1974**, 21, 65.
49. V. V. Ramakrishna; S. K. Patil; Synergic extraction of actinides. In *New Developments, Springer: 1984*, 56, 35.
50. S. Chaohong; B. Borong; B. Yizhi; W. Gaodong; Q. Ju; C. Zhengbei; Extraction of U (VI), Th (IV) and some fission products from nitric acid medium by sulfoxides and effect of γ - irradiation on the extraction. *J. Radioanal. Nucl. Chem.* **1994**, 178, 91.
51. J. P. Shukla; S. A. Pai; M. S. Subramanian; Solvent extraction of plutonium (IV), uranium (VI), and some fission products with di-n-octylsulfoxide. *Sep. Sci. Technol.* **1979**, 14, 883.
52. K. M. A. Malik; J. W. Jeffery; The crystal structure of tetranitratobis (triphenylphosphine oxide) thorium (IV). *Acta Cryst.* **1973**, **B** 29, 2687.
53. G. J. Lumetta; B. K. McNamara; B. M. Rapko; R. L. Sell; R. D. Rogers; G. Broker; J. E. Hutchison; Synthesis and characterization of mono- and bis-(tetraalkylmalonamide)uranium(VI) complexes. *Inorg. Chim. Acta* **2000**, 309, 103.
54. S. K. Singh; P. S. Dhama; A. Dakshinamoorthy; M. Sundersanan; Studies on the recovery of uranium from phosphoric acid medium using synergistic mixture of 2-ethyl hexyl hydrogen 2-ethyl hexyl phosphonate and octyl (phenyl)-N, N-diisobutyl carbamoyl methyl phosphine oxide. *Sep. Sci. Technol.* **2009**, 44, 91.
55. Z.-X. Zhu; Y. Sasaki; H. Suzuki ; S. Suzuki; T. Kimura; Cumulative study on solvent extraction of elements by N, N, N', N'-tetraoctyl-3-oxapentanediamide (TODGA) from nitric acid into n-dodecane. *Anal. Chim. Acta* **2004**, 527, 163.

56. S. Kannan; M. A. Moody; C. L. Barnes; P. B. Duval; Lanthanum (III) and Uranyl (VI) Diglycolamide Complexes: Synthetic Precursors and Structural Studies Involving Nitrate Complexation. *Inorg. Chem.* **2008**, 47, 4691.
57. G. F. Vandegrift; R. A. Leonard; M. J. Steindler; E. P. Horwitz; L. J. Basile; H. Diamond; D. G. Kalina; L. Kaplan; *Report ANL-84-45; Argonne National Laboratory: Argonne, IL, 1984.*
58. Y. Morita; J. P. Glatz; M. Kubota; L. Koch; G. Pagliosa; K. Roemer ; A. Nicholl, *Solv. Extr. Ion Exch.*, **1996**, 14, 385.
59. E. P. Horwitz; D. G. Kalina; H. Diamond; G. F. Vandegrift; W. W. Schulz; *Solvent Extr. Ion Exch.* **1985**, 3, 75.
60. E. P. Horwitz.; D. G. Kalina; H. Diamond; L. Kaplan; G. F. Vandegrift; R. A. Leonard; M. J. Steindler; W. W. Schulz, *German Patent DE85 010251, 1985.*
61. D. S. Wisnubroto; S. Nagasaki; Y. Enokida; A. Suzuki; *J. Nucl. Sci. Technol.* **1992**, 29, 263.
62. S. Nagasaki; K. Kinoshit; Y. Enokida; A. Suzuki; *J. Nucl. Sci. Technol.* **1992**, 29, 1100.
63. E.P. Horwitz; H. Diamond; D. G. Kalina; *ACS Symposium series No. 216*, W.T. Carnall and G. Choppin, Eds., ACS, Washington D.C. **1983**, 433.
64. J. N. Mathur; M. S. Murali.; P. R. Natarajan, *Talanta* **1992**, 39, 493.
65. K. Hatakeyama; Y.-Y. Park; H. Tomiyasu; *J. Nucl. Sci. Technol.* **1995**, 32, 1146.
66. E. P. Horwitz; H. Diamond; K. A. Martin; *Solvent Extr. Ion Exch.* **1987**, 5, 447.
67. A. E. Visser; M. P. Jensen; I. Laszak; K. L. Nash; G.R. Choppin; R. D. Rogers; *Inorg. Chem.* **2003**, 42, 2197.
68. OECD International Energy Agency World Energy Outlook, **2017**.
69. International Atomic Energy Agency Energy, electricity and nuclear power estimates

for the period up to 2030, **2008**, <http://www-pub.iaea.org/>.

70. S. A. Parry; L. O'Brien; A. S. Fellerman; C. J. Eaves; N. B. Milestone; N. D. Bryan; F. R. Livens; *Energy Environ. Sci.*, **2011**, 4, 1457.
71. D. M. Taylor; *Sci. Total Environ.*, **1989**, 83, 217.
72. J. L. Swanson; W. W. Schulz; L. L. Burger; J. D. Navratil; K. P. Bender; PUREX Process Flow sheets, *Science and Technology of Tributyl phosphate*, CRC Press Inc., Boca Raton, **1984**, 55.
73. T. Koyama; Y. Sakamura; M. Iizuka; *ECS Trans.*, **2010**, 33, 339.
74. Y. L. Liu; Y. D. Yan, W. Han; M. L. Zhang; L. Y. Yuan, Z. F. Chai ; W. Q. Shi ; *RSC Adv.*, **2013**, 3, 23539.
75. A. V. Bychkov ; O. V. Skiba; Review of non-aqueous nuclear fuel reprocessing and separation methods, in *Chemical Separation Technologies and Related Methods of Nuclear Waste Management*, **1999**, 71.
76. Spent Fuel Reprocessing Options Iaea, Vienna, IAEA-Tecdoc-1587 ISBN 978-92-0-103808-1 ISSN1011-4289, **2008**.
77. M. R. S. Foreman; *Cogent Chem.*, **2018**, 4, 1450944.
78. M. Poliakoff; N. J. Meehan; S. K. Ross; *Chem. Ind. (London)*.**1999**, 750, 175.
79. J. P. Hallett; T. Welton; *Chem. Rev.* **2011**, 111, 3508.
80. T. Welton; *Chem. Rev.* **1999**, 99, 2071.
81. Z. Kolarik; *Solvent Extr. Ion Exch.* **2013**, 31, 24.
82. A.P. Abbott; G. Frisch; J. Hartley; K.S. Ryder; *Green Chem.***2011**, 13, 471.
83. F. Zhao; X. Wu; M.K. Wang; Y. Liu; L.X. Gao; *Anal. Chem.*, **2002**, 18, 4960.
84. B.M. Quinn; Z.F. Ding; R. Moulton; A.J. Bard; *Langmuir*, **2002**, 18, 1734.
85. D. Wei; A. Avaska; *Anal. Chim. Acta*, **2008**, 607, 126.
86. O. Wallach; *Ber. Dtsch. Chem. Ges.* **1884**, 16, 535.

87. S. Sudgen; H. Wilkens; *J. Chem. Soc.* **1929**, 51, 1291.
88. P. Walden; *Bull. Acad. Impér. Sci.* **1914**, 8, 405.
89. B. K. M. Chan; N.-H. Chang; M. R. Grimmer; *Aust. J. Chem.* **1977**, 30, 2005.
90. M. Maase; V. Stegmann; *WO* 2006 10886, **2006**.
91. M. Masse; V. Stegmann; *DE Pat.* 102005017715, **2006**.
92. R. P. Swatlowksi; J. D. Holbrey; R. D. Rogers; *WO* 2003 029329, **2003**.
93. J.D. Holbrey; R. P. Swatlowksi; J. Chen, D. Daly, R. D. Rogers, *WO* 2005 098546, **2005**.
94. F. H. Hurley; Electrodeposition of Aluminum, *US Pat.* **1948**, 4,446,331.
95. T. P. Wier Jr., *US PAT* 4,446,350, **1948**; T. P. Wier Jr.; F. H. Hurley; *US Pat.* 4,446,349, **1948**.
96. F. H. Hurley; T. P. Wier; *J. Electrochem. Soc.* **1951**, 98, 203, 207;
97. J. S. Wilkes; *Green Industrial Applications of Ionic Liquids* (Eds.: R. D. Rogers, K. R. Seddon, S. Volkov), NATO Science Series II: Mathematics, Physics and Chemistry, Kluwer, Dordrecht, **2002**, 92, 295.
98. J. S. Wilkey; M. J. Zaworotko; *J. Chem. Soc., Chem. Commun.* **1992**, 965.
99. E. I. Cooper; E. J. M. O'Sullivan; Eighth International Molten Salts Symposium (Eds.: R. J. Gale, G. Blomgren, H. Kojima), *J. Electrochem. Soc., Inc.*, Pennington, New Jersey, **1992**, 92, 386.
100. J. D. Holbrey; K. R. Seddon; *Clean Prod. Proc.* **1999**, 1, 223.
101. P. Wasserscheid; W. Keim; *Angew. Chem. Int. Ed.* **2000**, 39, 3772; X. Y. Sheldon; *Chem. Commun.* **2001**, 2399.
102. C. M. Gordon.; *Appl. Catal. A* **2001**, 222, 101; H. Olivier-Bourbigou; L. Magna; *J. Mol. Catal. A* **2002**, 182, 419.
103. J. Dupont; R. F. de Souza; P. A. Z. Suarez; *Chem. Rev.* **2002**, 102, 3667.

104. K. R. Seddon; The International George Papatheodorou Symposium: Proceeding (Eds.: S. Boghosian, V. Dracopoulos, C. G. Kontoyannis, G. A. Voyiatzis), Institute of Chemical Engineering and High Temperature Chemical Processes, Patras, **1999**, 131.
105. A. Stark; K. R. Seddon; Kirk-Othmer Encyclopediadia of Chemical Technology (Ed.: A. Seidel), John Wiley & Sons, Inc., Hoboken, New Jersey, **2007**, 26, 836.
106. M. Freemantle; *Chem. Eng. News* **1998**, 76, 32.
107. J. H. Davis Jr; Task-Specific Ionic Liquids. *Chem. Lett.* **2004**, 33, 1072.
108. J. G. Huddleston; A. E. Visser; W. M. Reichert; H. D. Willauer; G. A. Broker; R.D.Rogers; Characterization and comparison of hydrophilic and hydrophobic room temperature ionic liquids incorporating the imidazolium cation. *Green Chem.* **2001**, 3, 156.
109. R. Hagiwara; Y. Ito; Room temperature ionic liquids of alkylimidazolium cations and fluoroanions. *J. Fluor. Chem.* **2000**, 105, 221.
110. K. R. Seddon; A. Stark; M. J. Torres; Influence of chloride, water, and organic solvents on the physical properties of ionic liquids. *Pure Appl. Chem.* **2001**, 72, 2275.
111. J. P. Mikkola; P. Virtanen; R. Sjöholm; Aliquat 336 - A versatile and affordable cation source for an entirely new family of hydrophobic ionic liquids. *Green Chem.* **2006**, 8, 250.
112. M. J. Earle; J. M. S. S. Esperança; M. A. Gilea; J. N.C. Lopes; L. P. N. Rebelo; J. W. Magee; K. R. Seddon; J. A. Widegren; The Distillation and Volatility of Ionic Liquids. *Nature* **2006**, 439, 831.
113. P. Wasserscheid; Chemistry: Volatile Times for Ionic Liquids. *Nature*, **2006**, 439, 797.

114. L. P. N. Rebelo; J. N. C. Lopes; J. M. S. S. Esperanca; E. Filipe; On the Critical Temperature, Normal Boiling Point, and Vapor Pressure of Ionic Liquids. *J. Phys. Chem. B*, **2005**, 109, 6040.
115. G. Le Rouzo; C. Lamouroux; V. Dauvois; A. Dannoux; S. Legand; D. Durand; P. Moisy; G. Moutiers; Anion effect on radiochemical stability of room-temperature ionic liquids under gamma irradiation, *Dalton Trans.* **2009**, 31, 6175.
116. D. Allen; G. Baston; A. E. Bradley; T. Gorman; A. Haile; I. Hamblett; J. E. Hatter; M. J. F. Healey; B. Hodgson; R. Lewin; K. V. Lovell; B. Newton; W. R. Pitner; D. W. Rooney; D. Sanders; K. R. Seddon; H. E. Sims; R. C. Thied ; An investigation of the radiochemical stability of ionic liquids. *Green Chem.* **2002**, 4, 152.
117. L. Berthon; S. I. Nikitenko; I. Bisel; C. Berthon; M. Faucon; B. Saucerotte; N. Zorz; P. Moisy; Influence of gamma irradiation on hydrophobic room-temperature ionic liquids [C₄MeIm]PF₆ and [C₄MeIm](CF₃SO₂)₂N. *Dalton Trans.* **2006**, 21, 2526.
118. E. Bosse; L. Berthon; N. Zorz; J. Monget; C. Berthon; I. Bisel; S. Legand; P. Moisy; Stability of [MeBu₃N][Tf₂N] under gamma irradiation. *Dalton Trans.* **2008**, 7, 924.
119. J.D. Holbrey; K.R. Seddon; The phase behaviour of 1-alkyl-3-methylimidazolium tetrafluoroborates: Ionic liquids and ionic liquid crystals. *J. Chem. Soc. Dalton Trans.* **1999**, 13, 2133.
120. P. Bonhote; A. P. Dias; N. Papageorgiou; K. Kalyanasundaram; M. Gratzel; Hydrophobic, Highly Conductive Ambient-Temperature Molten Salts. *Inorg. Chem.* **1996**, 35, 1168.

121. G. Turian; Polarity: From Electromagnetic Origins to Biological Take-Over, *Hamburg Kovač*, **1994**.
122. A. J. Carmichael; K. R. Seddon; "Polarity Study of Some 1-alkyl-3-Methyl imidazolium Ambient-Temperature Ionic Liquids with the Solvatochromic Dye, Nile Red." *Journal of Physical Organic Chemistry* **2000**, 13, 591.
123. S. N. V. K. Aki; J. F. Brennecke; A. Samanta; "How Polar are Room-Temperature Ionic Liquids?" *Chem. Comm.* **2001**, 5, 413.
124. A. Kawai; T. Hidemori; K. Shibuya; "Polarity of Room-Temperature Ionic Liquid as Examined by EPR Spectroscopy." *Chem. Lett.* **2004**, 33, 1464.
125. G. Angelini; C. Chiappe; P. D. Maria; "Determination of the Polarities of Some Ionic Liquids Using 2-nitrocyclohexanone as the Probe," *J. Org. Chem.* **2005**, 70, 8193.
126. C. Wakai; A. Oleinikova; M. Ott; "How Polar are Ionic Liquids? Determination of the Static Dielectric Constant of an Imidazolium-Based Ionic Liquid by Microwave Dielectric Spectroscopy." *J. Phys. Chem. B* **2005**, 109, 17028.
127. G. H. Tao; M. Zou; X. H. Wang; "Comparison of Polarities of Room-Temperature Ionic Liquids Using FT-IR Spectroscopic Probes," *Australian J. Chem.* **2005**, 58, 327.
128. T. Köddermann; C. Wertz; A. Heintz; "The Association of Water in Ionic Liquids: A Reliable Measure of Polarity," *Angew. Chem. Int. Ed.* **2006**, 45, 3697.
129. S.V. Dzyuba; R.A. Bartsch; Expanding the Polarity of Ionic Liquids. *Tetrahedron Lett.* **2002**, 43, 4657.
130. R. J. P. Williams; R. D. Gillard; "Coordination Chemistry and Analysis," *Pergamon Press, Oxford*, **1987**.

131. K. R. Seddon; "Ionic Liquids for Clean Technology." *J. Chem. Technol. Biotechnol.* **1997**, 68, 351.
132. M. Schmeisser ; P. Keil; J. Stierstorfer ; A. König ; T. M. Klapötke ; R. Eldik; An Ionic Liquid Designed for Coordination Chemistry Revisited: Synthetic Routes and Safety Tests for 1-Ethyl-3-methylimidazolium Perchlorate ([emim][ClO₄]); *Eur. J. Inorg. Chem.* **2011**, 31, 4761.
133. R. Sheldon; "Catalytic Reactions in Ionic Liquids". *Chem. Comm.* **2001**, 2399.
134. C. M. Gordon; "New Developments in Catalysis Using Ionic Liquids." *Appl. Catal. A* **2001**, 222, 101.
135. M. J. Earle; K. R. Seddon; "Ionic Liquids. Green Solvents for the Future". *Pure Appl. Chem.* **2000**, 72, 1391.
136. A.V. Mudering; A. Babai; S. Arenz; "The "Noncoordinating" Anion Tf₂N⁻ Coordinates to Yb²⁺: A Structurally Characterized Tf₂N⁻ Complex from the Ionic Liquid [MPPyr][Tf₂N]," *Angew. Chem., Int. Ed.* **2005**, 44, 5485.
137. D. B. Williams; M. E. Stoll; B. L. Scott; "Coordination Chemistry of the bis(trifluoromethylsulfonyl)imide Anion: Molecular Interactions in Room Temperature Ionic Liquids". *Chem. Commun.* **2005**, 11, 1438.
138. A. Babai; A. V. Mudering; "Crystal Engineering in Ionic Liquids. The Crystal Structures of [Mppyr]₃[NdI₆] and [Bmpyr]₄[NdI₆][Tf₂N]". *Inorg. Chem.*, **2006**, 45, 4874.
139. P. Wasserscheid; E. T. Welton; "Ionic Liquids in Synthesis," *Wiley-VCH verlag GmbH & Co. KGaA*, **2002**.

140. A. G. Avent; P. A. Chaloner; M. P. Day; K.R. Seddon; T. Welton; "Evidence for Hydrogen Bonding in Solutions of 1-ethyl-3-methylimidazolium Halides, and its Implications for Room-Temperature Halogenoaluminate(III) Ionic Liquids," *J. Chemical Soc. Dalton Trans.* **1994**, 23, 3405.
141. A. Elaiwi; P. B. Hitchcock; K. R. Seddon; "Hydrogen Bonding in Imidazolium Salts and its Implications for Ambient-Temperature Halogenoaluminate(III) Ionic Liquids" *J. Chemical Soc. Dalton Trans.* **1995**, 21, 3467.
142. D. R. MacFarlane; K.R. Seddon; Ionic liquids - progress in fundamental issues. *Aust. J. Chem.* **2007**, 60, 3.
143. R.P. Swatloski; J. D. Holbrey; R. D. Rogers; Ionic liquids are not always green: hydrolysis of 1-butyl-3-methylimidazolium hexafluorophosphate. *Green Chem.* **2003**, 5, 361.
144. R. Harjani; R. D. Singer; M. T. Garcia; "Biodegradable Pyridinium Ionic Liquids: Design, Synthesis and Evaluation". *Green Chem.* **2009**, 11, 83.
145. Y. Fan; M. Chen; C. Shentu, , F. El-Sepai, K. Wang, Y. Zhu, M. Ye; "Ionic liquids Extraction of Para Red and Sudan Dyes from Chilli Powder, Chilli Oil and Food Additive Combined with High Performance Liquid Chromatography," *Analytica Chim. Acta* **2009**, 650, 65.
146. T. Welton; Ionic liquids in green chemistry. *Green Chem.* **2011**, 13, 225.
147. M. L. Dietz; J. A. Dzielawa; Ion-exchange as a mode of cation transfer into room temperature ionic liquids containing crown ethers: implications for the 'greenness' of ionic liquids as diluents in liquid-liquid extraction. *Chem. Commun.* **2001**, 20, 2124.

148. M. L. Dietz; J. A. Dzielawa; I. Laszak; B. A. Young; M. P. Jensen; Influence of solvent structural variations on the mechanism of facilitated ion transfer into room-temperature ionic liquids. *Green Chem.* **2003**, 5, 682.
149. D. C. Stepinski, M. P. Jensen, J. A. Dzielawa, M. L. Dietz, Synergistic effects in the facilitated transfer of metal ions into room-temperature ionic liquids. *Green Chem.* **2005**, 7, 151.
150. C. Xu; L. Yuan; X. Shen; M. Zhai; Efficient removal of caesium ions from aqueous solution using a calix crown ether in ionic liquids: mechanism radiation effect. *Dalton Trans.* **2010**, 39, 3897.
151. N. Turanov; V. K. Karandashev; V. E. Baulinc; Extraction of Alkaline Earth Metal Ions with TODGA in the Presence of Ionic Liquids. *Solvent Extr. Ion Exch.* **2010**, 28, 367.
152. P. Giridhar; K. A. Venkatesan; T. G. Srinivasan; P. R. Vasudeva Rao; Extraction of uranium(VI) from nitric acid medium by 1.1M tri-n-butylphosphate in ionic liquid diluent. *J. Radioanal. Nucl. Chem.* **2005**, 265, 31.
153. P. Giridhar; K. A. Venkatesan; T. G. Srinivasan; P. R. Vasudeva Rao; Effect of alkyl group in 1-alkyl-3-methylimidazolium hexafluorophosphate ionic liquids on the extraction of uranium by tri-n-butylphosphate diluted in various ionic liquids. *J. Nucl. Radiochem. Sci.* **2004**, 5, 21.
154. M.L. Dietz; D. C. Stepinski; Anion concentration-dependent partitioning mechanism in the extraction of uranium into room-temperature ionic liquids. *Talanta* **2008**, 75, 598.
155. I. Billard; A. Ouadi; E. Jobin; J. Champion; C. Gaillard; S. Georg; Understanding the extraction mechanism in ionic liquids: UO₂²⁺/ HNO₃/ TBP/ C₄mimNTf₂ as a Case Study, *Solvent Extr. Ion Exch.* **2011**, 29, 577.

156. I. Billard; A. Ouadi; C. Gaillard; Liquid–liquid extraction of actinides, lanthanides and fission products by use of ionic liquids: from discovery to understanding. *Anal Bioanal Chem.* **2011**, 400, 1555.
157. H. S. Ho; R. N. Menchavez; Y. M. Koo; Reprocessing of spent nuclear waste using ionic liquids. *Korean J. Chem. Eng.* **2010**, 27, 1360.
158. V. A. Cocalia; K. E. Gutowski; R. D. Rogers; The coordination chemistry of actinides in ionic liquids: A review of experiment and simulation. *Coordination Chem. Rev.* **2006**, 250, 755.
159. P.R. Vasudeva Rao; K.A. Venkatesan; T. G. Srinivasan; “Studies on applications of room temperature ionic liquids”, *Progress in Nuclear Energy*, **2008**, 50, 449.
160. K.A. Venkatesan; T.G. Srinivasan; P. R. Vasudeva Rao; A Review on the Electrochemical Applications of Room Temperature Ionic Liquids in Nuclear Fuel Cycle. *J. Nucl. Radiochem. Sci.* **2009**, 10, R1.
161. P.R. Vasudeva Rao; K.A. Venkatesan; Alok Rout; T. G. Srinivasan; Potential Applications of Room Temperature Ionic Liquids for Fission Products and Actinide Separation. *Sep. Sci. Technol.* **2012**, 47, 204.
162. A. V. Mudring; S. Tang; Ionic Liquids for Lanthanide and Actinide Chemistry. *Eur. J. Inorg. Chem.* **2010**, 18, 2569.
163. T. J. Bell; Y. Ikeda; The application of novel hydrophobic ionic liquids to the extraction of uranium(VI) from nitric acid medium and a determination of the uranyl complexes formed. *Dalton Trans.* **2011**, 40, 10125.
164. K. V. Lohithakshan; S. K. Aggarwal; Solvent extraction studies of Pu(IV) with CMPO in 1-octyl 3-methyl imidazolium hexa fluorophosphate (C₈mimPF₆) room temperature ionic liquid (RTIL). *Radiochim. Acta* **2008**, 96, 93.

165. A. E. Visser; R. D. Rogers; Room-temperature ionic liquids: new solvents for f element separations and associated solution chemistry. *J. Solid State Chem.* **2003**, 171,109.
166. K. Nakasima; F. Kubota; T. Maruyama; M. Goto; Feasibility of ionic liquids as alternative separation media for industrial solvent extraction process. *Ind. Eng. Chem. Res.* **2005**, 44, 4368.
167. K. Nakasima; F. Kubota; T. Maruyama; M. Goto; Ionic liquids as a novel solvent for lanthanides extraction. *Anal Sci.* **2003**, 19, 1097.
168. K. Shimojo; K. Kurahashi; H. Naganawa; Extraction behavior of lanthanides using a diglycolamide derivative TODGA in ionic liquids. *Dalton Trans.* **2008**, 37, 5083.
169. P. M. Jensen; J. Neuefeind; V. J. Beitz; S. Skanthakumar; L. Soderholm; Mechanisms of metal ion transfer into room-temperature ionic liquids: the role of anion exchange. *J Am. Chem. Soc.* **2003**, 125, 15466.
170. P. Nockemann; B. Thijs; S. Pittois; J. Thoen; C. Glorieux; K.V. Hecke; L. Van Meervelt; B. Kirchner; K. Binemanns; Task specific ionic liquid for solubilising metal oxides. *J. Phys. Chem. B*, **2006**, 110, 20978.
171. A. Ouadi; B. Gadenne; P. Hesemann; J. E. Moreau; I. Billard; C. Gaillard; S. Mekki; G. Moutiers; Task-Specific Ionic Liquids Bearing 2-Hydroxybenzylamine Units: Synthesis and Americium-Extraction Studies. *Chem. Eur. J.* **2006**, 12, 3074.
172. A. Ouadi; O. Klimchuk; C. Gaillard; I. Billard; Solvent extraction of U(VI) by task specific ionic liquids bearing phosphoryl groups. *Green Chem.* **2007**, 9, 1160.
173. G. Modolo; S. Seekamp; H. Vijgen; K. Scharf; P. Baron; Recent developments in the ALINA process for An(III)/Ln(III) group separation during the partitioning of minor actinides, Proceedings of the 8th International Conference on Radioactive

- Waste Management and Environmental Remediation. ICEM 01, Bruges, Belgium, Sept. 30–Oct. 4, **2001**, ASME.
174. J. H. Olivier; F. Camerel; R. Ziessel; Lanthanide Ion Extraction by Trifluoromethyl-1, 3-diketonate-Functionalised Ionic Liquids Adsorbed on Silica, *Chem. Eur. J.* **2011**, 17, 9113.
175. H. Mehdi; K. Binnemans; V. Hecke; L.V. Meervelt; P. Nockemann; Hydrophobic ionic liquids with strongly coordinating anions. *Chem. Commun.* **2010**, 46, 234.
176. X. Sun; Y. Ji; F. Hu; Bo. He; Ji. Chen,; D. Li; The inner synergistic effect of bifunctional ionic liquid extractant for solvent extraction. *Talanta* H. Mehdi, K. Binnemans, V. Hecke, L.V. Meervelt, P. Nockemann, Hydrophobic ionic liquids with strongly coordinating anions. *Chem. Commun.* **2010**, 81, 1877.
177. A. Bard; S.Faulkner, *Electrochemical Methods: Fundamentals and Applications*, ed. Harris. **2001**: John Wiley & Sons, Inc.: pp. 5, 23-26, 227, 231, 419, 581, 591.
178. M. Faraday; *Experimental Researches in Electricity*, Bernard Quaritch, London, UK, **1839**.
179. D. Pletcher; *A First Course in Electrode Processes*, Electrochemical Consultancy, **1991**.
180. R. P. Buck; Diffuse layer charge relaxation at the ideally polarized electrode *J. Electroanal. Chem.* **1969**, 23, 219.
181. A. Fick; On liquid diffusion. *J. Membr. Sci.* **1995**, 100, 33.
182. A. M. Bond; *Broadening Electrochemical Horizons*, Oxford University Press, Oxford, **2002**.
183. D. Grujcic; B. Pesic; Electrodeposition of copper: the nucleation mechanisms. *Electrochim. Acta* **2002**, 47, 2901.

184. F. Neese; *The ORCA program system. Wiley Interdiscip. Rev.: Mol. Sci.* **2012**, 2, 73.
185. J. P. Perdew; K. Burke; M. Ernzerhof; *Phys. Rev. Lett.*, **1996**, 77, 3865.
186. D. A. Pantazis; F. J. Neese; *Che. Theory m Comput.* , **2011**, 7, 677.
187. A.D. Becke, *Phys. Rev. A* **1988**, 38, 3098.
188. J.P. Perdew, *Phys. Rev. B* **1986**, 33, 8822.
189. F. Weigend; R. Ahlrichs; *Phys. Chem. Chem. Phys.* **2005**, 7, 3297.
190. TURBOMOLE version 6.0 *A Development of University of Karlsruhe and Forschungszentrum Karlsruhe GmbH*, **2009**.
191. F. Neese; *ORCA Version 3.0, An ab initio density functional and semi empirical program package*, **2013**.
192. D. Pantazis; F.J. Neese; *Chem. Theor. Comp.* **2009**, 5, 2229.
193. D. Pantazis; X.Y. Chen; C.R. Landis; F.J. Neese; *Chem. Theor. Comp.* **2008**, 4, 908.
194. F. Baumgartner; *Kerntechnik* **1978**, 20, 74.
195. F. Baumgartner; D. Ertel; *J. Radioanal. Chem.* **1980**, 58, 11.
196. J.M. McKibben; *Radiochim. Acta* **1984**, 36, 3.
197. D.D. Sood; S.K. Patil; *J. Radioanal. Nucl. Chem.* **1996**, 203, 547.
198. C. Musikas; W. W. Schultz; J.-O. Liljenzin; J. Rydberg; M. Cox; C. Musikas, G. Choppin (Eds.), *Solvent Extraction Principles and Practice, 2nd ed.*, M. Dekker; Inc., New York, **2004**, 507.
199. K.L. Nash; C. Madic; J.N. Mathur; J. Lacquement; J.J. Katz, L.R. Morss, N.M. Edelstein, J. Fuger (Eds.), *The Chemistry of the Actinide and Transactinide Elements*, Springer, Dordrecht, The Netherlands, **2006**, 1, 2622.
200. L.E. Barrosse- Antle; A.M. Bond; R.G. Compton; A.M. OMahony; E.I. Rogers; D.S. Silvester; *Chem. Asian J.* **2010**, 5, 202.

201. A. Sengupta; M. S. Murali; P. K. Mohapatra, M. Iqbal, J. Huskens, W. Verboom, *Monatshefte fuer Chemie* **2015**, 146, 1815.
202. A. Sengupta; M. S. Murali; P. K. Mohapatra; M. Iqbal; J. Huskens; W. Verboom; *J. Radioanal. Nucl. Chem.* **2015**, 304, 563.
203. S. I. Nikitenko; P. Moisy; *Inorg. Chem.* **2006**, 45, 1235.
204. R. Gupta; S. K. Gupta; J.S. Gamre; K.V. Lohithakshan; V. Natarajan; S.K. Aggarwal; *Eur. J. Inorg. Chem.* **2015**, 1, 104.
205. R. Gupta; K. Jayachandran; S. K. Gupta; K.V. Lohitakshan; J.V. Kamat; *Eur. J. Inorg. Chem.* **2015**, 26, 4396.
206. L.S. Natarajan; *Coord. Chem. Rev.* **2012**, 256, 1583.
207. M. Mohapatra; V. Natarajan; *J. Radioanal. Nucl. Chem.* **2014**, 302, 1327.
208. P.K. Verma; P.N. Pathak; P.K. Mohapatra; V.K. Aswal; B. Sadhu; M. Sundararajan; *J. Phys. Chem. B*, **2013**, 117, 9821.
209. P.K. Verma; P.N. Pathak; N. Kumari; B. Sadhu; M. Sundararajan; V.K. Aswal; P.K. Mohapatra; *J. Phys. Chem. B*, **2014**, 118, 14388.
210. M. Sundararajan; S.K. Ghosh; *J. Phys. Chem. A* **2011**, 115, 6732.
211. P.K. Verma; N. Kumari; P.N. Pathak; B. Sadhu; M. Sundararajan; V.K. Aswal; P.K. Mohapatra; *J. Phys. Chem. A* **2014**, 118, 3996.
212. B.G. Vats; S. Kannan; M. Sundararajan; M. Kumar; M.G.B. Drew; *Dalton Trans.* **2015**, 44, 11867.
213. P. Kumar; P.G. Jaison; M. Sundararajan; V.M. Telmore; S.K. Ghosh; S.K. Aggarwal, *Rapid Commun. Mass Spectrom.* **2013**, 27, 947.
214. E.R. Brown; J.R. Sandifer; Cyclic voltammetry AC polarography and related techniques, B.W. Rossiter, J.F. Hamilton (Eds.), Physical Methods of Chemistry—Volume II, *Electrochemical Methods*, Wiley, New York, **1986**.

215. S. Matsika; M.J. Pitzer; *J. Phys. Chem. A* **2000**, 104, 4064.
216. R. Bradshaw; D. Sykes; L.S. Natrajan; R.J. Taylor; F.R. Livens; S. Faulkner; IOP Conf. Series: *Mater. Sci. Engg.* **2010**, 9, 012047.
217. G.A. Shamov; G.J. Schreckenbach; *J. Phys. Chem. A* **2005**, 109, 10961.
218. J.P. Austin; M. Sundararajan; M.A. Vincent; I.H. Hillier, *Dalton Trans.* **2009**, 30, 5902.
219. C.Z. Wang; J.-H. Lan; Y.-L. Zhao; Z.-F. Chai; Y.-Z. Wei; W.-Q. Shi; *Inorg. Chem.* **2013**, 52, 96.
220. K. Long; G. Goff; W. Runde; *Chem. Comm.* **2014**, 50, 7766.
221. A. Chaumont; G. Wipff; *Phys. Chem. Chem. Phys.* **2006**, 8, 494.
222. N. Kumari; D. R. Prabhu; A.S. Kanekar; P.N. Pathak; Validation of solvent extraction scheme for the reprocessing of advanced heavy water reactor spent fuel using N, N-dihexyl octanamide as extractant. *Ind. Eng. Chem. Res.* **2012**, 51, 14535.
223. J. N. Mathur; M.S. Murali; K. L. Nash; Actinide partitioning—a review. *Solvent Extr. Ion Exch.* **2001**, 19, 357.
224. S. A. Ansari; P. Pathak; P.K.Mohapatra; V.K. Manchanda; Aqueous partitioning of minor actinides by different processes. *Sep. Purif. Rev.* **2011**, 40, 43.
225. R. Natarajan, B. Raj; Fast reactor fuel reprocessing technology in India. *J. Nucl. Sci. Technol.* **2007**, 44, 393.
226. C. Cuillerdier, C. Musikas, P. Hoel, L. Nigond ; X. Vitart; Malonamides as new extractants for nuclear waste solutions. *Sep. Sci. Technol.* **1991**, 26, 1229.
227. S.A. Ansari; P. Pathak; P.K. Mohapatra; V.K. Manchanda; Chemistry of diglycolamides: promising extractants for actinide partitioning. *Chem. Rev.* **2012**, 112, 1751.

228. S. Kannan; K.V. Chetty; V.Venugopal; M.G.B. Drew; Extraction and coordination studies of the unexplored bifunctional ligand carbamoyl methyl sulfoxide (CMSO) with uranium(VI) and cerium(III) nitrates. Synthesis and structures of $[UO_2(NO_3)_2(PhSOCH_2CONiBu_2)]$ and $[Ce(NO_3)_3(PhSOCH_2CONBu_2)_2]$. *Dalton Trans.* **2004**, 21, 3604.
229. J.H. Matonic; M.P. Neu; A.E. Enriquez; R.T. Paine, B.L. Scott; Synthesis and crystal structure of a ten-coordinate plutonium(IV) ion complexed by 2-[(diphenylphosphino) methyl] pyridine N, P-dioxide: $[Pu(NO_3)_3\{2-[(C_6H_5)_2P(O)CH_2]C_5H_4NO\}_2]$ $[Pu(NO_3)_6]_{0.5}$. *J. Chem. Soc. Dalton Trans.* **2002**, 11, 2328.
230. S. Pailloux; C.E. Shirima; A.D. Ray; E.N. Duesler; K. A. Smith; R.T. Paine; J.R. Klaehn; M.E. McIlwain; B.P. Hay; Synthesis and lanthanide coordination chemistry of trifluoromethyl derivatives of phosphinoylmethyl pyridine N-oxides. *Dalton Trans.* **2009**, 36, 7486.
231. B.G. Vats; J.S. Gamare; S. Kannan; I.C. Pius; D.M. Noronha; M. Kumar ; Synthesis, structural and extraction studies of new bifunctional ligand with uranium. *Inorg. Chim. Acta* **2017**, 467, 1.
232. S. Kannan, B.G. Vats; I.C. Pius; D.M. Noronha; P.S. Dhimi; P.W. Naik; M. Kumar; Extraction and structural studies of an unexplored monoamide, N, N'-dioctyl, α -hydroxy acetamide with lanthanide(III) and actinide(III) ions. *Dalton Trans.* **2014**, 43, 5252.
233. P. Hapiot; C. Lagrost; Electrochemical reactivity in room temperature ionic liquids. *Chem. Rev.* **2008**, 108, 2238.
234. H. Ohno; Electrochemical aspects of ionic liquids. Wiley, Hoboken. ISBN: 978-0-471-76252-2, **2005**.

235. J.Zhang, A.M. Bond; Practical considerations associated with voltammetric studies in room temperature ionic liquids. *Analyst* **2005**, 130, 1132.
236. M.C. Buzzeo; R.G.Evans; R.G. Compton; Non-haloaluminate room-temperature ionic liquids in electrochemistry—a review. *Chem. Phys. Chem.* **2004**, 5, 1106.
237. N. Fietkau, A.D.Clegg; R.G.Evans; C. Villagran; C. Hardacre; R.G. Compton; Electrochemical rate constants in room temperature ionic liquids: the oxidation of a series of ferrocene derivatives. *Chem. Phys. Chem.* **2006**, 7, 1041.
238. K. Jayachandran; R. Gupta; M. Sundararajan; S.K. Gupta; M. Mohapatra; S.K. Mukerjee; Redox and photophysical behaviour of complexes of NpO_2^+ ions with carbamoyl methyl phosphine oxide in 1-hexyl-3-methylimidazolium bis (trifluoromethylsulfonyl) imide ionic liquid, *Electrochim. Acta* **2017**, 224, 269.
239. P.K. Mohapatra; **1993**, Ph.D. Thesis, University of Bombay.
240. T.D. Dolidze; D.E. Khoshtariya; P. Illner; L. Kulisiewicz; A.Delgado; R.V. Eldik; A model for self-diffusion of guanidinium based ionic liquids: a molecular simulation study. *J. Phys. Chem. B* **2008**, 112, 13849.
241. J. Dupont; P.A.Z. Suarez; Physico-chemical processes in imidazolium ionic liquids. *Phys. Chem. Chem. Phys.* **2006**, 8, 2441.
242. P.K. Mohapatra; Actinide ion extraction using room temperature ionic liquids: opportunities and challenges for nuclear fuel cycle application. *Dalton Trans.* **2017**, 46, 1730.
243. T. Prathibha; B. R.Selvan; K. A.Venkatesan; S. Rajeswari; M. P. Antony; Radiolytic stability of N,N-di-alkyl-2-hydroxyacetamides, *J. Radioanal. Nucl. Chem.* **2017**, 311, 1929.

244. M.S. Sajun; V.V. Ramakrishna; S.K. Patil; The effect of temperature on the extraction of plutonium (IV) from nitric acid by tri-n-butyl phosphate.
Thermochim. Acta **1981**, 47, 277.
245. P. Nockemann; B.Thijs ; T. N. Parac-Vogt; K. V. Hecke; L.V. Meervelt; B. Tinant; I. Hartenbach; T. Schleid; V. T. Ngan; M. T. Nguyen; K. Binnemans.; Carboxyl functionalized task-specific ionic liquids for solubilizing metal oxides.
Inorg. Chem. **2008**, 47, 9987.
246. P. Nockemann; B.Thijs; K.V. Hecke; L. V. Meervelt; K.. Binnemans; Polynuclear metal complexes obtained from the task-specific ionic liquid betainium bistrifimide.
Cryst. Growth Des. **2008**, 8, 1353.
247. P. Nockemann; R. V. Deun; B.Thijs; D. Huys; E. Vanecht; K..Van Hecke; L. V. Meervelt; K. Binnemans; *Inorg. Chem.*, **2010**, 49, 3351.
248. C. J.Rao; K. A.Venkatesan; K. Nagarajan.; T. G. Srinivasan; *Radiochim. Acta*, **2008**, 96, 403.
249. O. Palumbo; F.Trequatrini; M.A. Navarra; J.B. Brubach; P. Roy; A. Paolone;
Phys. Chem. Chem. Phys. **2017**, 19, 8322.
250. A. Sengupta; M. S. Murali; P. K. Mohapatra; S.M Ali. ; K. T.Shenoy; *Radiochim. Acta* **2016**, 104, 153.